COMPACTION AND EXTRUSION OF METAL POWDERS

THE ISOSTATIC COMPACTION AND HYDROSTATIC EXTRUSION OF SOME METAL POWDERS

By

ROY LAWRENCE HEWITT, B.Sc., M.Eng.

A Thesis

Submitted to the School of Graduate Studies

in Partial Fulfilment of the Requirements

for the Degree

Doctor of Philosophy

McMaster University

May 1973

DOCTOR OF PHILOSOPHY (1973)
(Mechanical Engineering)

McMASTER UNIVERSITY
Hamilton, Ontario.

TITLE: The Isostatic Compaction and Hydrostatic Extrusion of Some Metal Powders

AUTHOR: Roy Lawrence Hewitt, B.Sc. (Bristol University)
M.Eng. (McMaster University)

SUPERVISOR: Professor M.C. de Malherbe

NUMBER OF PAGES: xiv, 191

SCOPE AND CONTENTS: The purpose of this work was to examine the processes of isostatic compaction and hydrostatic extrusion and to evaluate their potential for the cold consolidation of metal powders to bar stock.

Equipment for isostatic compaction and hydrostatic extrusion at pressures up to 1600 MN/m^2 is described. A numerical technique is presented for calculating the internal pressure required to produce a given bore strain in a tapered pressure vessel set of the type used. The method is applicable to open or closed ended vessels of elastic-plastic work hardening material and assumes the Mises criterion of yielding.

From a review of the literature of powder compaction it is concluded that there is some confusion as to the role and extent of plastic deformation in powder compaction and that the means by which compacts consolidate and achieve green strength is uncertain. It is suggested that the Shapiro-Konopicky pressure-density equation has most capability for further development.

Results of mechanical testing, metallographic examination and x-ray diffraction analyses of some atomized iron powder compacts are presented, together with a metallographic examination of compacted spherical superalloy powders. From these it is concluded that extensive plastic deformation occurs even during the first stage of compaction, but is not solely responsible for consolidation. A sequence of compacting mechanisms is described for the iron powder and it is suggested that the transition from stage 1 to stage 2 compaction corresponds to the change from local to homogeneous plastic flow.

Torre's model of a hollow sphere subjected to external pressure, that was deveioped to represent the compaction behaviour of a porous body, has been modified to cover strain hardening of the material. Theoretical predictions of density are compared with experimental results for Atomet 28 iron powder and Alcoa grade 1202 aluminum powder. There is good agreement in the second stage of compaction; outside of this stage the theoretical values are higher than the experimental results. Some possible reasons for the discrepancy are discussed.

Results are presented showing the extrusion pressure required for iron compacted at different pressures; from these it is concluded that the extrusion characteristics of compacts can be influenced by their porosity and an expression is derived relating the extrusion pressure to the relative density of the compact.

Results of mechanical testing and metallographic and fractographic examinations of extruded aluminum compacts are presented,

together with their extrusion characteristics. These show that good bonding can be developed in these compacts by hydrostatic extrusion at reduction ratios of 6.25, and that their strengths can be higher than wrought material of similar composition. This strength improvement is attributed to the strain hardening undergone by the material during compaction. An interpretation of the mechanism of bonding is also given.

Although it is shown that isostatic compaction and hydrostatic extrusion can be used to produce well bonded bar material from metal powders, it is suggested that the potential of the method is limited by the very high pressures that would be required to produce materials of commercial interest.

ACKNOWLEDGEMENTS

The author wishes to express his sincere appreciation of the help, advice and encouragement of his supervisor and friend, Professor M.C. de Malherbe. He is also grateful to Professor R. Newcombe for acting as supervisor in Professor de Malherbe's absence.

The author would like to thank Professor J.M. Alexander, of Imperial College, England, for suggesting the area of investigation and for assistance with the initial design of the equipment.

The assistance of the Division of Mechanical Engineering, National Research Council of Canada, who manufactured the high pressure equipment is also gratefully acknowledged.

The support of the Structures and Materials Laboratory, National Aeronautical Establishment, National Research Council of Canada, in providing facilities for and assistance with the experimental work is acknowledged.

In particular, the author would like to thank Dr. W. Wallace of the Materials Section, for his keen interest in this work. His advice and encouragement and the many stimulating discussions that have taken place have been invaluable. His assistance in the preparation of this thesis is also gratefully acknowledged.

TABLE OF CONTENTS

LIST OF ILLUSTRATIONS

LIST OF PRINCIPAL SYMBOLS

a	inner radius of hollow sphere
a_o	initial value of a
b	outer radius of hollow sphere
b_o	initial value of b
D	relative density (density/theoretical density)
D_o	initial relative density of model
D_1	relative density of compact prior to extrusion
D_2	relative density after extrusion
E	Young's modulus
E_p	plastic tangent modulus = $d\bar{\sigma}/d\bar{\varepsilon}_p$
H	porosity (=1-D)
H_v	Vicker's hardness
K	ratio of external radius to internal radius
K_c	compaction constant
L	effective length of liner
m	index in empirical stress-strain relationship
N	normal stress on outside of liner due to taper
P	compaction pressure
P_E	extrusion pressure
P_{E1}	external pressure on liner due to taper alone
P_{E2}	external pressure on liner due to container without taper
P_{EX}	total external pressure on liner

r	radius of point within wall of sphere or current radius of any point within wall of tube
r_o	initial radius of any point within wall of tube
r_{E1}	external radius of liner
r_{E2}	external radius of container
r_I	internal radius of liner
R	extrusion ratio (billet c.s.a./product c.s.a.)
u	radial displacement
u_a	radial displacement of inner surface of sphere
u_b	radial displacement of outer surface of sphere
Y	yield strength of compacted powder
β	strain hardening constant
δ	operator indicating increment of a quantity associated with an increment of pressure
Δ	operator referring to a change in a quantity between two neighbouring points
$\varepsilon_r, \varepsilon_\theta, \varepsilon_z$	natural strains in radial, circumferential and axial directions
$\bar{\varepsilon}_p$	equivalent plastic strain
θ	semi-angle of taper
μ	coefficient of friction
ν	Poisson's ratio
ρ	density
$\sigma_r, \sigma_\theta, \sigma_z$	normal stresses in radial, circumferential and axial directions
$\sigma'_r, \sigma'_\theta, \sigma'_z$	deviatoric stresses in radial, circumferential and axial directions

σ_{rn}	radial stress at $r = r_n$
σ_{rp}	previous radial stress at $r = r_{n-1}$ (i.e. when the interface was one step further in)
$\bar{\sigma}$	equivalent stress
$\bar{\sigma}_o$	equivalent stress at first yield

1 INTRODUCTION

There has been a tremendous increase in the use of powder metallurgy over the past twenty years; many new fabrication processes have been developed and many more powders made available. Traditionally, powder metallurgy processing has been explored with a view to lowering production costs by minimizing machining operations and material and scrap losses. However, continuing demands for extreme levels of alloy homogeneity and hence uniformity and reliability of mechanical properties in high strength and low weight engineering components have added new impetus to the development of powder metallurgy techniques.

Dendritic segregation in cast ingots is normally eliminated by combinations of hot-working and homogenization annealing treatments. For heavily alloyed materials, these operations may be difficult to perform, time consuming and therefore expensive. For example, nickel-base superalloys such as Udimet 700 and Astraloy are extremely resistant to forging deformation; they exhibit very narrow hot-working temperature ranges and they suffer from hot shortness. Other more heavily alloyed materials such as IN-100 and MAR M246 cannot be hot-worked by conventional means and consequently they must be used in investment cast form.

These problems of alloy segregation and poor workability can be overcome by converting the molten alloy to powder form by atomization. The rapid rates of solidification achieved by atomization effectively eliminate segregation, and that which does occur is confined within each powder particle.

Consolidation of these metal powders can be achieved in a variety of ways. Techniques such as cold pressing and sintering, hot pressing, hot isostatic pressing, hot forging and hot extrusion have been widely used. In order to avoid excessive contamination of the powder particle surfaces during high temperature processing, operations must often be performed in a vacuum or in a carefully controlled inert or reducing atmosphere. The sintering of aluminum alloy powder compacts, for example, must be carried out in a controlled humidity environment. In other cases costly vacuum canning operations may be required. Even when these precautions are observed, undesirable metallurgical reactions can occur during high temperature processing which degrade the properties of the product. A reaction of this type often seen in hot isostatically pressed nickel-base superalloy powders is the preferential precipitation of brittle carbide particles on prior powder particle boundaries. The resulting carbide networks impede grain boundary migration during subsequent grain growth treatments and also lead to alloy embrittlement. Such problems might be avoided if means could be found to compact and consolidate these powders at temperatures much lower than those currently used.

Recent developments in hydrostatic extrusion, together with the similarity of the equipment used for this and cold isostatic compaction, suggest that they might be combined to provide a method for compacting and consolidating metal powders to bar stock without recourse to high temperature treatments. The feasibility of this approach has been partially demonstrated by Alexander and Dove[1] and more recently by Alexander and Quainton[2]. These workers showed that isostatically compacted sponge iron powder could be hydrostatically extruded without

cracking if a sufficiently high extrusion ratio was employed. No examinations of the microstructure and mechanical properties were performed, however, and therefore the degree of powder particle bonding developed by this process is not known.

The final properties of the extrude will depend on the extrusion ratio and the flow characteristics and degree of bonding of the initial compact. These in turn will depend on the inherent strength of the alloy powder, the particle geometry, the density of the compact and on the extent of interparticle bonding and strain hardening developed during compaction. Knowledge of these mechanical and physical processes occurring during metal powder compaction appears to be very limited, and consequently even less is known about the hydrostatic extrusion of metal powder compacts.

The purpose of this work was to examine the processes of isostatic compaction and hydrostatic extrusion and to evaluate their potential for the cold consolidation of metal powders to bar stock. Three commercially available atomized powders, Alcoa grade 1202 aluminum, Atomet 28 iron powder from Quebec Metal powders and INCO 713LC nickel-base superalloy powder from Federal Mogul Corporation have been studied. These three powders have quite different particle geometries and mechanical properties and thus provide a broad base for the study.

2 LITERATURE SURVEY

2.1 POWDER COMPACTION

2.1.1 Historical Survey

Of principal concern in powder compaction is the relationship between the applied pressure and resulting density of a compact. One of the earliest attempts to relate these two quantitatively was made by Walker[3] in 1923. By using an analogy with Hooke's law he proposed the expression:

$$\ell nP = -\frac{L}{D} + C \qquad (2.1)$$

where P is the applied pressure, D the relative density of the powder and L and C are constants.

A similar expression was proposed in 1938 by Balshin[4] who applied the concepts of fluid mechanics to the problem. It is found in practice, however, that the values of L and C are not constant but vary with the powder and the conditions of the experiment. Further, the equation clearly becomes invalid at high pressures as the relative density becomes greater than one. Shapiro and Kolthoff[5] have suggested that this invalidity stems from the applied assumption of elastic deformation, whereas the pressing of powder is essentially plastic deformation as noted by Wretblad and Wulf[6].

An expression which has gained much popularity is that proposed by Shapiro and Kolthoff[5] in 1947 and independently by Konopicky[7] in 1948 i.e.

$$H = H_o e^{-K_c P} \qquad (2.2)$$

where H_o is the initial (extrapolated) porosity at zero applied pressure, H is the porosity at a pressure P and K_c is a constant. This equation may be rewritten in terms of relative densities to give

$$\ln \frac{1}{1-D} = K_c P + \ln \frac{1}{1-D_o} \qquad (2.3)$$

Shapiro and Kolthoff found that this expression adequately represented the behaviour of die compacted silver bromide powders over the first half of the pressure range studied (1 to 310 MN/m^2). Since the apparent density of the powder at higher pressures was within a few percent of the true density, the accuracy of the porosities was insufficient to allow any conclusions to be drawn with respect to the second half of the pressure range. They concluded from their experiments with particles of different size that the value of K_c increases with particle size or decreasing surface development and/or temperature. Also they noted that H_o remains essentially constant for samples of particles of uniform size but decreases for samples composed of particles of different size.

Shapiro and others have pointed out the connection with Athy's[8] work on the compaction of shale beneath the earth's surface. He found that the porosity of shale at a depth x below the surface was given by

equation (2.2) with the pressure P replaced by the depth x, and where H_o was the porosity of the surface clays. Shapiro and Kolthoff thought the agreement of experimental findings for two very different materials, both of which are considered very plastic, to be significant.

Smith[9] proposed the following empirical formula to describe the pressing of metal powders in 1948:

$$CF = \frac{D - d}{\sqrt[3]{P}} \qquad (2.4)$$

where CF is the compressibility factor associated with a particular powder, and d is the relative apparent density. He claimed that predicted results for iron powders were surprisingly close to experiment. Comparisons for different types of bronze were also close. The pressure range covered, however, was only up to about 250 MN/m^2, and Smith observed that at higher pressures this formula gave results higher than experienced in practice, and he attributed this to work hardening of the particles.

In the same year, Balshin[10] proposed a formula which still receives much attention today, especially in the Russian literature. He supposed the compacting of powder to obey an analogous law to Hooke's Law, i.e.

$$\frac{dP}{S_c} = K' \frac{dh}{h} \qquad (2.5)$$

where S_c is the "contact cross section", K' a constant, and $\frac{dh}{h}$ is the relative reduction of the briquet height. But

$$\frac{dh}{h} = \frac{d\beta}{\beta} \qquad (2.6)$$

where β is the relative volume of the material ($= 1/D$). If particle hardening is excluded then

$$\frac{P}{S_c} = \text{constant} \qquad (2.7)$$

Hence, substituting equations (2.6) and (2.7) into (2.5), and integrating gives the result

$$\ell nP = -n\ell n\beta + \ell nP_{max} \qquad (2.8)$$

where n is a constant.

Also in 1948 Torre[11] proposed a new concept in powder compaction to lend theoretical support to Konopicky's equation. He used a model of a hollow metal sphere with negligible internal pressure and a hydrostatic external pressure to represent a pore surrounded by solid material. Assuming a rigid-perfectly plastic material he obtained the Shapiro-Konopicky equation (equation 2.3) theoretically. The proportionality constant K_c was shown to be

$$K_c = \frac{3}{2\sigma_o} \qquad (2.9)$$

where σ_o was the upper yield stress of the material. Unfortunately, this expression for K_c is in considerable disagreement with experiment.

More recently in 1961 Van Buren and Hirsch[12] instituted an experimental program to produce some generalizations concerning the more favourable conditions for hydropressing different classes of powder. They investigated three different general types of powder:

(i) a ductile metal - iron, (ii) a non-ductile metal - tungsten, and (iii) a single component ceramic - aluminum oxide. Each material was studied using a fine and a coarse powder and the effect of deairing was also investigated.

Using a maximum compacting pressure of 775 MN/m^2 they concluded that for unsintered hydropressed compacts, the green density and green strength increase with forming pressure, and that the slope of the density versus forming pressure curve decreases with increasing particle hardness. Further they observed that the higher the apparent density the higher the green density for a given pressure and that deairing had no significant effect on green properties.

Heckel[13,14] developed a method of die compaction to measure densities from very low compaction pressures up to about 850 MN/m^2. He used this to determine pressure-density curves for various grades of iron, nickel, copper, tungsten and steel (SAE 4630) powders. He modified the Shapiro-Konopicky equation and suggested that densification could be represented as a three stage process expressed in terms of the formula:

$$\ell n \frac{1}{1-D} = K_c P + \ell n \frac{1}{1-D_o} + B \qquad (2.10)$$

where B increases from 0 at P = 0 to a constant value at the end of the second stage.

The first stage is the filling of the die and the amount of densification is indicated by D_o; by using particles of differing geometries he showed that D_o was primarily a function of the geometry of the powder particles, decreasing with increasing particle size.

The second stage is characterized by individual particle movement and rearrangement at low pressures before interparticle bonding becomes appreciable. This was shown by compacting -80+140 mesh alumina powder (which densifies by crushing); there was little interparticle bonding and no transition from non-linear to linear behaviour of the $\ell n \frac{1}{1-D}$ versus P plot over the pressure range studied (up to about 435 MN/m^2). He also observed that the transition to linear behaviour for the iron, nickel, copper and tungsten powders occurred very close to the minimum pressure necessary to form a coherent compact. The densification taking place in this stage is again primarily a function of particle geometry, the amount of densification decreasing as the particle size decreases or as the particle shape becomes more nearly spherical. The third stage is characterized by the proportionality of the rate of change of density with pressure and the void fraction of the compact, which corresponds with the work of Shapiro[5] and others. The proportionality constant K_c is a material constant, being larger for softer and more ductile powders. He concluded that the value of K_c in die compaction could be approximated by

$$K_c = \frac{1}{3\sigma_o} \qquad (2.11)$$

where σ_o is the yield strength of the material. The similarity between this experimental value for K_c and Torre's theoretical expression should be noted.

This expression relating pressure and density was further developed by Heckel[15]. He noted that increases in D_o were almost always

accompanied by decreases in B. In general the sum

$$\ell n \frac{1}{1-D_o} + B = A \qquad (2.12)$$

was approximately constant. Thus he was able to normalize density - pressure data for different powders to a common set of axes by plotting relative density D against reduced pressure $P/3\sigma_o$. Such a plot was given together with tolerance bands for future data points.

While he observed that this figure was limited to die compaction, he suggested that it should be possible, at least in theory, to construct a similar diagram for isostatic compaction.

Nikolaev[16] published a paper in 1962 in which he proposed to derive a new formula for relating die compacting pressure and density which did not involve any empirically determined constants. He suggested that above a certain pressure compaction was made possible mainly by penetration of particles into the pores, and thus used the idea of extrusion through a conical die. Determining the average pressure transmitted to a particle in terms of the compacting pressure and relative density, he then related this to the highest specific pressure in extrusion through a conical die. Relating the cross sectional areas of the hypothetical conical die to the particle and pore surface areas he obtained the formula:

$$P = \sigma_s C D \ell n \frac{D}{1-D} \qquad (2.13)$$

where σ_s is the creep limit of the material and C is a coefficient related to the 'die angle', i.e. the particle geometry, and equal to 2.5 to 3.0. He noted that equation (2.13) could only be used for D > 0.5 and showed that predictions using this equation were in good agreement with experimental data for steel, iron, electrolytic copper and aluminum powders at pressures up to the maximum pressure used (about 620 MN/m^2).

Cooper and Eaton[17] put forward a new concept of powder compaction in 1962. They suggested that the compaction process was dependent upon the size of the voids in the material. As an initial analysis they divided the processes into two broad classes: (i) filling of holes of the same order of size as the original particles, and (ii) filling of voids that are substantially smaller. The first process occurs primarily by particles slipping past each other while the second occurs because of fragmentation or plastic flow.

By using a probability density function to represent the variation of hole filling of each type with pressure, they arrived at the following expression relating fractional volume compaction and applied pressure:

$$\frac{V_o - V}{V_o - V_\infty} = a_1 \exp \frac{-K_1}{P} + a_2 \exp \frac{-K_2}{P} \qquad (2.14)$$

where V_o is the initial total volume, V is the compact volume and V_∞ is the compact volume when all holes are filled, i.e. the theoretical fully compacted volume. The dimensionless coefficients a_1 and a_2 indicate the fraction of theoretical compaction that would be achieved at infinite pressure by each particular process. The coefficients K_1 and K_2 indicate the magnitude of the pressure at which the particular process has the

greatest probability density.

They confirmed this expression experimentally by compacting four ceramic powders, alumina, silica, magnesia and calcite at pressures up to about 620 MN/m^2. By selecting suitable values of a and K they were able to calculate a curve of fractional compaction versus pressure that was in excellent agreement with their experimental results.

They observed that the empirically determined values of the coefficients a and K were consistent with the mechanisms which they had assumed to govern compaction. Further they concluded that the harder and more brittle the powder, the higher was the ultimate porosity. They tentatively explained this by the difference in the predominant process for small pore filling; hard particles depend primarily on fracture to fill these small pores with fragments, but as the pores become smaller this becomes more difficult and some plastic flow is necessary before ultimate compaction is achieved; with softer powders, however, plastic flow occurs at lower pressures and hence small pore filling is easier.

Again in 1962, Meerson[18] published a discussion of some of the Soviet literature on powder compacting. He concluded that the formula put forward by Balshin[4] was based on unsound assumptions and that the relationship later proposed by Balshin[10] was more reasonable. Meerson derived this relationship in three different ways, thereby, he suggested, confirming its soundness. If powders of ductile metals are compressed corrections have to be introduced to make allowance for particle hardening during compression.

Donachie and Burr[19] in a review of the effects of pressing on metal powders in 1963 treat the literature as four separate areas:

packing, pressing, strains and the effect of lubricants. They conclude from this review that packing and strains are intimately related to the development of a formula expressing the pressing characteristics of powders; only the effect of lubricants may be considered separately.

They suggest that certain discrete regions of pressure-density behaviour exist and justify an expression of the form:

$$D = f_1(P) + f_2(P) + f_3(P) + A \qquad (2.15)$$

where $f_1(P)$, $f_2(P)$ and $f_3(P)$ are functions of pressure applying to the regions of transitional restacking, local flow and isostatic compression respectively and A is a geometrical constant related to material shape and size, etc. Of the various experimental formulae previously suggested they conclude that the best quantitative correlation of the pressing process is expressed by equation (2.10) due to Heckel[14]. They note, however, that this equation is inaccurate for very low (less than 150 MN/m^2) and high (greater than 775 MN/m^2) pressures. Further, they doubt the validity of the relationship between the constant K_c and the yield strength suggested by Heckel[15] and expressed in equation (2.11) since yield strength is a defined parameter whose observed values vary with the definition and sensitivity of the measurement technique; it is also a sensitive function of composition and purity. In their pressing experiments they observed virtually no metallographic evidence of gross plastic deformation in brass powders and little X ray line broadening in commercial copper powders, both compacted up to 700 MN/m^2. Thus they suggest that although the intuitive feeling is that extensive

plastic deformation occurs in pressing, little in fact does with commercial powders.

Burr and Donachie[20] have also given more detailed results of the effect of die pressing on copper powders in the pressure range of 78 to 1540 MN/m^2. They confirm the validity of Heckel's results which were obtained for pressures up to 850 MN/m^2, and agree that they can be suitably expressed by equation (2.10). However, above this pressure there is a marked non-linearity in the P versus $\ell n \frac{1}{1-D}$ plot. They conclude that this casts doubts on the theoretical significance of K_c as a material constant which measures the ability of a compact to deform.

A detailed study of the compressibility of powders undertaken by Shapiro[21] was published in 1963. A broad spectrum of powders ranging from "plastic" to "brittle" were investigated to determine both their compressibility and the mechanism by which compaction was achieved. The particle size was kept fairly uniform both within a sample and between different powders to reduce the number of variables. Shapiro concluded from the study that powder compaction takes place via plastic deformation for plastic type powders such as magnesium, or via fragmentation for brittle powders like thoria, or via a combination of the two as in the case of molybdenum disulphide. Within the pressure range studied (up to 700 MN/m^2) the effect of pressure on porosity for plastic materials could be expressed by the Shapiro-Konopicky equation. For other materials, two terms of the general equation,

$$H = \sum_i a_i \, e^{-K_i P} \qquad (2.16)$$

are required. One term whose influence is in the low pressure range is believed to be related to the porosity of the individual particles. The initial or bulked porosity was found to be a function of particle size, size distribution, particle shape and the porosity of the individual particles.

Photomicrographs taken during the compression process revealed that particles do not slide past one another during compaction regardless of the type of compaction. The same mechanism applies in filling large holes or small pores in any one system. This contradicts the suggestion of Cooper and Eaton[17] and Shapiro discounts their compaction equation as having no physical significance.

A further observation of Shapiro was that fragmentation of ceramic-type particles results in the formation of many fine fragments as well as several large fragments. The concept of fine fragments falling away from the bearing surface in the initial stages of compression may account for the changing slope of the logarithm porosity - pressure curve.

A formula for relating compacting pressure and density that is often cited in the Russian literature is that proposed by Kunin and Yurchenko[22], again in 1963. Compressing powders of bismuth, cadmium, copper, tin, zinc, iron, alumina (dust), graphite, sulphur and rock salt at pressures from 0 to 310 MN/m^2, they observed that the compacting curves had much in common and thus justified a search for general regularities governing their behaviour during compacting.

Introducing a coefficient of compaction, K_p, given by

$$K_p = \frac{d\rho}{dP} \qquad (2.17)$$

where ρ is the density, and plotting its value against density, they concluded that the compaction process could be schematically divided into three regions. The first region is characterized by the particles being brought closer together, the second by the particles undergoing brittle and plastic deformation and the third by bulk compression. They suggested that the coefficient of compaction in the plastic region of compaction is given by an exponential function of the form:

$$K_p = K_{po} e^{-\alpha P} \qquad (2.18)$$

where α is a constant, and from this derived the following powder compaction equation:

$$\rho = \rho_{lim} - \frac{K_{po}}{\alpha} e^{-\alpha P} \qquad (2.19)$$

where ρ_{lim} is some arbitrary limiting density; it is arbitrary in the sense that it would be the limiting density only if equation (2.18) were valid up to infinitely high pressures. In general ρ_{lim} will be higher than the theoretical density. The constants α, K_{po} and ρ_{lim} characterize the material under given compacting conditions and must be found experimentally.

In a further paper published in 1964, Kunin and Yurchenko[23] compare their pressing equation with those proposed by Balshin[4], Konopicky[7], Torre[11], and polytropic equations of the type:

$$P\rho^n = C \qquad (2.20)$$

where n and C are constants. Analysing the same data as reported in reference 22 in terms of these equations they concluded that the polytropic equation could be used with satisfactory approximations in special cases only. Similarly, the logarithmic expression of Balshin[4] was considered to have extremely limited application.

They noted that the formulas of Konopicky[7], Torre[11] and their own[22] were equivalent except for the difference of using ρ_{lim} instead of the single crystal theoretical density, though as they were derived independently from different concepts of the nature of the compaction process the physical meaning imparted to the constants was different. Analysing their data in terms of these equations led them to the conclusion that use of the theoretical density instead of a limiting density gave results which did not agree with experiment, while their own equation (2.19) was "well justified for all metals in a wide range of pressures".

Greenspan[24] isostatically compacted beryllium, iron, copper and aluminum powders using pressures up to about 1250 MN/m^2 in 1964. He observed that the order of easiest pressing was aluminum, copper, iron and beryllium where the end point porosities (at 1040 MN/m^2) were respectively of the order of 1%, 4.2%, 7.4% and 8.6%. He suggested that the degree of densification was of the same order as the degree of plasticity expected for these materials. Further, expressing the porosity-pressure data in terms of the Shapiro-Konopicky equation, he observed that it was represented nearly by two straight line segments and suggested that strain hardening effects might be important with respect to the

change point. In fact he showed the influence of strain hardening by interjecting a stress annealing operation on the pressing cycle; beryllium compacts initially pressed to 8.0 - 9.5% porosity, stress annealed and pressed again at the same pressure were densified further to a porosity of 2.7 - 3.3%. Repeating the entire cycle produced further densification to about 1.0 - 1.6% porosity.

In 1965 Kawakita and Tsutsumi[25] compared several powder compression equations including those of Balshin[4], Konopicky[7] and Athy[8] and an empirical formula previously used for soft, fluffy medical powders by Kawakita, namely:

$$\frac{V_o - V}{V_o} = \frac{abP}{1 + bP} \qquad (2.21)$$

where V_o is the initial apparent volume corresponding to P = 0, V is the volume under the applied pressure P and a and b are the characteristic constants. Rearranging equation (2.21) in the form

$$\frac{P}{1-V/V_o} = \frac{P}{a} + \frac{1}{ab} \qquad (2.22)$$

they plotted $P/(1-V/V_o)$ against P for various sets of previously published data to determine whether the expected straight line resulted. They similarly plotted appropriate values to get expected straight lines from the other predictions. From comparison of these plots, which were all in the pressure range of less than 775 MN/m^2 they concluded that the plot represented by equation (2.22) gave the best straight line and that, therefore, equation (2.22) gave the best fit to the experimental data.

A further paper by Kawakita and Tsutsumi[26] again compared these various compaction equations, but from a more analytical viewpoint. They classified the equations into two types by means of the gradient of porosity with the pressure. One was

$$\frac{dH}{dP} = - AH^x \qquad (2.23)$$

where A is a constant. This type includes those of Shapiro (x=1) and Kawakita (x=2). The other type was

$$\frac{dH}{dP} = \frac{A(1-H)^y}{P^z} \qquad (2.24)$$

which includes the equation of Balshin (y=2, z=1) and Smith (y=0, z=2/3). By evaluating the porosities predicted by the various equations as $P \to 0$ and $P \to \infty$, they concluded that only the equations of Shapiro and Kawakita were applicable over the entire range of pressures as only these gave $H = H_o$ at $P = 0$ and $H = 0$ at $P = \infty$. Of these, Kawakita's equation indicates a considerable decrease in porosity at lower pressures, while Shapiro's shows that a major portion of the compaction occurs at higher pressures. According to their experiments on tablet compression, Kawakita's equation gave good agreement for powders of common nonspherical particles, while powder of spherical glass or metal particles followed Shapiro's equation. They noted that it was difficult to find a single equation which is in exact accord with experimental data for different kinds of powder and different experimental conditions.

A different approach to powder compaction was presented by Bockstiegel[27] in 1966. Considering Cooper and Eaton's[14] idea of the importance of pore size in the compaction process, he investigated the distribution of pore size in iron powder compacts pressed at varying pressures. Isostatically compacting an electrolytic iron powder at pressures up to about 775 MN/m^2, and measuring the pore size distribution using microscopic lineal analysis, he observed that the accumulated porosity (calculated from the pore size distribution) as a function of the pore diameter very closely approximates the logarithmic - normal type curve. Neither the slope nor the position of these curves appeared to be greatly influenced by the applied pressure or powder hardness. However, the diameter of the largest pores in a compact decreased with increasing pressure and showed a pronounced dependence on powder hardness. An expression was also given relating the compact porosity, pore size distribution and compacting pressure in terms of a complementary error function.

Plotting porosity - pressure data in terms of the Shapiro-Konopicky equation gave non-linearities which he felt could not reasonably be explained in terms of an increase in yield strength due to cold working. Further, he showed that pure iron powder, slightly precompacted at 20 MN/m^2 and presintered 1 hour at 1150°C yielded the same porosity - pressure curve as the loose powder when subsequently pressed. This he claimed contradicted Konopicky's[7] and Heckel's[14] explanations that deviations from the theoretical curve at low pressures were due to rearrangement processes involving loose powder particles sliding past each other.

Bockstiegel has also criticized Torre's[11] calculations, claiming that they were based on unsound assumptions, and recalculated them to give the pressure at which a hollow sphere would just begin to yield. This latter calculation is itself wrong, however, and it appears that Bockstiegel has not sufficiently understood Torre's assumptions; Torre's calculations are, in fact, correct.

Radomysel'skii and Shcherban'[28] reported an investigation of the die compaction of two component materials in 1966. They used three different materials: a reduced iron powder containing up to 12% by mass of glass, an iron-chromium carbide and iron-chromium (electrolytic) containing 1 and 7% by mass respectively of the chromium carbide and chromium. In the pressure range studied (up to 925 MN/m^2), they observed that the pressure density relationship could be expressed by equation (2.8) of Balshin[10], and that the index n in this equation could be expressed in terms of the second component by the equation:

$$n = n_o(1 + kW) \qquad (2.25)$$

where n_o is a constant for the main component, k is a constant characterizing the properties of a given system and W is the weight fraction of the second component. Plotting their data also using the method of Kunin and Yurchenko[22], equation (2.19), they noted a linear dependence on $e^{-\alpha P}$ in the range 230 - 700 MN/m^2; above and below this range, non-linear behaviour was observed.

Morgan and Sands[29], reviewing isostatic compaction in 1969, suggest that Heckel's[14] interpretation of the constant K_c in equation (2.10)

is a useful means of expressing the densification that is caused by particle deformation. They present data to show a pronounced change in slope on a $\ell n \frac{1}{1-D}$ versus P plot for die compacted sponge iron powder at about 775 MN/m^2 and note that a similar change in slope also appears to occur for isostatic compaction. The authors remark that further studies of change point with respect to density and pressure would be very valuable in comparing the fundamental mechanisms of these processes and finding the cause of the change. Comparing die and isostatic compaction they conclude that there is a distinct advantage in using isostatic conditions except for aluminum and iron compacted to high densities.

Savin, Ukhina and Fedotov[30] investigated the die pressing of nickel powders in terms of Balshin's[4,10] equations and the equation of Kunin and Yurchenko[22]. Using a maximum compaction pressure of 465 MN/m^2 and several different nickel powders they concluded that a single equation could not be used to describe the pressing of these different powders. They suggested that Balshin's first equation could be applied for carbonyl powder in the pressure range 30 to 465 MN/m^2, whereas for enlarged carbonyl powder and spherical electrolytic powder in the pressure range 90 to 465 MN/m. Balshin's second equation was more applicable. They also noted that for these two groups, deviation from a linear plot of ℓnP versus ℓnD occurred at lower pressures for larger powders. It also appears from the plot of ℓnD versus P given in this paper, that Kunin and Yurchenko's equation is valid at the higher pressures (above about 230 MN/m^2).

Yurchenko, Pugina and Shcherban'[31] have reported further work on the densification of two component materials in die pressing. Using a base of iron powder with additions of graphite, zinc sulphide and electrolytic nickel and a maximum compaction pressure of 925 MN/m^2, they observed that the pressure-density data could be represented by Balshin's second equation except at high pressures (over 850 MN/m^2). The parameter n, in equation (2.8), varied linearly over a wide range when the second component was introduced into a ductile material; the second component may be either a ductile or brittle material. The intensity of variation of n is dependent on the physico-mechanical properties and is given by equation (2.25). The authors further noted that addition of graphite generally lowered the porosity, as with other additions, except at high pressures; this, they suggested, might be due to increased elastic after-effect.

Petrova, Shcherban' and Sleptsov[32] studied the densification behaviour of iron, nickel and cobalt powders with additions of 20% to 85% by weight of zirconium, niobium and molybdenum carbides at pressures up to 385 MN/m^2 using die pressing. They found that the pressure-density data conformed with Balshin's[10] equation and that the value of the index n varied almost linearly over the range 0 - 60% by weight of carbides, and could be expressed by equation (2.25) proposed previously by Radomysel'skii and Shcherban'[28]. They also observed that raising the carbide content of mixtures raised their porosity at pressures above 155 MN/m^2 and lowered it at lower compaction pressures. It was demonstrated that the presence of a lubricant had no significant

influence on the value of n and on its rate of variation.

Meerson, Islankina, Mel'nikov and Gol'man[33] made an experimental investigation of the hydrostatic compaction of stainless steel powder and compared it with compaction in both single and double acting dies. Using a maximum compacting pressure of about 1300 MN/m^2 they observed that to get compacts of a given relative density, the pressure used in hydrostatic compaction is about 1.5 to 2 times lower than required with a double action press and as much as 3 times lower than with a single acting press. In this pressure range the pressure - density relationship could be well expressed by equation (2.8) of Balshin[10]. Some specimens were hydrostatically compressed up to about 2800 MN/m^2 and it was observed that there was a marked deviation from linearity on the ℓnP versus ℓnD plot above about 1300 MN/m^2; in fact this plot could be fairly well represented by two intersecting straight lines. It may be noted that the maximum relative density obtained was only about 92% at 2800 MN/m^2.

Radomysel'skii and Serdyuk[34] published a survey on the shaping of metal powders in 1970 in which reference is made to both die and isostatic compaction. They classified the researches concerning die compaction into two main classes; one represented by the researches of Nikolaev[16] and Kunin and Yurchenko[22] in which the theoretical analysis is based on the hypothesis of continuity of the material being pressed. The other is represented by studies based on Balshin's[4] theory, where the concept of a contact cross section is used.

The only work on isostatic pressing that is referred to is that of Il'in and Gol'dman[35] who derived a relationship between pressure and density using the method of slip lines. The relationship can only be used in the region of plastic deformation as the authors chose an idealized model of powder material consisting of a multitude of spheres with a regular, orthogonal system of packing, for which the initial relative density is 50%.

Meerson, Rasskazov and Chulkov[36], in an investigation of the die compaction of copper, iron, tungsten and tungsten carbide powders at pressures of up to about 775 MN/m^2, observed that the hard, low ductility materials (W and WC) conformed to the relationship given by equation (2.8) of Balshin, whereas for ductile metals (Fe and particularly Cu) deviations were observed. They attributed these deviations to the influence of work hardening of severely deformed particles at high pressure. Also, the harder the material the less effective was pressure in inducing densification.

Boiko and Shcherban'[37] investigated the densification of dispersed Ni-ZrC, Ni-NbC and Ni-WC powders in a die at pressures up to about 775 MN/m^2, and compared it with the densification of pure nickel powder. They observed that the relationship between pressure and density was well represented by equation (2.8). The dependence of the constant n on the amount of second component was seen to be given by equation (2.25) proposed by Radomysel'skii and Shcherban'[28]. The overall effect of the additions was to reduce the densification of the nickel for a given pressure, the ZrC producing the greatest effect and the WC the least;

this was attributed to the differences in hardness and particle size between the carbides.

Severdenko and Iosifov[38] have investigated the effect of pressing on aluminum grandules. Using a double acting die set and pressures up to 620 MN/m^2 they found that the equation of Kunin and Yurchenko[22] gave good agreement with experimental plots. They also observed that the size of the granules used had no marked effect on the relationship between compact density and compacting pressure.

In 1971 Alexander and Quainton[2] reported their results of isostatically compacting a sponge iron powder in the pressure range of 465 to 1540 MN/m^2. They observed that their results were very close to the few points published by Morgan and Sands[29] for isostatic compaction and by comparing them with Morgan and Sands results for die compaction confirmed the higher density achievable by isostatic compaction. They found no consistent proportionality between $\ell n \frac{1}{1-D}$ and pressure, and no marked change in slope.

Compaction of powder using a combination of isostatic and unidirectional pressing was reported by Koerner and Quirus[39] in the same year. They showed isostatic and unidirectional compaction curves for MH-100 sponge iron powder at pressures up to 690 MN/m^2; these indicated a higher green density for isostatically pressed compacts which was most pronounced at low pressures. The curves shown nearly converge at the higher pressures and Koerner and Quirus concluded that the overall behaviour suggested that the use of shear stresses to continually reorient the particles into their optimal density state might lead to yet higher green densities.

The compaction curves mentioned above are misleading however. The points plotted at the higher pressures for isostatic compaction do not correspond to those mentioned later in the paper. Further, plotting Alexander and Quainton's data[2] for the same powder type, while showing agreement at the lower pressures, indicates higher densities at the higher pressures. The difference in densities between the two methods then remains almost constant over the range studied.

The device used to produce the shear stresses was designed so that the powder could be isostatically compacted to any desired pressure while an axial load was applied through a piston on top of the compact. Results were presented showing the density response to the applied shear stress for various isostatic pressures. For a given isostatic pressure the density increased almost linearly as the shear stress increased up to a certain limit, after which there was little further increase. The slope of these curves decreased and the limiting value of shear stress increased a little as the isostatic pressure was increased. Comparing the densities obtained by Alexander and Quainton[2] at high isostatic pressures and the apparent trends in this work, it appears that there would be little advantage to be gained from the applied shear stress at higher pressures as the slope of the curves would be near zero. Where higher pressures are not attainable, however, the technique looks promising.

The generality of the method was demonstrated by Koerner[40] by using it to compact iron, aluminum, nickel, copper and tungsten. Each powder showed the compaction trends described above. The isostatic pressure required for a near zero slope of the density - applied shear stress curve increased with powder strength.

2.1.2 Review

From the preceding survey, it is apparent that most of the work has been involved with determining pressure-density relationships. One of the more popular, especially in the Russian literature, is the polytropic type due to Balshin[10], i.e.

$$PD^{\gamma} = \text{constant} \qquad (2.26)$$

This equation only agrees with experiment over a limited range of pressures, however. Further, its derivation is based on an analogy with Hooke's law which does not seem reasonable, especially at high pressures.

The more general equations of Cooper and Eaton[17] and Shapiro[21], although they can be made to fit the data over a wider range, are essentially exercises in curve fitting and do not warrant further theoretical investigation at this stage.

Kawakita's[25] equation is another empirical equation with little or no theoretical justification. The accuracy with which it can approximate the data is also in doubt since the observed linearity in Kawakita's plots seems to result from the method of plotting (i.e. P versus $P/(1-V/V_o)$).

Balshin's[4] first equation and Smith's[9] equation do not warrant further attention as they are clearly incapable of approximating the data except in very limited circumstances.

Nikolaev's[16] equation was intended as an equation that did not involve any empirically determined constants, but in fact the constant C in equation (2.13) must still be found experimentally. Furthermore, the concept on which the derivation is based does not seem to agree with

experimental observation, i.e. particles do not slide past each other.

The complex equation of Il'in and Gol'dman[35] is only valid over the second stage of compaction, and would not be expected to be very accurate due to the idealistic assumptions made in its derivation.

The pressure-density equation which appears to have most capability for further development is of the type

$$\ln(1/1-D) = K_c P + \text{constant} \qquad (2.27)$$

which includes the equations of Shapiro and Kolthoff[5], Konopicky[7], Torre[11], Heckel[14] and Kunin and Yurchenko[22]. This equation is particularly interesting in that Torre has provided some theoretical basis for it and Bockstiegel's[27] results impart some measure of validity to Torre's model. Perhaps the theoretical value of compaction constant obtained by Torre could be improved by including strain hardening in the model, and this is certainly worth pursuing.

Equation (2.27) adequately represents the compaction process over a limited range of pressures, but overestimates the observed densities at very low and high pressures to give the three characteristic regions shown in Fig. 1.

It is widely held that these three regions correspond to different mechanisms of compaction. Kunin and Yurchenko[22] define the first region as being characterized predominantly by the particles being brought closer together and densified without undergoing deformation; the second region is characterized by the particles undergoing brittle and plastic deformation and the third by bulk compression.

Heckel[14] makes a very similar classification, characterizing the first region by individual particle movement and rearrangement before interparticle bonding becomes appreciable, and the second by plastic deformation and cold working. He did not observe the third region since he was using relatively low compaction pressures.

Donachie and Burr[19] suggest that the first region is one of transitional restacking, the second corresponds to local plastic flow and the third to isostatic compression, both elastic and plastic. They suggest that there is very little severe plastic deformation during pressing.

Shapiro[21] has discounted the theory that particles slide past each other during compaction and states that compaction takes place via plastic deformation for plastic type powders such as magnesium, via fragmentation for brittle powders like thoria or by a combination of the two as in the case of molybdenum disulphide. He suggested that deviations at the low pressure end were related to the porosity of individual particles.

Greenspan[24] observed the change in slope between the second and third regions for several metal powders and suggested that the change point was a function of the strain hardening characteristics of the material. Smith[9] and Meerson[33] have also attributed deviations at high pressures to the effects of strain hardening.

It can be seen, therefore, that there is still some confusion as to the role and extent of plastic deformation in powder compaction, and that there has been little work aimed directly at this problem.

The inclusion of strain hardening in Torre's model may provide some insight, but direct measurements of the plastic strain in a compact would be most valuable.

It is also apparent that the means by which compacts consolidate and achieve green strength is uncertain; this must be clarified before it is possible to understand the bonding of extruded compacts.

2.2 HYDROSTATIC EXTRUSION

The subject of hydrostatic extrusion is now well founded and it would be inappropriate to include an exhaustive review of its literature here. It may be useful, however, to briefly trace its development and draw attention to some of the principal process variables encountered. A short discussion of some of the more recent developments will also be included together with references to some of the major publications in the field.

The first description of the hydrostatic extrusion process was given by Robertson[41] in patents taken out in England, but the first practical attempt was performed by Bridgman[42] in the U.S.A. The majority of the original research and development work, however, has been carried out independently in England by Pugh[43] and his colleagues at the National Engineering Laboratory, and in Russia by Beresnev, Vereshcagin, Ryabinin and Livshits[44] and others at the High Pressure Laboratory of the Academy of Sciences. Since then work has started in many other places including Canada, Czechoslovakia, France, Norway, Sweden and the U.S.A..

The principal advantages of hydrostatic extrusion over the conventional process are reviewed as follows. In hydrostatic extrusion the billet is surrounded by fluid, and it is the fluid pressure that provides the extruding force and not the direct action of a ram. With the elimination of the billet-ram contact, there is no longer any need to stop extruding when the end of the billet reaches the beginning of the die; hence the length of the discard may be reduced.

Since the discard length is now more or less independent of die length, the possibility of using smaller die angles arises. The billet-die friction is generally lower in hydrostatic extrusion because the high pressure fluid, in which a lubricant is often dispersed, is continually being drawn along the billet-die interface[43]. Reducing the die angle increases this frictional work because of the longer interface, but the increase is not as significant as in conventional extrusion because of the improved lubrication. Conversely, reduction of the die angle decreases the redundant work required in the extrusion, and this is larger than the increase in friction work except for very small angles. Thus small angle dies require lower extruding pressures for a given ratio. They also produce products with more uniform properties because of the more uniform deformation of the material; this helps make it possible to extrude many materials that are too brittle to extrude by conventional means.

Further differences in the design of the dies result by taking advantage of the supporting fluid pressure. Hydrostatic extrusion dies may be constructed with thin walls and the fluid pressure on the outside of the die used as a support in place of the heavy shrink or tapered

rings used in conventional tooling.

Another result of having fluid surrounding the billet is the elimination of the friction at the billet-container interface with a consequent reduction in extrusion force. More important, perhaps, the extrusion force then becomes independent of the billet length which allows the use of longer billets. Also there is no tendency to buckle as the sides of the billet are always supported by the fluid pressure.

The process does have some disadvantages, nonetheless, chiefly associated with the attainment of the high pressures required. Since the liquid is compressed by maybe one fifth to achieve a pressure of 1500 MN/m^2, there is a considerable amount of stored energy in the system which presents a potential hazard; this is minimized by keeping the volume of fluid used to a minimum and providing adequate safety shields, etc. The other major problem is in the design and construction of the pressure vessel and seals, etc. required to contain the high pressures used and withstand the cyclic nature of the process when discrete billets are used. Davidson and Kendall[45] have discussed this in some detail, and a description of several different types of equipment already in use has been given by Pugh[46].

Among the various process parameters involved in hydrostatic extrusion, the most important are the extrusion pressure and ratio, the billet material and geometry, the die angle and lubrication used and the speed of extrusion. The relationship between extrusion pressure, P_E, and extrusion ratio, R, can be expressed[47] by the empirical equation:

$$P_E = a(\ell nR + n) \qquad (2.28)$$

where a and n are constants that depend on the material and conditions. The value of n is invariably small for small die angles, such as 45^o, being related to the amount of redundant work involved in the extrusion.

To get an estimate of the extrusion pressure required to extrude a particular billet, Pugh[48] proposed a relationship involving the Vickers hardness, H_V, of the billet. Plotting the ratio $P_E/\ell nR$ for a 45^o die against H_V, he showed that all his results for round product from round billets of many different materials lay near a straight line given by the empirical equation:

$$P_E = (5.78\ H_V + 62)\ell nR \qquad (2.29)$$

where the extrusion pressure is given in MN/m^2. More recently Lowe and Goold[49] obtained a similar expression for their own experiments, namely

$$P_E = (4.24\ H_V + 144.5)\ell nR \qquad (2.30)$$

The billet geometry also plays an important part in the extrusion process. If a square ended billet is used, or even one with a nose tapered to the die angle, severe stick-slip conditions will generally be encountered, with the initial peak pressure being considerably higher than the run-out pressure. By making the nose taper some 2^o less than the die angle, Low and Donaldson[50] found that under certain conditions the peak pressure and stick-slip were virtually eliminated. A similar effect can also be obtained by providing a generous radius instead of a

sharp transition between the tapered nose and the rest of the billet[43]. One of the reasons for these effects is the improved lubrication, as more fluid is dragged through in the initial part of the extrusion, but probably more important is that, by having a smaller taper on the billet, extrusion is initiated at a lower extrusion ratio and hence pressure; then the pressure rises gradually with the extrusion ratio until the full ratio is achieved and the static friction condition is effectively eliminated.

The surface finish of the billets is important too; rough billets tend to drag more lubricant with them entrapped in the surface pores which reduces the initial pressure peak and the amount of stick-slip behaviour observed[43]; unfortunately, rough billets also tend to produce rough extrusions.

As mentioned previously, the die angle has an important effect on the extrusion pressure required for a given reduction. Typically, for an extrusion ratio of 2, a drop in extrusion pressure of about 40% is observed as the die angle is decreased from 150^{o} to 40^{o}[47], and there is a minimum pressure at some critical angle (generally between 50^{o} and 20^{o}). Experimental results suggest that the optimum die angle increases with extrusion pressure no matter whether this results from an increase in extrusion ratio or in the flow stress in the material or both[43].

The experimental evidence concerning the effect of lubricants and pressurizing fluids on the hydrostatic extrusion process is inconclusive and in some cases conflicting. It appears that in general, however, the viscosity of the fluid has little effect on the extrusion pressure as long as there is no lubricant breakdown due to decreasing viscosity as

the pressure is raised; further, the fluid must remain effective as a pressure transmitting medium. A decrease in viscosity does tend to cause stick-slip behaviour, however, as the lubrication conditions are more critical and lubrication breakdown becomes more apparent. For the same fluid, variations in solid lubricant have little effect on the run-out pressure, but the breakthrough pressure may be higher if no lubricant is used. There is also some evidence to suggest that certain combinations of liquid and lubricant are incompatible. More information on the topic of liquids and lubricants is contained in the works of Beresnev et al[51], Bobrowsky and Stack[52], Fiorentino et al[53,54,55], Lowe and Goold[49] and Pugh[46,47].

The speed of extrusion also has some effect on the process. Fiorentino et al[54,56] have shown that the peak pressure may be reduced by as much as 8% by increasing the speed of the ram; for several different materials and extrusion ratios they found a decrease in peak pressure up to a certain speed in each case, above which there was no further change in the peak pressure. More important, perhaps, they observed that an increase in ram speed often prevented stick-slip during run-out, thereby eliminating surface cracks on the product.

Similar work by Low[57] suggests that there are three types of stick-slip behaviour, the type occurring depending on the speed. Low found that at slow speeds, stick-slip was very irregular and showed no tendency towards stability; at intermediate speeds the pressure variation was progressively reduced and the oscillations damped out; above a certain critical speed no cyclic phenomena were apparent. He observed

that the extrusion speed had little effect on either the peak or run-out pressures above a certain critical speed.

Pugh[43] has suggested a quantitative explanation of these results in terms of conventional lubrication theory. He assumed that the extrusion speed, and hence sliding speed, influences the coefficient of friction in a similar manner to conventional lubrication theory, and proposed that the first region in Low's results corresponds to boundary lubrication, the second to mixed lubrication and the third to hydrodynamic lubrication.

There have been numerous reports on the effect of hydrostatic extrusion on the mechanical properties of many different materials, but it is difficult to make any generalizations about them other than that they are similar to those produced by conventional extrusion.

For some of the more difficult to work materials it has been found advantageous to employ back pressure extrusion, also known as fluid to fluid or differential pressure extrusion. In this process the material is extruded from the main high pressure chamber into a second, back pressure, chamber, the differential pressure being the same as in the standard method. The back pressure has the effect of inhibiting the surface cracking which occurs in the extrusion of very brittle materials. The process is inconvenient, however, especially from a production viewpoint, in that the length of the extrudate is limited by the length of the second chamber; further, the main pressure must be higher, necessitating more complex pressure vessels and tooling, etc..

To obtain the same beneficial effects of an applied back pressure, Fiorentino et al[58] have suggested the use of a double reduction die. The second reduction, which is about thirteen mm after the first and of the order of 2%, requires very little extra fluid pressure over that for the first reduction and in no way limits the length of extrudate. It was suggested that these double reduction dies prevent surface cracking by favourably altering the residual stress pattern, changing the residual surface longitudinal stresses from tensile to compressive. Fiorentino's qualitative description of the stress pattern on exit from a standard die has been partially verified by Osakada et al[59] who measured the residual stresses in hydrostatically extruded copper rod and concluded that the fir tree type surface cracking was due to the longitudinal residual tensile stresses. Little work relating to the use of double reduction dies has been published, however.

2.3 HYDROSTATIC EXTRUSION OF POWDER COMPACTS

Very little work has been published on the subject of hydrostatic extrusion of powder compacts. Bobrowsky[60] has briefly discussed the use of hydrostatic extrusion for the consolidation of powder, but has given no indication of any experimental work in this area. In a private communication, however, he suggested that it was probable that some proprietary investigations have been made.

Gardner, Donaldson and Yans[61] have discussed the conventional extrusion of metal powders, which for most materials of technical interest must be performed at temperatures in excess of 500°C. Various areas where

this process might be of interest are discussed, the first being the extrusion of pure metals such as tungsten. This material is processed almost exclusively by powder metallurgy means, and can be hot extruded to yield rod and tubing. Molybdenum is also often produced by means of powder metallurgy and might be suitable for extrusion direct from powders. Again, beryllium powder must be used for the production of rod and tubing of that material and direct extrusion of powder should be a useful way of producing it.

Another potentially fertile area of investigation suggested by Gardner et al involves the manufacture of superalloys since these are difficult to both cast and fabricate. By producing Rene 41 by means of blending and extruding elemental powders at a temperature of 925°C and a reduction ratio of 16:1, they were able to cold work the resulting product over 70%. They further point out that this process would permit a greater flexibility in choosing the amount and type of alloying components.

Another area which they suggest deserves attention is the manufacture of hard facing alloys. These cobalt and nickel base materials are generally produced by finger casting which limits their length to diameter ratio, and segregation and voids within the castings give rise to problems during welding.

Martynov et al[62] hydrostatically extruded some hot pressed molybdenum and found that the mechanical properties were considerably enhanced by the extrusion and, most importantly, that a high ductility was retained by the hydrostatically extruded molybdenum after a high temperature annealing treatment. They suggested that this latter effect

was due to the development of a perfect recrystallization texture; because of the high uniformity of deformation, and the lack of high-temperature effects in hydrostatic extrusion, a more perfect deformation texture of the <110> is created than with hot pressing, hence an improved recrystallization texture.

Mochalov et al[63] extended this work to include different kinds of molybdenum. They used commercial powder compacts with no prior plastic treatment, forged powder compacts with a total reduction of about 70%, and hot forged, commercial cast molybdenum containing small additions of titanium and zirconium. This last material had a reduction of more than 95% and some samples of it were annealed in vacuo for one hour at 2000°C before extrusion.

In the initial state, the powder metal molybdenum had a relative density of about 91%; this was increased to close to 100% after about 50% reduction by hydrostatic extrusion. There was a big improvement in hardness, strength and impact toughness as the degree of reduction was increased. The plasticity also increased, which was attributed to the disappearance of pores and the development of texture.

The hardness, strength and plasticity of the forged powder metal molybdenum also increased with the degree of deformation.

Similar behaviour was noticed in the case of the annealed forged cast molybdenum, though the increase in plasticity was less marked. The other forged cast molybdenum showed a decrease in elongation with increase of deformation, but still remained quite high.

Mochalov et al[64] further investigated the mechanical properties of these same hydrostatically extruded materials after annealing at various temperatures. They found that the strength and plasticity decreased as the annealing temperature increased, but even after total recrystallization the unalloyed extruded powder metal molybdenum retained higher plasticity and strength than the unextruded material. They attributed the high plastic characteristics of the extruded material to the formation of a fine-grain recrystallized structure and the development of a pronounced <110> recrystallized texture. In contrast, the low alloy molybdenum in any state underwent embrittlement after recrystallization annealing. This was attributed to the disintegration of the supersaturated solid solution of interstitial impurities on the molybdenum base.

The first work to be published on the use of hydrostatic extrusion for consolidating unsintered powder compacts seems to have been that by Alexander and Dove[1]. They isostatically compacted sponge iron powder in thin rubber envelopes at pressures of 518 MN/m^2 and 710 MN/m^2, which resulted in compacts with relative densities of 86.6% and 91.9% respectively. The specimens compacted at the lower pressure disintegrated as the pressure was applied to extrude them, but those compacted at the higher pressure were successfully extruded through an extrusion ratio of 6.75 when coated with PTFE. The extrusion pressure required at this ratio was 1500 MN/m^2. Extrusion ratios of less than 6.75 resulted in cracked extrudates, but the empirical equation of pressure-hardness, obtained by Pugh[47], was found to apply. The final relative density of the extruded compact increased to 97.4% and the hardness had increased

a little, suggesting an improvement in mechanical properties, though these were not measured.

This work was extended by Alexander and Quainton[2], who extruded a series of sponge iron powder billets compacted at 710 MN/m^2 through several different ratios. They observed that sound products could be produced by simple hydrostatic extrusion at extrusion ratios greater than 4.7. This was considerably lower than found previously and was attributed to the different lubricant used; in this series of experiments a graphite based chemically active lubricant had been used instead of PTFE, and the extruded products had been found to be still completely coated with the lubricant. They observed that fluid to fluid extrusion enabled smaller extrusion ratios to be used to produce sound products. They also found that a double reduction die, although incorrectly made with a 90° semi-angle at the second reduction instead of 20°, produced sound products at extrusion ratios as low as 2.25; a back pressure of 620 MN/m^2 was required for sound products at the same ratio using a standard die.

Unfortunately, Alexander and Quainton have given no details concerning the densities of the extruded products; nor have they obtained any mechanical test data on the material. Thus although they have shown that the hydrostatic extrusion of powder compacts is possible, it is still uncertain as to how effective the process is as a means of consolidating the material and creating interparticle bonding. Alexander and Dove[1] observed an increase in hardness and density of the extruded material as compared with the compact, but a similar increase would be obtained merely by pressurizing to the extrusion pressure used.

Similarly, in the work of Mochalov et al[63], the extent to which the porosity of the sintered powder compacts was reduced by the application of the extrusion pressure alone was not studied; it might be expected to be quite high as the material would have softened in the sintering treatment and would then repress to a lower porosity as found by Greenspan[24] for beryllium.

In order to obtain a better understanding of the process it will be necessary to extrude a series of billets compacted at different pressures through extrusion ratios chosen such that the extrusion pressure is no greater than the compaction pressure of the billet extruded. Detailed mechanical tests will have to be performed on both the compacted and extruded material so that variations in mechanical properties with compacting pressure and extrusion ratio can be studied.

Although the work reviewed above is inconclusive in regard to the consolidating effect of hydrostatic extrusion, there is other experimental evidence which suggests that it is a useful tool in closing up microporosity and material defects. Bulychev et al[65] created microporosity and crack-type defects in copper by extending at elevated temperatures and observed the effect of hydrostatic pressure and plastic deformation on the density of the material. They found that even very high hydrostatic pressures (up to about 10,000 MN/m^2) unaccompanied by plastic deformation did not eliminate the pores and cracks. With a sufficiently large amount of plastic deformation, however, the pores and cracks were either completely eliminated or reduced in size to such an extent that they could no longer be observed under an optical microscope, nor worsen

the mechanical properties of the material.

Beresnev et al[66], using the same type of copper material as Bulychev et al[65], found that there were improvements in both mechanical properties and density when specimens with defects were deformed by hydrostatic extrusion. These were slight at low degrees of deformation but increased rapidly as the deformation was increased from 5 to 20% reduction in area. Thereafter the improvement in properties became less rapid. They also found that for a given degree of deformation the density was improved two to three times faster using hydrostatic extrusion as compared with wire drawing.

Thus hydrostatic extrusion does have the potential for eliminating porosity in compacts.

3 THEORETICAL ANALYSIS OF POWDER COMPACTION

3.1 INTRODUCTION

Although Donachie and Burr[19] have questioned the existence of a relationship between the compaction constant K_c in the Shapiro-Konopicky equation and the yield stress of the material, it still seemed rational to the present author that densification behaviour should be related to the yielding characteristics of the material. Since it is not sufficient to characterize a metal merely by its yield stress, it is necessary to include the entire stress-strain behaviour in some way. This, together with a desire to determine whether the curvature in the $\ell n(1/1-D)$ - pressure plot at high pressures could be attributed to strain hardening, prompted the author to attempt to produce a model for compaction which included the effects of strain hardening.

Since the concept of Torre's[11] model has been given some experimental backing by Bockstiegel[27] and produces a form of result which agrees with experiment, at least over part of the pressure range, it was decided to use this as a basis for the new model. This now consisted of a hollow metal sphere with negligible internal pressure and a hydrostatic external pressure with the sphere material assumed to be rigid-plastic instead of rigid-perfectly plastic, i.e. the material was assumed to strain harden.

3.2 THEORY

3.2.1 Basic Equations

Assume that the porous material can be represented by a hollow sphere of a rigid-plastic material with internal radius a and external radius b. Let the initial radius of some point within the wall of the sphere be r and let its radial displacement due to an external pressure P be u.

The equilibrium equation for the sphere may be written

$$d\sigma_r = \frac{2}{r-u}(\sigma_\theta - \sigma_r)d(r-u) \qquad (3.1)$$

where σ_r and σ_θ are the radial and circumferential stresses respectively. If the sphere is fully plastic, then using either the Tresca or Von Mises yield criterion (since the circumferential and tangential stresses are equal by symmetry)

$$\bar{\sigma} = (\sigma_\theta - \sigma_r) \qquad (3.2)$$

where $\bar{\sigma}$ is the equivalent yield stress. Substituting equation (3.2) into (3.1) and integrating gives the result

$$\sigma_r = 2\int \frac{\bar{\sigma}}{r-u} d(r-u) \qquad (3.3)$$

Evaluating this equation from $\sigma_r = P$ at the outside to $\sigma_r = 0$ inside gives

$$P = \int_{b_o-u_b}^{a_o-u_a} \frac{\bar{\sigma}}{r-u}\, d(r-u) \qquad (3.4)$$

where the subscript o refers to initial conditions (i.e. P=0) and u_a and u_b are the radial displacements of the inner and outer surfaces of the sphere respectively.

The radii of the sphere can be related to the relative density by the expression

$$D = 1 - \left[\frac{a_o-u_a}{b_o-u_b}\right]^3 \qquad (3.5)$$

3.2.2 Without Strain Hardening

For a non strain hardening material as assumed by Torre, $\bar{\sigma}$ is a constant and equation (3.4) can be integrated directly to give

$$P = 2\bar{\sigma}_o \ell n \left[\frac{b_o-u_b}{a_o-u_a}\right] \qquad (3.6)$$

which by using equation (3.5) may be written in terms of the relative density as

$$P = \frac{2}{3}\bar{\sigma}_o \ell n \left(\frac{1}{1-D}\right) \qquad (3.7)$$

When plotted as $\ell n(1/1-D)$ versus P, equation (3.7) is represented by a straight line of slope $3/2\bar{\sigma}_o$ passing through the origin. This does not agree with experiment in that the extrapolated straight line always gives

a positive intercept on the $\ell n(1/1-D)$ axis as in Fig. 1. This has led to the addition of a constant in equation (3.7) to make it conform with equation (2.27), but there is no mathematical justification for this in terms of the model; a rigid-perfectly plastic hollow sphere can assume only one size and hence one value of $\ell n(1/1-D)$, for any given pressure. The failure of the straight line to pass through the origin must be due to an inadequacy in the model.

3.2.3 Introduction of Strain Hardening

For a strain hardening material, equation (3.4) cannot be integrated directly since $\bar{\sigma}$ is an unknown function of (r-u), and a numerical method must be used to evaluate $\bar{\sigma}$ at the various values of r. The method used follows that proposed by Manning[67] for thick tubes.

From considerations of symmetry,

$$\delta\varepsilon_\theta = \delta\varepsilon_\phi \qquad (3.8)$$

where $\delta\varepsilon$ refers to a plastic strain increment. Thus, since all elastic strains are to be neglected following the assumption of a rigid-plastic material, it follows from the Prandtl-Reuss equations that

$$\delta\varepsilon_\theta + \delta\varepsilon_\phi + \delta\varepsilon_r = 0 \qquad (3.9)$$

Substituting equation (3.8) into (3.9) gives

$$\delta\varepsilon_r = -2\delta\varepsilon_\theta \qquad (3.10)$$

The equivalent plastic strain increment, $\delta\bar{\varepsilon}_p$, is given by the expression

$$\delta\bar{\varepsilon}_p = \frac{\sqrt{2}}{3} \left| (\delta\varepsilon_r - \delta\varepsilon_\theta)^2 + (\delta\varepsilon_r - \delta\varepsilon_\phi)^2 + (\delta\varepsilon_\theta - \delta\varepsilon_\phi)^2 \right|^{\frac{1}{2}} \qquad (3.11)$$

which may be simplified using equation (3.10) as

$$\delta\bar{\varepsilon}_p = 2\delta\varepsilon_\theta \qquad (3.12)$$

Thus by integrating,

$$\bar{\varepsilon}_p = 2\int \delta\varepsilon_\theta \qquad (3.13)$$

But the circumferential strain increment can be expressed in terms of the displacement as

$$\delta\varepsilon_\theta = \frac{\delta u}{r} \qquad (3.14)$$

which can be substituted into equation (3.13) to give

$$\bar{\varepsilon}_p = 2\int_r^{r-u} \frac{dr}{r} \qquad (3.15)$$

or

$$\bar{\varepsilon}_p = 2\ell n \left(\frac{r}{r-u}\right) \qquad (3.16)$$

the change of sign being introduced to keep $\bar{\varepsilon}_p$ positive.

The other equation required for the solution is obtained from the assumption of incompressibility, i.e. constant volume. Hence

$$\frac{4}{3}\pi(r^3-a_o^3) = \frac{4}{3}\pi\left[(r-u)^3-(a_o-u_a)^3\right]$$

or

$$r-u = r(1+C^3/r^3)^{1/3} \qquad (3.17)$$

where

$$C^3 = -3u_a a_o^2 + 3u_a^2 a_o - u_a^3 \qquad (3.18)$$

3.2.4 Method of Solution

Using equations (3.16) and (3.17), equation (3.4) may be integrated numerically as follows: splitting the sphere into a series of concentric shells, choose a value of internal displacement u_a so that values of u at any other radius may be calculated from equation (3.17). Then using equation (3.16) $\bar{\varepsilon}_p$ may be calculated at each radius. Using the equivalent stress-strain data for the material, the equivalent yield stress can be found at each radius. Thus values are known for all the variables in equation (3.4) at each station and a standard numerical technique may be used to evaluate the integral. Finally the relative density corresponding to this pressure is calculated from the internal and external radii as in equation (3.5). Repeating the procedure for different values of u_a produces the pressure-density data.

In order to get a further check on the validity of the model, a value for the average strain in the material at any pressure was calculated. This was achieved by summing the products of the plastic strain for any

shell and the volume of the shell, then dividing this sum by the total volume of material in the hollow sphere.

3.3 NUMERICAL RESULTS

To obtain an idea of the effects of different amounts of strain hardening on the graph of $\ell n(1/1-D)$ against P, a series of hypothetical stress-strain curves were employed. Fig. 2 shows the graphs for various degrees of linear strain hardening. The graph for the non strain hardening material obtained by the same numerical technique is as predicted from simple integration. It does not pass through the origin, however, but bends toward the horizontal at some finite value of pressure. This is because the sphere is initially taken to be of finite size and a finite pressure is needed to produce plastic flow in the material. The horizontal part of the graph thus corresponds to pre-yield behaviour but it is not accurate since the assumptions made in the theory are violated in this region; the numerical results are only valid when the plastic strains are large enough for the elastic strains to be ignored. Similar bending toward the horizontal is apparent in all the graphs of $\ell n(1/1-D)$ against $P/\bar{\sigma}_o$.

As the amount of linear strain hardening increases, so the slope of the graphs decreases. This is as expected from the simple Torre model, but less obvious is the shape of the new graphs. One might have expected greater curvature, but it is clear from Fig. 2 that curvature occurs mainly at the lower pressures. For large amounts of strain hardening the plots become very nearly linear (e.g. $\beta = 10.0$). Also, even with as

little strain hardening as $\beta = 0.2$, the slope is decreased by as much as 50% compared to no strain hardening.

It is also apparent from Fig. 2 that if the straight line segments of the graphs are extrapolated to zero pressure, they do not pass through the origin, but give a finite value of D which increases with the degree of strain hardening. Thus the discrepancy between experiment and the predictions from Torre's model can be explained, at least partially, in terms of strain hardening.

Fig. 3 shows the variation of average strain in the material with compacting pressure for the same stress-strain curves as are used for Fig. 2. The strains for a given pressure decrease as the amount of strain hardening increases and the curvature becomes less; for $\beta = 10.0$, the strain versus pressure curve has become almost linear. The effect of small amounts of strain hardening on the strain-pressure relationship is less pronounced than on the graph of $\ell n(1/1-D)$ against pressure.

Although the chosen initial density has little effect on the density-pressure curve for a non strain hardening material, it does affect the strain-pressure results quite significantly as can be seen in Fig. 4. As it is raised the slope is reduced and the curvature increased. Also, for a higher initial density, a larger compacting pressure is required to produce a finite strain; this is easily understood in terms of the model in that a thick hollow sphere will yield at a higher pressure than a thin one.

In a strain hardening material the initial density also affects the pressure-density curve. Fig. 5 shows the graphs for a material

with $\beta = 5.0$. Raising the initial density moves the line up and to the right, while increasing the slope slightly, as would be expected from physical considerations. It is interesting to note that the points at which these curves tend toward the horizontal at the low pressure end lie along the line obtained for the non strain hardening material. This is because, at the pressure the material yields, it is still in the unhardened condition.

Since the assumption of linear strain hardening is somewhat unrealistic in terms of engineering materials, giving too great an increase in flow stress at high strains, the effect of using a three step linear material was investigated. A stress strain curve given by the following equations was employed:

$$\left.\begin{aligned} \bar{\sigma} &= \bar{\sigma}_o & 0 &< \bar{\varepsilon}_p < 0.02 \\ \bar{\sigma} &= \bar{\sigma}_o\,(1+5\bar{\varepsilon}_p) & 0.02 &< \bar{\varepsilon}_p < 0.18 \\ \bar{\sigma} &= \bar{\sigma}_o\,(1.9+0.5(\bar{\varepsilon}_p-0.18)) & 0.18 &< \bar{\varepsilon}_p < \infty \end{aligned}\right\} \quad (3.19)$$

where $\bar{\sigma}$ is given in MN/m^2.

Such a material has an initially constant flow stress, then strain hardens rapidly and finally levels out to a low rate of further hardening. It can be seen from Figs. 6 and 7 that the effect of this levelling-out is very apparent at quite low pressures and tends to increase both the slope of the $\ln(1/1-D)$ graph and the strains. The initial step appears to have very little effect.

4 THE ELASTIC-PLASTIC EXPANSION OF TAPERED PRESSURE VESSEL SETS

4.1 INTRODUCTION

Although the pressure vessel set used in the present experiments was based on an existing piece of equipment, there appear to be no reports of any elastic-plastic stress analyses of such vessels and therefore the ultimate pressure capability of the equipment was unknown. A suitable technique was therefore developed.

It is advantageous in the design of high pressure cylinders to provide a variable external pressure which increases with the internal pressure. This can be achieved by placing the cylinder within another vessel or vessels and subjecting it directly to a controllable external hydrostatic pressure. A simpler method, proposed by Bridgman[42] and subsequently used by Beresnev[44] and Pugh[43] among others, consists of making the cylinder with a tapered or conical outside surface, and fitting it into another cylinder having a matching taper on the bore. This container is supported as shown in Fig. 8 and the action of the plunger pressurizes the fluid within the bore and forces the liner into the container, thus providing an external pressure on the liner.

Since an elastic-plastic analysis of such cylinders is not available it is difficult to achieve the optimum relationship between the taper, liner length, and the K ratios of the liner and container. The present work presents a method of analysis for such a tapered

pressure vessel set which, although does not optimize the parameters, does allow the designer to check on his proposed design.

The method is applicable to open or closed ended liners of elastic-plastic work hardening materials in an elastic container and assumes the Mises criterion of yielding. The pressures required to produce an equivalent bore strain of ½% and 1% are calculated for pressure vessel sets of various lengths and tapers and with several assumed coefficients of friction between the liner and container.

4.2 OUTLINE

4.2.1 Simplifications

In practice it is usually unnecessary to calculate the burst pressure of a vessel; it is normally sufficient to calculate the pressure required to produce yielding to a specified depth through the wall or to produce a specified bore strain. This means that in the present problem it is sufficient to find a method which can account for expansion of the liner where the bore is plastic but the outside is still elastic.

Also, since the container is larger than the liner and is consequently more difficult to heat treat, it is made of a different material from the liner. This introduces an extra variable, i.e. the relationship between the flow characteristics of the liner and container materials. To avoid this added complication, it is assumed that the container remains elastic. For each solution obtained the equivalent stress at the bore of the container is calculated to check on the validity of this assumption.

Considering the pressure vessel shown in Fig. 9, it is reasonable to assume that the liner will expand more between x and x' as the pressure is increased. Thus most of the vertical force in the liner will be taken between x and x'. For simplicity it is assumed that the force is taken uniformly between these two points. Further, although this distance will decrease as the pressure is applied because of the fluid compressibility, a constant value is assumed in the calculations and is denoted by the effective length of the liner, L. The liner can now be considered as a thick cylinder subjected to an internal and external pressure. The top of the liner is basically open-ended while the bottom is closed-ended, but only the latter is considered in the results since with an external pressure the closed-ended case generally allows the lower usable pressure.

4.2.2 External Pressure on Liner

The external pressure on the liner can be considered as being composed of two separate parts, one due to the taper and one to the restraining effect of the container. This latter pressure can be calculated by assuming the liner and container to be one vessel and finding the radial stress at the radius corresponding to the container bore. If the stresses at the elastic-plastic interface are known, this can easily be accomplished using Lamé's equations.

The external pressure due to the taper alone can be calculated since the total downward load due to the fluid pressure on the closed end of the liner is supported by the taper of the container bore. Thus a simple equilibrium of forces is sufficient to determine this pressure.

4.2.3 Method of Solution

The problem has been reduced to that of the elastic-plastic expansion of an open or closed ended thick tube subjected to internal and external pressures, where the external pressure is a function of the internal one. A solution to this problem, using the Prandtl-Reuss equations and the Mises yield criterion does not seem to exist. Marcal[68] has published a numerical technique for the solution of the problem of a thick cylinder without external pressure using a stiffness concept that he developed previously[69]. However, this method does not appear amenable to variations in boundary conditions as occur in this problem. Thus a more direct method was developed which traces the path of the elastic-plastic interface and alters the boundary conditions after each step.

Consider a thick tube under pressure such that yielding has occurred. Suppose the elastic-plastic interface has reached some point distant r from the centre and that at this stage the stress and strain distributions throughout the tube are known. The interface is then allowed to move out a distance Δr. The stresses and strains at the interface may be calculated using Lamé's equations and the yield criterion. Using this interface as a datum the stress and strain increments of a surface Δr inside the interface may be found using the Prandtl-Reuss equations, the equilibrium equations, the stress-strain relationship, yield criterion and strain compatibility equation. Having obtained the stresses and strains for this surface, they may then be found for another surface Δr inside this one, and so on, until the bore is reached.

Thus, the stress and strain distribution throughout the tube is known with the elastic-plastic interface at $(r + \Delta r)$. By starting with the elastic-plastic interface at the bore, it is possible to progress in the above manner until the tube becomes fully plastic. A matrix formulation of the equations is used based on the methods put forward by Alexander and Gunasekera[70].

4.3 THEORY

4.3.1 Prandtl-Reuss Equations

The Prandtl-Reuss equations may be written in matrix form as

$$\begin{bmatrix} 1/E & -\nu/E & -\nu/E & 0 & 3\sigma'_r/2\bar{\sigma} \\ -\nu/E & 1/E & -\nu/E & -1 & 3\sigma'_\theta/2\bar{\sigma} \\ -\nu/E & -\nu/E & 1/E & 0 & 3\sigma'_z/2\bar{\sigma} \end{bmatrix} \begin{bmatrix} \delta\sigma_r \\ \delta\sigma_\theta \\ \delta\sigma_z \\ \delta\varepsilon_\theta \\ \delta\bar{\varepsilon}_p \end{bmatrix} = \begin{bmatrix} \delta\varepsilon_r \\ 0 \\ \delta\varepsilon_z \end{bmatrix} \qquad (4.1)$$

where $\sigma'_{r,\theta,z}$ are the deviatoric stresses, $\bar{\sigma}$ is the equivalent stress, $\delta\bar{\varepsilon}_p$ is the equivalent plastic strain increment and the other symbols have their normal meaning.

4.3.2 Equilibrium Equation

Equilibrium of the stresses requires that

$$d\sigma_r = \left(\frac{\sigma_\theta - \sigma_r}{r}\right) dr \qquad (4.2)$$

This equation may be written in incremental form as

$$(\sigma_r)^r - (\sigma_r)^{r-\Delta r} = \left[\left(\frac{\sigma_\theta - \sigma_r}{r}\right)^r + \left(\frac{\sigma_\theta - \sigma_r}{r}\right)^{r-\Delta r}\right] \frac{\Delta r}{2} \qquad (4.3)$$

which, when expanded and simplified, can be written

$$\Delta\sigma_r(2r_n - 3\Delta r) + \Delta r\Delta\sigma_\theta = (\sigma_{\theta_n} - \sigma_{r_n})(2r_n - \Delta r)\frac{\Delta r}{r_n} \qquad (4.4)$$

where σ_n is the stress at $r = r_n$ and $\Delta\sigma$ is the change in stress associated with the change in position from $r = r_{n-1}$ to $r = r_n$. Thus it is possible to write

$$\sigma_{r_{n-1}} = \sigma_{r_n} - \Delta\sigma_r \qquad (4.5)$$

and

$$\sigma_{r_{n-1}} = \sigma_{r_p} + \delta\sigma_r \qquad (4.6)$$

where σ_{r_p} is the previous radial stress at $r = r_{n-1}$ and $\delta\sigma_r$ is the change in radial stress at $r = r_{n-1}$ associated with a movement of the elastic-plastic interface. Eliminating $\sigma_{r_{n-1}}$ between equations (4.5) and (4.6) gives an expression for $\Delta\sigma_r$, i.e.

$$\Delta\sigma_r = (\sigma_{r_n} - \sigma_{r_p}) - \delta\sigma_r \qquad (4.7)$$

and similarly

$$\Delta\sigma_\theta = (\sigma_{\theta n} - \sigma_{\theta p}) - \delta\sigma_\theta \qquad (4.8)$$

Substituting equations (4.7) and (4.8) into equation (4.4) gives an equilibrium equation

$$- (2r_n - 3\Delta r)\delta\sigma_r - \Delta r\delta\sigma_\theta$$

$$= (\sigma_{\theta_n} - \sigma_{r_n})(2r_n - \Delta r)\frac{\Delta r}{r_n} - (\sigma_{r_n} - \sigma_{r_p})(2r_n - 3\Delta r) \qquad (4.9)$$

$$- (\sigma_{\theta n} - \sigma_{\theta p})\Delta r$$

or denoting the right hand side by KK,

$$- (2r_n - 3\Delta r)\delta\sigma_r - \Delta r\delta\sigma_\theta = KK \qquad (4.10)$$

4.3.3 Stress-Strain Equation

An empirical stress-strain equation which closely fits many engineering materials can be written

$$\bar{\sigma} = \bar{\sigma}_o(1 + \beta\bar{\varepsilon}_p)^m \qquad (4.11)$$

where m and β are constants and $\bar{\sigma}_o$ is the equivalent stress at first yield. Differentiating this equation gives

$$0 = \delta\bar{\sigma} - E_p\delta\bar{\varepsilon}_p \qquad (4.12)$$

where

$$E_p = m\bar{\sigma}_o\beta(1 + \beta\bar{\varepsilon}_p)^{m-1} \qquad (4.13)$$

4.3.4 Yield Criterion

The Mises yield criterion may be written

$$2\bar{\sigma}^2 = (\sigma_r - \sigma_\theta)^2 + (\sigma_\theta - \sigma_z)^2 + (\sigma_z - \sigma_r)^2 \qquad (4.14)$$

Differentiating this equation leads to the result,

$$0 = 3\sigma_r'\delta\sigma_r + 3\sigma_\theta'\delta\sigma_\theta + 3\sigma_z'\delta\sigma_z - 2\bar{\sigma}\delta\bar{\sigma} \qquad (4.15)$$

4.3.5 Strain Compatibility

Compatibility of strains requires that

$$\delta\varepsilon_r = \frac{\partial}{\partial r}(\delta u) \qquad (4.16)$$

where u is the radial displacement. In incremental form this equation becomes

$$\delta\varepsilon_r = \frac{1}{\Delta r}\left[(\delta u)^{r+\Delta r} - (\delta u)^r\right] \qquad (4.17)$$

But

$$\delta\varepsilon_\theta = \frac{\delta u}{r} \qquad (4.18)$$

Thus equation (4.17) can be written in terms of ε_θ as

$$\delta\varepsilon_{r_{n-1}} = \frac{1}{\Delta r}\left[r_n\delta\varepsilon_{\theta_n} - r_{n-1}\delta\varepsilon_{\theta_{n-1}}\right] \qquad (4.19)$$

4.3.6 Solution Matrix

Eliminating $\delta\bar{\sigma}$ between equations (4.12) and (4.15) and $\delta\varepsilon_r$ between equations (4.1) and (4.19) and combining the results with equation (4.10) gives

$$\begin{bmatrix} 1/E & -\nu/E & -\nu/E & r_{n-1}/\Delta r & 3\sigma'_r/2\bar{\sigma} \\ -\nu/E & 1/E & -\nu/E & -1 & 3\sigma'_\theta/2\bar{\sigma} \\ -\nu/E & -\nu/E & 1/E & 0 & 3\sigma'_z/2\bar{\sigma} \\ (3\Delta r - r_n) & -\Delta r & 0 & 0 & 0 \\ 3\sigma'_r & 3\sigma'_\theta & 3\sigma'_z & 0 & -2E_p\bar{\sigma} \end{bmatrix} \begin{bmatrix} \delta\sigma_r \\ \delta\sigma_\theta \\ \delta\sigma_z \\ \delta\varepsilon_\theta \\ \delta\bar{\varepsilon}p \end{bmatrix} = \begin{bmatrix} r_n\delta\varepsilon_{\theta_n}/\Delta r \\ 0 \\ \delta\varepsilon_z \\ KK \\ 0 \end{bmatrix} \tag{4.20}$$

4.3.7 External Pressure on Liner

Considering Fig. 9 the external pressure on the liner due to the taper can be calculated as follows. For vertical equilibrium

$$P\pi r_I^2 = 2\pi r_{EI} L(N\sin\theta + \mu N\cos\theta)/\cos\theta \tag{4.21}$$

where r_{EI} is the external radius of the liner, L the effective length, θ the semi-angle of the taper, N the normal stress and μ the coefficient of friction between liner and container. Thus

$$N = Pr_I^2/2r_{EI} L(\tan\theta + \mu) \tag{4.22}$$

Resolving horizontally, the radial pressure on the outside of the liner due to the taper is therefore given by

$$P_{E1} = \frac{Pr_1^2(\cos\theta - \mu\sin\theta)}{2r_{E1}L(\tan\theta + \mu)} \tag{4.23}$$

which can be written

$$P_{E1} = \alpha_1 P \tag{4.24}$$

where α_1 is a function of the geometry of the system and the coefficient of friction.

The external pressure due to the restraining effect of the container can be found by considering the total pressure vessel set but without the taper. The pressure at the outside of the liner with the elastic-plastic interface at $r = r_{int}$ is given by the usual expression

$$P_{E2} = \frac{-\sigma r_{int} r_{int}^2(1 - r_{E2}^2/r_{E1}^2)}{(r_{int}^2 - r_{E2}^2)} \tag{4.25}$$

where r_{E2} is the outside radius of the container. Equation (4.25) may be rewritten as

$$P_{E2} = -\alpha_2 \sigma r_{int} \tag{4.26}$$

where α_2 is a function of the geometry of the system and the position of the elastic-plastic interface. Denoting the total external pressure on the liner by P_{EX},

$$P_{EX} = \alpha_1 P - \alpha_2 \sigma r_{int} \tag{4.27}$$

4.3.8 Boundary Conditions

At the elastic-plastic interface, using the Mises yield criterion

$$2\bar{\sigma}_o^2 = (\sigma_r - \sigma_\theta)^2 + (\sigma_\theta - \sigma_z)^2 + (\sigma_z - \sigma_r)^2 \qquad (4.28)$$

and from the elastic stress-strain relationships

$$\sigma_z = \nu(\sigma_\theta + \sigma_r) + E\varepsilon_z \qquad (4.29)$$

Combining equations (4.28) and (4.29) leads to the result

$$2\bar{\sigma}_o^2 = (\sigma_r - \sigma_\theta)^2 + \left[\sigma_\theta(1-\nu) - \nu\sigma_r - E\varepsilon_z\right]^2 + \left[\sigma_r(1-\nu) - \nu\sigma_\theta - E\varepsilon_z\right]^2 \qquad (4.30)$$

For the elastic part of the tube, the Lamé equations are

$$\sigma_r = A + B/r^2 \qquad (4.31)$$

and

$$\sigma_\theta = A - B/r^2 \qquad (4.32)$$

Substituting these two equations into equation (4.30) produces the following condition which must be satisfied at the interface, i.e.

$$\bar{\sigma}_o^2 = \frac{3B^2}{r_{int}^4} + (1-2\nu)^2A^2 + (E\varepsilon_z)^2 - 2(1-2\nu)AE\varepsilon_z \qquad (4.33)$$

At $r = r_{EI}$, σ_r is equal to the external pressure on the liner, P_{EX}. Thus substituting equation (4.27) into equation (4.31) yields the following

$$A = \frac{B}{1-\alpha_2}\left(\frac{\alpha_2}{r_{int}^2} - \frac{1}{r_{EI}^2}\right) - \frac{\alpha_1 P}{(1-\alpha_2)} \tag{4.34}$$

which can be written

$$A = BD - CP \tag{4.35}$$

where C and D are constants defined by equation (4.34). Substituting this into equation (4.33) yields the following quadratic in B:

$$\begin{aligned} 0 = {} & B^2\left[\frac{3}{r_{int}^4} + (1-2\nu)^2 D^2\right] \\ & + B\left[-2DCP(1-2\nu)^2 - 2(1-2\nu)E\varepsilon_z D\right] \\ & + \left[C^2P^2(1-2\nu)^2 + (\varepsilon_z E)^2 + 2(1-2\nu)CPE\varepsilon_z - \bar{\sigma}_o^2\right] \end{aligned} \tag{4.36}$$

Initially, with the interface at the liner bore, $\sigma_{r_{int}} = -P$ and $r_{int} = r_l$, which substituted into equation (4.31) gives

$$P = -A - B/r_l^2 \tag{4.37}$$

Substituting this into equation (4.34) leads to

$$A = \frac{B}{(1-\alpha_1-\alpha_2)}\left(\frac{\alpha_1 + \alpha_2}{r_l^2} - \frac{1}{r_{EI}^2}\right) \tag{4.38}$$

which may be written

$$A = BD' \tag{4.39}$$

where D' is defined by equation (4.38). Substituting equation (4.39) into (4.33) yields the following quadratic in B:

$$0 = B^2\left[\frac{3}{r_1^4} + (1-2\nu)^2 D'^2\right] + B\left[-2(1-2\nu)E\varepsilon_z D'\right] + \left[(E\varepsilon_z)^2 - \bar{\sigma}_o^2\right] \qquad (4.40)$$

4.4 NUMERICAL METHOD

The liner is initially split into a number of shells with undeformed inner radii designated by r_{on} where n is the index number of the shell. Suppose that the elastic-plastic interface is at r_{n-1} where r is the current radius of the point r_o, and that the stress and strain distributions are known throughout the tube. The elastic-plastic interface is then allowed to move out a distance Δr to r_n. Then the stresses and subsequently strains are calculated at the interface using equations (4.36), (4.35), (4.32) and (4.31). Equation (4.36) contains the quantity P, the current internal pressure, which will not be known at this stage, and so an iterative technique is required for the solution. Similarly, the axial strain, ε_z, in equation (4.36) is unknown. Thus values are assumed for P and ε_z, generally their previous values, i.e. when the interface was at r_{n-1}, and the stresses and strains calculated at the next inner surface, i.e. at r_{n-1}, using equation (4.20). In this equation, $E_p\bar{\sigma}$ is known from the previous equivalent strain at that surface, and the stresses σ_r' etc. also refer to previous values at that

surface. Thus the only unknown, apart from the stress and strain increments, is the current radius of the surface, i.e. r_{n-1}. This is assumed as its previous value and a solution obtained. From the new value obtained for ε_θ, a better value of r_{n-1} is calculated and iteration continued until the desired degree of convergence is obtained. The stresses and strains are then calculated for the next inner surface in the same way, and so on until the bore is reached. The end load on the liner can now be calculated from the axial stresses and this is checked against zero for the open-ended case or against the product of the new internal pressure and the current bore area for the closed-ended case. The axial strain is then adjusted using a simple search technique, and using this together with the new value of P, the whole procedure with the interface at r_n is repeated until suitable convergence of ε_z and P is obtained. The interface is then allowed to move out to r_{n+1} and so on until the outside of the liner is reached or the bore strain has reached some preselected value.

Initially, with the interface at the bore, equations (4.40) and (4.39) are used instead of (4.36) and (4.35); in this case it is unnecessary to guess a value for P as it does not enter into the equations.

The method is summarized in the simplified flow chart shown in Fig. 10.

4.5 TEST PROBLEM

4.5.1 Problem

To check on the validity of the method and on the existence of any program errors the problem of the thick tube without external pressure

using the Tresca yield criterion was tried. This was selected since a very simple, but relatively accurate method is available for the solution of this problem, i.e. Manning's method[67]. This method does not allow for any elastic expansion, however, and thus is only accurate after the tube has become fully plastic. Thus to make a meaningful comparison between the two methods it is necessary to calculate pressures higher than those required to make the tube fully plastic. A convenient pressure is the maximum one.

4.5.2 Additions to Program

When the tube becomes fully plastic, a new method is required to find the boundary conditions. Of equations (4.20), the equilibrium equation and the relationship between $\delta\varepsilon_r$, and $\delta\varepsilon_\theta$ cannot be used, as they would require values from a surface outside the tube. So the number of equations available is effectively reduced by 2. However, since σ_r is known at the outside (equal to the constant external pressure) then $\delta\sigma_r$ is zero at the boundary. Also, a value may be chosen for one of the other variables, say $\delta\sigma_\theta$ (this is equivalent to setting the distance that the interface moves). Thus, the number of variables is reduced by 2 also and the following set of equations may be solved to determine the conditions at the outside surface:

$$\begin{bmatrix} -1 & 0 & -\frac{\nu}{E} & \frac{3\sigma'_r}{2\bar{\sigma}} \\ 0 & -1 & -\frac{\nu}{E} & \frac{3\sigma'_\theta}{2\bar{\sigma}} \\ 0 & 0 & \frac{1}{E} & \frac{3\sigma'_z}{2\bar{\sigma}} \\ 0 & 0 & 3\sigma'_z & -2E_p\bar{\sigma} \end{bmatrix} \begin{bmatrix} \delta\varepsilon_r \\ \delta\varepsilon_\theta \\ \delta\sigma_z \\ \delta\bar{\varepsilon}_p \end{bmatrix} = \begin{bmatrix} \frac{\nu}{E}\delta\sigma_\theta \\ -\frac{1}{E}\delta\sigma_\theta \\ \frac{\nu}{E}\delta\sigma_\theta + \delta\varepsilon_z \\ -3\sigma'_\theta\delta\sigma_\theta \end{bmatrix} \qquad (4.41)$$

for Mises or as above with the bottom line replaced by:

$$\begin{bmatrix} 0 & 0 & 0 & \frac{2E_p}{\sqrt{3}} \end{bmatrix} \qquad \begin{bmatrix} \delta\sigma_\theta \end{bmatrix} \quad \text{for Tresca}$$

4.5.3 Numerical Results

Results were obtained for the two methods using a stress-strain equation of the form given in equation (4.11) with values of the constants taken as

$$\sigma_o = 616 \quad MN/m^2$$
$$\beta = 215.827$$
$$m = 0.096264$$

This stress-strain curve is for EN25T steel. Since Manning's method gives an accurate solution for an incompressible material, letting $E \to \infty$ and $\nu \to 0.5$ should produce the same result using both methods. Since the computer is unable to handle ∞, a very high value of 1.54×10^6 MN/m^2 was used for E. This gave a burst pressure of 570.2 MN/m^2 with a hoop

bore strain of 0.080 using the new method. Manning's method for the same material and K ratio (= 2) gave the burst pressure as 570.25 MN/m^2 with a hoop bore strain of 0.079. This is very good agreement; the bore strain using Manning's method should be the lower of the two since $E = \infty$ was not used in the new method and so there is still some small elastic strain present. Also, the burst pressure should be lower using the new method as it decreases with decreasing values of E. For a more realistic value of $E = 2.06 \times 10^5$ MN/m^2, the burst pressure is calculated as 567.0 MN/m^2.

Further results were obtained for this material using the Mises yield criterion and open and closed-ended conditions instead of plane strain as used to compare with Manning's method. These were quite similar and varied in a predictable manner which demonstrated that the method was working satisfactorily.

4.6 NUMERICAL RESULTS AND DISCUSSION

Numerical results were obtained for a pressure vessel set with a liner made of 300M, a vacuum arc remelted steel of basically SAE 4340 composition plus about 1½% silicon. A typical stress strain curve for this material may be represented by the equation

$$\bar{\sigma} = 1544\ (1 + 200\bar{\varepsilon}_p)^{0.09}$$

where $\bar{\sigma}$ is given in MN/m^2.

The results were obtained for a vessel having a 44 mm diameter bore, an external liner diameter of 13.4 cm and an overall diameter

of 43.1 cm. These dimensions were chosen as being typical of the type of equipment in use and correspond to the equipment described in section 5. For this size of container it is practical to use a container material having a yield strength of 850 - 930 MN/m^2 while still retaining a reasonable ductility. This means that the container bore pressure is limited to about 462 MN/m^2 if yielding of the container is to be prevented. Thus in Figs. 11 - 13, which show the effect of various assumed coefficients of friction, liner lengths and tapers, results are presented to show the internal pressure required to produce a container bore pressure of 462 MN/m^2 as well as that to produce an equivalent bore strain of ½% and 1%.

Fig. 11 shows the variation of these internal pressures with the coefficient of friction for a taper of 2° included angle and an effective liner length of 17.8 cm. For coefficients of friction greater than about 0.2, the internal pressure required to produce a container bore pressure of 462 MN/m^2 increases quite slowly with the friction, while the pressure required to produce a given equivalent bore strain decreases slowly. In this region, a container bore pressure of 462 MN/m^2 is always associated with an equivalent bore strain of greater than 1%, and so it is the bore strain which limits the usable internal pressure. For coefficients of friction between 0.1 and 0.2 the same trend of pressure versus friction is observed, but the rate of change is greater. At the lower end of this range, the critical container bore pressure is produced at an equivalent bore strain of less than ½%. For lower values of the coefficient of friction, the pressures to produce a given bore strain increase very

rapidly for decreasing friction, but the pressure to produce the critical container bore pressure decreases rapidly. Thus in this region it is the container strength which imposes limitations on the design rather than the bore strain.

Fig. 12 shows the variation of the internal pressures with effective liner length for the same taper as in Fig. 11 and a coefficient of friction of 0.2. The variation of pressure against length is of the same type as that against friction. This is to be expected since, considering equation (4.23), for small tapers and a fixed radial geometry, the restraint imposed on the liner due to the taper is inversely proportional to the product of the coefficient of friction and the effective length of the liner. For the conditions shown, it is the bore strain which limits the usable pressure for any effective liner length greater than about 15 cm.

Fig. 13 shows that the internal pressures are not very sensitive to changes in the angle of the taper. The pressure for the limiting container bore pressure increases by only about 3% as the included taper angle increases from 2^{o} to 8^{o}, and the pressures for limiting bore strains decrease by even less over the same range. The limiting value of taper will be determined more by manufacturing limitations on the diameter tolerances rather than theoretical design considerations. For example, for an included angle taper of 2^{o} the relative vertical displacement between the liner and container is about ± 2.9 mm for diameter tolerances of ± 0.025 mm on each, and double that for a 1^{o} taper.

A further point of interest which became apparent from the numerical results is that at some value of internal pressure, the pressure on the outside of the liner begins to increase faster than the inside pressure. Once this pressure has been reached, the radial bore strain can no longer increase and the equivalent bore strain decreases, though the present calculations are not valid in this region. Fig. 14 shows the variations in this maximum equivalent bore strain value with coefficient of friction; the associated values of internal pressure are also shown. Both the strain and pressure increase very rapidly with friction for coefficients of friction less than 0.2 and then tend toward a more gradual, almost linear, increase. This observation is academic, however, since even for a coefficient of friction of 0.5, the container bore pressure is 695 MN/m^2 at the limiting strain; this would require a container material almost as strong as the liner. For smaller coefficients of friction the container material would have to be even stronger.

It is apparent from these results that it is the product of the coefficient of friction and the effective length of the liner that has the greatest effect on the usable pressure in any tapered pressure vessel set design once the diameter ratios and materials have been chosen. Typical values for the coefficient of friction between two metal surfaces are often given, e.g. Beer and Johnston[71], as 0.15 to 0.6, but these may be altered quite significantly by placing lead foil between the liner and container, or interspersing graphite or molybdenum disulphide powder between the two. Ideally, before finalizing a design, one should determine the coefficients of friction between pieces of

liner and container material using the various possible lubricants; the pieces should have the same hardness and surface finish as in the proposed design and the range of normal pressures studied should be comparable to those expected in use.

The effective length of the liner is also a difficult quantity to ascertain. It will change as the pressure is applied due to the plunger motion and may also change while the pressure remains constant, as in the extrusion process where the plunger is continually moving downward. Thus it is necessary to take a range of lengths that might be used. A reasonable estimate for any one effective length might be the length of the pressure chamber at that point, or perhaps 10% more.

The other factor to be decided upon before making any design decision is the criteria to be used in assessing the design. Those used in the present paper are the pressure required to cause yielding of the container and the pressures to produce a given equivalent bore strain. The first is dictated by the method of analysis, though it would be possible to extend the analysis to allow for plastic expansion of the container. The second is more arbitrary, though an equivalent bore strain of greater than 1% will generally correspond to a bore expansion larger than that acceptable for leak-free operation of the system. The permissible bore strain will be dependent on the type of sealing devices employed and the ductility of the liner material.

No attempt has been made to demonstrate the effect of different diameter ratios since it is generally accepted that a ratio of about 3 is "optimum"; less than that causes a significant drop in the pressure

capability while anything greater produces only small improvements for large increases in material size, cost and required handling capacity.

The results suggest that for the pressure vessel set used, which is described in section 5.2, a pressure of about 1600 MN/m^2 can be achieved without causing the container to yield nor make the equivalent liner bore strain exceed 0.5%.

5 COMPACTION AND EXTRUSION APPARATUS

5.1 GENERAL ARRANGEMENT

The equipment built for isostatic compaction and hydrostatic extrusion is shown in cross section in its initial state in Fig. 15. It was based on a piece of working equipment at Imperial College, but due to the special problems encountered with the available press, the original design has been considerably modified. The pressure vessels and plunger closely follow the original equipment, but substitutions were made for the materials and treatments.

Load was applied from the top platen of the press (1) through a bolster (3), retaining plate (5) and plunger (8) to the fluid within the bore of the liner (9). The fluid passage was blocked at the lower end of the bore either by a compaction pad for the compaction experiments or by the extrusion die and billet in the extrusion process; these rested on the hard pad (13). Sealing at the plunger and die or compaction pad was effected by neoprene O-ring seals (11) and beryllium copper mitre rings.

The plunger was held in its locating hole in the retaining plate by means of one large nut (7) which allowed easy removal and replacement of the plunger without the necessity of realignment. A steel tube (6) was placed around the plunger when pressurizing as a safety precaution in case the plunger or seals failed. Electrical leads from the manganin coil terminals (10) were taken out through a centre hole in the plunger and a passage within the retaining plate.

The tapered liner fitted within the tapered bore of the container (12) which was supported on a large tubular stool (14), 75 cm high. This allowed extrusions nearly one metre long to be obtained if necessary. A series of openings were machined in this stool to permit observation of the extruding material. The stool was attached to a base plate (15) which in turn was fixed to the base of the press.

The press used for these experiments was a 2.669 MN Baldwin universal testing machine, which stood ten metres high and three metres across. Vertical positioning was by two screws and the load was applied hydraulically via two pillars more than two metres apart. It was expected that the crosshead of such a press would not necessarily come down in the same place each time and therefore the plunger could not be attached directly to the platen as in the design at Imperial College. It was thought, however, that the hydraulic motion of the press would be straight over the short distance required for pressurization. Consequently the die set (4) shown in the figure was designed to locate the plunger with respect to the bore of the pressure vessel. Attachment to the platen was fairly loose to allow motion of the die set plate with respect to the crosshead when lifting the plate on or off the pins; this was necessary to permit sufficient access to the bore for insertion and removal of the extrusion dies and billets.

5.2 PRESSURE VESSEL SET

The pressure vessel set consisted of a tapered liner which fitted into a matching tapered bore of a large container, the taper being about 2^{o} included angle.

The liner was made of Atlas Alloy's 300M, a vacuum arc remelted steel of high strength and reasonable ductility. Its composition is basically that of an SAE 4340 steel with an additional 1½% silicon content. A vacuum arc remelted steel was used because it gives a better guarantee of transverse ductility. The material was machined and heat treated to the following schedule:

1) Rough machine to within 6 mm of finished size.
2) Stress relieve at 620°C.
3) Finish machine to leave grinding allowance.
4) Austenitize at 870 ± 14°C in salt bath or controlled atmosphere furnace. (Protect threaded holes if necessary.)
5) Quench in oil at 60°C maximum.
6) Double temper at 300 ± 8°C for 2 hours minimum each temper. Air cool between tempers.

This heat treatment schedule was designed to give the following properties in the liner:

Hardness	54-56	Rockwell C
UTS	1930 MN/m^2	min.
0.2% yield stress	1540 MN/m^2	min.
Transverse elongation	6%	min.

The container was made from Atlas Steel's AHT 28, a material of lower strength but higher ductility, especially in large sections. It was machined and heat treated to the following schedule:

1) Rough machine to within 6 mm of finished size.
2) Stress relieve at 620°C.

3) Finish machine to leave grinding allowance.

4) Austenitize at 815 ± 14°C.

5) Air cool.

6) Temper at 540°C x 6 hours minimum.

7) Check hardness and retemper if necessary to adjust hardness.

This heat treatment schedule was designed to give the following properties in the container:

Hardness	32-34	Rockwell C
UTS	1080 MN/m^2	min.
0.2% yield stress	850 MN/m^2	min.
Elongation	12%	min.

The outside of the liner and inside of the container were both coated with a graphite powder lubricant before assembly to reduce the friction between the two.

5.3 EXTRUSION DIES

The extrusion dies shown in Fig. 16, compaction pad and hard pad (part (13) in Fig. 15) were made from a Kayser, Ellison and Co. Steel, KE970*, which corresponds to an SAE cast tool steel CD-3. This is an air hardening steel which deforms very little on heat treating; this was important in the manufacture of the extrusion dies since all the intricate machining could be completed on the annealed material before vacuum hardening to a minimum Rockwell C hardness of 62.

---

* see section 5.7.2

The dies were made with an included angle of 40° to correspond with the work of Alexander[1,2] and were threaded on the outside to enable insertion and extraction by means of an internally threaded tool. The compaction pad was also made with this extraction thread.

A hard pad was machined to fit the radiused end of the liner bore. In this way it was possible to simplify the design of the extrusion dies and compaction pad by allowing them to be made with a square bottom edge instead of a radius; the bore could not be made with a square corner because of the undesirable stress concentration.

5.4 PLUNGER

The plunger was made of the same steel as the dies, KE 970*, but was tempered at 480°C instead of 150°C used for the dies. This reduced the hardness slightly from 62 to 58-60 Rockwell C, but improved the toughness.

Conical holes were machined in the end of the plunger into which conical ceramic insulators were lapped. Conical hardened terminals of KE 970 were in turn lapped into these insulators to carry the electrical connections from the manganin pressure gauge. The ends of these terminals were given a square cross section to assist in their removal if necessary.

The radial clearance between the plunger and bore was kept very small (about 0.025 mm) for the satisfactory operation of the seals and therefore, since the radial expansion of the plunger was quite large when

---

* see section 5.7.2

the designed load of nearly 2.7 MN was applied, the plunger was radially relieved about 0.075 mm from 25 mm above the seals. Although the plunger still expands slightly in this bottom 25 mm, the bore also expands here due to the effect of the internal pressure; the expansion at the top of the bore is negligible, however.

In an effort to prevent the plunger scoring the bore in the event of any misalignment, a small copper collar, slightly bigger than the plunger was attached to the nose below the seals. Several openings were machined on it so that the fluid pressure was easily transmitted past it and so was able to provide it with support.

To assist in checking the alignment of the plunger and bore when in the press, a dummy plunger of smaller diameter was machined from aluminum, and a differential transformer was attached to its end by means of a special clamp. By moving this plunger up and down and monitoring the output from the transformer, any discrepancy in the plunger alignment could be detected very easily.

5.5 PRESSURE MEASURING SYSTEM

Several manganin resistance gauges of about 100 ohms were wound to measure the fluid pressure during the compaction and extrusion experiments. They consisted of about 60 cm of 0.06 mm diameter manganin wire non-inductively wound onto a threaded 6 mm diameter lucite core. After winding they were dipped in coil varnish for protection and were seasoned using the following schedule:

1. Place coils in test tube and bake at about 140^{o}C for about 8 hours.

2. Remove from furnace and cork test tube (to minimize condensation on the coils in the next step).
3. Place in solid carbon dioxide (-80°C) for a few hours.
4. Replace in furnace and repeat over several days.

5.6 COMPACTION BAGS

A rubber bag for holding the powders during compaction is shown in Fig. 17. Several of these bags were moulded from Flexane 95, a cold curing urethane liquid rubber compound. The advantage of using a rubber bag is that it returns to its original shape when the pressure is released and can be used many times. Flexane 95 was used since it was very hard and the powders did not penetrate its surface under pressure.

5.7 EQUIPMENT MODIFICATIONS

5.7.1 Attachment to Press

Contrary to expectations, it was found that the motion of the press was not at all straight and wandered randomly through almost one millimetre. Since it was unreasonable to expect the die set to be able to contain this motion it became necessary to provide a fitting between the crosshead and top die set plate which would allow lateral motion of the crosshead under load without transmitting any appreciable transverse loading to the die set plate.

The fitting that was designed for this purpose is shown in Fig. 18. It consisted of two 25 mm thick hardened steel plates separated by about 500 steel balls of 12.7 mm diameter. Another set of about one hundred balls were incorporated at the attachment to the hemispherical

seat to allow free lateral motion when the system was not under load, i.e. when withdrawing the plunger, or lowering it under its own weight. The hemispherical seat was used to ensure that the die set plate was allowed to remain perpendicular to the bore of the pressure vessel.

The use of the hemispherical seat made it necessary to employ longer bushings on the die set as with the short bushings originally specified the die set plate tended to tip if allowed to fall freely. As a further precaution against any tipping or binding, the pins were increased in diameter from 38.1 to 50.8 mm and the bushings made with a tubular steel backing. The complete assembly finally used is shown in Fig. 19.

5.7.2 Plunger Failures

On the forty-ninth application of load, after two previous load applications of 2.23 MN, it became difficult to fit the plunger to the retaining plate. There was no apparent cause other than that the diameter of the plunger head had increased marginally.

A load of 2.23 MN was applied in the normal way, and when the plunger was removed from the retaining plate, two radial cracks originating from the centre hole were observed in the top face. One had progressed to the edge and extended the whole depth of the cross section, while the other had extended through about 80% of the wall. Stress analysis showed that the nominal applied stresses could not have caused failure.

The most obvious explanation of the cause of failure was that stress raisers present in the bore layers caused compressive yielding

under load and subsequent tensile fracture occurred due to residual tensile stresses that were set up when the load was removed. The cause of the stress raisers was thought to be either a flaw in the material or the surface condition of the centre hole. Thus on the next plunger the centre hole was polished after heat treating, and a larger and more carefully finished radius made where the hole emerges at the plunger head.

This plunger was carefully examined after every load application and after a third time of loading to 2.0 MN, a small crack was noticed as before. It was then found that instead of a D-2 steel as requested, a D-3 steel, with inferior fracture toughness properties to D-2, had been sent in error by the supplier.

A D-2 steel was obtained (KEA 180) and two more plungers machined. The first was made without the centre hole for the leads, both to save time and avoid further problems.

No further difficulties were encountered with the plunger.

6 EXPERIMENTAL PROCEDURE

6.1 PRESSURE CALIBRATION

It was originally intended to use the manganin wire coils to measure the hydrostatic pressure produced in the chamber. The change in resistance of manganin wire with pressure is very nearly linear, and, for use in the pressure range 0 - 1600 MN/m^2, assuming linearity introduces errors of no more than 1%[72]. The assumption of linearity simplifies the calibration procedure considerably since only one calibration point is then required.

The calibration is usually made at some fixed point, and a convenient one for the pressure range used in these experiments is the freezing pressure of mercury at room temperature which is about 1154 MN/m^2. This is usually detected by its change in volume, and the procedure is outlined in detail in reference 72.

Unfortunately this procedure requires the pressure to be maintained within quite close limits for relatively long times, and this was found to be extremely difficult with the available press. Because of this and the untimely failures of the plungers, a secondary pressure measuring system, namely the press load indicator, was used.

The calibration of this load indicator was checked before use with a proving ring and found to be accurate to better than ½%. Thus the load on the plunger could be measured to the same accuracy, but this could not necessarily be directly transformed to a pressure

because of the unknown effects of the friction of the plunger seals and any friction in the die set. Alexander and Quainton[2], using a very similar plunger with similar seals and clearances, observed a difference of 3% between the plunger load pressure and that measured with a manganin coil, with a pressure medium of castor oil and 10% methylated spirits. Lowe and Goold[49] observed that the difference between the pressure calculated from the plunger load and that measured with a manganin coil was dependent upon the pressure medium used. For castor oil they observed a difference of about 3%.

Since, in the present system, the bushings in the die set could have been subject to some sideways loading if there was any assembly misalignment, a small allowance was made for friction in these bushings. The friction must have been quite small, however, since no binding was observed in these bushings and no wear was apparent after many pressurizations. An estimate of 1% of the load should be conservative.

Thus all the experimental pressures quoted in this thesis were calculated by subtracting 4% from the applied load multiplied by the bore area. They should be accurate to better than ±2%.

6.2 ISOSTATIC COMPACTION

6.2.1 Description of Powders

Three types of powder were used in the investigation, (i) an atomized iron powder, Atomet 28, (ii) an atomized aluminum powder, Alcoa grade 1202 and (iii) an argon atomized nickel base superalloy, INCO 713 LC. These powders had very different hardness values, yield strengths and particle geometries as shown in Figs. 20 and 21.

6.2.2 Packing Procedure

For the iron compacts, a rubber compaction bag was filled with 425 g of powder and gently vibrated for 2 minutes to promote better packing within the bag but without causing too much segregation of large and small particles. The bag was sealed with a cylindrical rubber bung with a thin Flexane washer interposed between the bung and the powder. This prevented the powder penetrating into the soft rubber of the bung. A thin coating of an adhesive rubber solution was applied to the periphery of the bung to prevent any initial fluid leakage into the bag.

Smaller samples of the superalloy were used since these did not compact. A tube of Flexane made from one of the compaction bags with the nose removed was filled with 200 g of the powder and sealed with a rubber bung and Flexane washer at either end.

Since the aluminum powder was much softer than the other two powders, it was unnecessary to use the moulded Flexane bags, and a length of ordinary latex tubing sealed at each end with a standard rubber bung was adequate. 50 g of powder were placed in the tube and gently vibrated for 2 minutes as for the iron, and sealed with the rubber bung. These filled tubes, unlike the Flexane bags, were not very rigid, and a perforated metal tube was used to support them in the pressurizing medium.

6.2.3 Pressurizing Procedure

With the compaction pad in the bottom of the pressure chamber, a small quantity of castor oil was added. This pressure medium has been shown[49] to remain sufficiently fluid to transmit pressures to at

least 1700 MN/m^2. A filled compaction bag, with a string attached to the top to facilitate removal, was inserted into the chamber and gently pushed to the bottom. More castor oil was added to within 45 mm of the top of the chamber and the plunger, which was not yet attached to its retaining plate, placed inthe bore; for the compaction experiments the plunger was removed between each compaction to permit insertion and removal of the bag without lifting the die set plate off the pins, a time consuming operation. The die set plate was lowered to meet the plunger and the latter fixed in place by means of its retaining nut. The plunger was then withdrawn by raising the crosshead of the press and the tightness of its attachment checked. The crosshead was gently lowered so that the plunger entered the bore of the pressure vessel under the weight of the retaining plate and attachment. As a check that there was no binding of the plunger at this stage, a close watch was kept on the clearance between the hemispherical head and the top hardened plate, and the lateral motion of the plunger was monitored with a dial gauge.

When the plunger reached the fluid level, the die set bushings were pumped full of grease to minimize binding on the pins under pressure, and the load slowly applied. Full pressure was maintained for two minutes and the load removed slowly. The plunger and most of the castor oil were removed and the compact extracted. If most of the castor oil was not removed first it was found very difficult to extract the compact.

A total of 44 iron compacts were produced at pressures between 35 and 1400 MN/m^2; some were used for pressure-density determinations

and mechanical testing and the rest for extrusion.

Only 5 superalloy compacts were attempted at pressures between 700 and 1400 MN/m^2, but no coherent compacts were produced.

Fifteen aluminum compacts were produced; a series compacted at pressures from 70 to 700 MN/m^2 were employed for pressure-density determinations, and the rest compacted at 551 MN/m^2 were used for extrusion.

6.3 MECHANICAL TESTING OF COMPACTS

6.3.1 Iron

One iron compact produced at each of the pressures employed was used for determining the compact properties. The nose section was cut off and two 3 mm thick slices cut from the larger end; the first was used for a metallographic examination and hardness test and the second for x-ray diffraction analysis. The rough cylinder was turned down to a constant diameter and both ends were faced off. It was then weighed and measured to give an initial indication of its density.

Since most of the green iron compacts were too brittle to have tensile test specimens machined from them, a three point bend test was used to determine an approximate value of their strengths. Test specimens were cut from the cylindrical density specimen and the surfaces ground to a size of 6.350 x .953 x .478 cm. They were accurately weighed and measured to determine their individual densities; the average of these densities for the two specimens was used in subsequent analyses since this was determined to a greater accuracy than that for the cylinder.

The bend tests were performed on a table model Instron testing machine (model TM) using a crosshead speed of 0.508 cm/min and a span of 3.810 cm. The maximum stress was calculated from the formula

$$\sigma_{max} = \frac{3P_mL}{2bd^2}$$

where P_m is the maximum load, L the span, b the width of the specimen and d its depth.

6.3.2 Aluminum

The extruded aluminum was produced from material compacted at a fixed pressure of 551 MN/m^2. Thus, since the mechanical test data for the aluminum compacts was needed only for comparison with the properties of the extruded material, it was only necessary to test compacts produced at this one pressure. Two tensile test specimens were prepared from several compacts and tested as described in section 7.6.3 for the extrusions.

Density measurements were performed on specimens compacted at the other pressures.

6.4 X-RAY ANALYSIS OF IRON COMPACTS

To obtain experimental information on the amount of strain hardening that occurred in the powder during compaction, a method was required to measure the flow stress of the compacted powder. This could not be achieved by direct mechanical testing of the compacts since their flow and fracture properties were not representative of the solid

material forming the powder particles, but were dependent on the inter-particle bond strength and void content of the compacts. However, it is known that plastic deformation causes broadening of high angle x-ray diffraction line profiles by an amount that depends upon the degree of deformation. Hence this provided a method of measuring the average plastic strains in loose compacted metal powders without interference from interparticle bonding or porosity effects.

Slices approximately 3 mm thick, cut from the nose section of the iron compacts used for mechanical testing, were mechanically polished to provide a flat surface and then electropolished in 85% orthophosphoric acid for 10 minutes at 2.4 volts to remove any surface strains. A slice from a sintered and annealed specimen was similarly prepared in order that the line profiles of the stress-free material could be obtained. A sample of the uncompacted powder was also prepared for comparison.

These samples were examined using a Phillips x-ray diffractometer and the x-ray line widths were measured at half the peak height on graphically resolved Co $K\alpha_1$ peaks from the composite $K\alpha_1 K\alpha_2$ profiles of the (220) reflection occurring at a Bragg angle of $\theta = 61.8^{o}$. The resulting variation of line width with pressure is shown in Fig. 22.

In order to quantitatively relate the line broadening to flow stress, some calibration samples were prepared. A sample of iron compacted at 1100 MN/m^2 was sintered for one hour at 1150°C under a vacuum of 2×10^{-5}torr to produce a material which could be tested in the conventional manner. Tensile test specimens were machined from

it and annealed for half an hour at 650°C under argon. They were mechanically polished to remove any oxidation and electropolished as above to remove surface strains before being strained various amounts from 5 to 20% elongation on an Instron universal testing machine (model TT-D) at a crosshead speed of 0.05 cm/min. These were then examined in a similar manner to the compacted material. The resulting calibration curve of line width versus strain is shown in Fig. 23. Combining this with the previous figure gave a relationship between the strain in the compact and compacting pressure.

A stress-strain curve up to 20% elongation was also obtained from one of the test specimens. This is shown in Fig. 24 together with the fitted curve used for subsequent comparison of the theoretical and experimental pressure-density results. The fitted curve is composed of two straight lines and a quadratic and is defined by the equations:

$$\bar{\sigma} = 207 \qquad 0 < \bar{\varepsilon}_p < 0.02$$

$$\bar{\sigma} = 178 + 2{,}455\ \bar{\varepsilon}_p - 6{,}460\ \bar{\varepsilon}_p^2 \qquad 0.02 < \bar{\varepsilon}_p < 0.18$$

$$\bar{\sigma} = 396\ [1 + (\bar{\varepsilon}_p - 0.18)] \qquad 0.18 < \bar{\varepsilon}_p < \infty$$

where $\bar{\sigma}$ is again given in MN/m^2.

6.5 HYDROSTATIC EXTRUSION

6.5.1 Iron

The iron compacts were machined to the billet shape shown in Fig. 25 with the diameter D chosen to give a reduction ratio between

1.36 and 3.36 when extruded through a 9.53 mm diameter die. For a series compacted at any one pressure, the highest ratio was chosen such that the extrusion pressure was about equal to the compaction pressure.

A large cone was left on the end of the billet to prevent complete extrusion and a consequent sudden loss of pressure. The nose of the billet was made with a 38^{o} included angle (2^{o} less than the die), the transition to the main diameter was well rounded and the billets were sandblasted before coating with lubricant. These are standard procedures used to reduce the initial breakthrough pressure and the tendency toward stick-slip behaviour.

The lubricant used was Acheson - 'dag' 144, a warm forming chemically active graphite based lubricant, which corresponds to the Acheson 'dag' 1870 suggested by Alexander and Quainton[2]. This lubricant reacts chemically with ferrous metals and produces a thin, adherent dry film on the billet.

The general procedure for hydrostatic extrusion was first to remove the die set plate from the pins to permit access to the bore. The die and seals were inserted and then the billet and guide lowered into the die. The nose of the billet was coated with MoS_2 grease to create an initial seal. The guide was necessary to stop the billet tipping initially. It consisted of a 25 mm thick teflon disc which was a loose sliding fit in the bore. A series of 6 mm diameter holes were drilled near the periphery to allow the pressurizing fluid to pass through. A seat was machined in one face for the rear of the billet to fit into and a central threaded hole was provided to facilitate removal. This also allowed easy insertion of the billet which was fitted into the

seat in the guide with a little grease and then the guide and billet lowered into the bore on the end of a threaded bar.

When the billet was in place, 200 cc of castor oil were added, and the die plate lowered onto the pins. The plunger was fitted and the system pressurized as in section 6.2.3, except that the hydraulic system of the press was bled each time before extrusion. The mean pressurizing rate for extrusion was about 250 MN/m^2 per minute.

On completion of the extrusion, the pressure was released and the plunger withdrawn from the bore and removed from the retaining plate. The die set plate was lifted off the pins and the guide ring and castor oil removed from the chamber. The die, extrusion and remaining part of the billet were then withdrawn together using the special die removal tool.

6.5.2 Aluminum

The aluminum compacts were smaller in diameter than the iron because the tubing used instead of the Flexane bags was smaller. As a consequence, there was generally insufficient material to allow a large cone to be left on the rear of the billet. Thus the compacts were machined to the billet shape shown in Fig. 25. One separate mild steel cone was machined to fit on the end of these billets to prevent loss of fluid after extrusion. The diameter D was chosen to give reduction ratios of from 2.25 to 7.60 when extruded through a 6.53 mm die. The billets were sandblasted before use and MoS_2 grease was used as a lubricant. The extrusion procedure thereafter was the same as for the iron above.

6.6 MECHANICAL TESTING OF EXTRUDED MATERIAL

6.6.1 Iron

No mechanical tests were performed on the iron extrusions since no sound products were obtained. Longitudinal and cross sections were mounted, however, to study the macroscopic crack pattern.

6.6.2 Aluminum

Two tensile test specimens were machined from each aluminum extrusion, together with specimens from the as-compacted material and some extruded wrought IS aluminum (99.5% Al) for comparison. Since the extrusions were not perfectly straight, fairly short specimens (44.5 mm long) were used which were turned down to 6.1 mm diameter to ensure the specimen was perfectly straight, and the centre section, 19 mm long, was reduced to 5.08 mm diameter. A gauge length of 15.7 mm was marked on this section.

The specimens were tested in an Instron universal testing machine (model TT-D) using a cross head speed of 1 mm/min.

6.7 METALLOGRAPHY AND FRACTOGRAPHY

Sections from the iron compacts were mounted and polished for metallographic examination and hardness measurements. The following polishing procedure was used.

Initial grinding was carried out on 240 grit wet silicon carbide papers followed by successively finer grinding on 320, 400 and 600 grit wet silicon carbide papers, the specimens being ultrasonically cleaned between grits. Final polishing was carried out on diamond wheels

using 9μ, 3μ and 1μ diamond paste successively, again cleaning ultrasonically between pastes. Etching was performed by swabbing with a 2% Nital solution.

Sections from the aluminum compacts and extrusions were also mounted and polished for metallographic examination and hardness measurements. The aluminum is difficult to polish mechanically, however, since it is very soft and so an electropolishing technique was used. After grinding on SiC papers as for the iron, the edges and other parts of the specimen were covered with lacquer to leave an area of about 1.5 cm^2. This area was then completely immersed in Lenoir's solution (328 mL orthophosphoric acid (85%), 67 mL sulphuric acid, 78 g chromic oxide and 100 mL distilled water) and a slow controlled electropolishing carried out at a potential of 10-12 V and a current of 0.1 amp for 9 minutes, the bath temperature being maintained at 75°C. The specimen was then removed from the bath and carefully washed in distilled water. The specimens were already etched by this polishing technique and no further etching was required.

Although no coherent compacts were produced from the superalloy powders, some of the loose compacted powder at each compaction pressure used was mounted and polished to observe the deformed shape of the powders and permit microhardness measurements to be made. The polishing procedure was as outlined for the iron.

To obtain further insight concerning the bonding in the extruded aluminum, one fracture surface from the tensile test specimen of each extrusion ratio was examined in a scanning electron microscope. Carbon replicas were also made of two fracture surfaces and examined in a transmission electron microscope.

7 RESULTS AND DISCUSSION

7.1 COMPARISON OF EXPERIMENTAL AND THEORETICAL PRESSURE-DENSITY DATA

7.1.1 Iron

The experimental pressure-density data expressed directly are shown in Fig. 26.

Before a suitable numerical prediction can be made it is necessary to have some estimate of the initial density of the material. This will not be the tap density of the powder, for the material is not 'solid' at that stage. It is the density at which the powder has been sufficiently consolidated for the model to become valid. As a first estimate, this might be taken as the density at the beginning of stage 2 compaction which Heckel[14] associated with the minimum density in a compact that enables it to be handled. The experimental results show that this would make $D_o = 0.65$ approximately.

An alternative estimate can be derived from the model. Fig. 3 shows that the degree of strain hardening has little effect on the pressure for minimum strain which, however, depends considerably on the initial density as shown in Fig. 4. Assuming the model to be valid above a certain density, the pressure corresponding to the beginning of plastic flow (i.e. the yield pressures of the spheres) should correspond to the pressure required to produce that density experimentally. Hence plotting this variation of pressure for minimum strain against D_o on the same graph as the experimental pressure-density relationship gives

a point of intersection of the two which corresponds to the initial density at which the model becomes valid. This value of D_o was found to be 0.8.

Using this value together with $D_o = 0.85$ and $D_o = 0.90$ and the fitted stress strain curve shown in Fig. 24, the $\ell n(1/1-D)$-pressure relationship for Atomet 28 iron powder was predicted numerically. The results are shown in Fig. 27 along with the experimentally determined relationship. The predictions do not, of course, hold for pressures below the 'yield' pressure discussed previously, and it seems that it is not until after a further small increase in pressure that the predictions tend toward the experimental results. This may be because of inaccuracies in the numerical results at low plastic strains; the transition between elastic and plastic behaviour might be more distinct than shown. This disagreement at low pressures would also explain why $D_o = 0.85$ gives better agreement with the experimental results than $D_o = 0.80$; to obtain this latter value, the numerical and experimental results have been matched at the low-pressure end.

The numerical results show an almost linear variation of $\ell n(1/1-D)$ over the whole range of pressures studied, whereas the experimental results show a marked non-linearity at higher pressures, as observed by many other investigators. It is clear, however, that there is good agreement over the linear portion of the experimental results (300 to 1000 MN/m^2).

Fig. 28 shows the changes of both computed and experimental strains with pressure, corresponding to the $\ell n(1/1-D)$-P graphs of Fig. 27.

The experimental strains are much higher at the low-pressure end but this is to be expected, since the model is still elastic at this stage. At greater pressures the computed strains are higher for any initial density below about 0.89, whereas one would expect them to be lower because of the initial plastic deformation undergone by the powder before the model becomes valid. Some of this discrepancy may be due to error in the x-ray line width measurements and calibration. However, it appears that an initial density between 0.85 and 0.90 provides reasonable agreement between theoretical and experimental data.

7.1.2 Aluminum

Since the sintering conditions for the aluminum are more critical than for the iron, a stress-strain curve for the aluminum powder was not obtained directly. Instead, the data obtained by Pugh[73] for 99.5% pure aluminum using an incremental compression test was employed. This, together with the fitted curve used for the analysis is shown in Fig. 29. The fitted curve is described by the equations:

$$\bar{\sigma} = 34.5 \qquad 0 < \bar{\varepsilon}_p < 0.012$$

$$\bar{\sigma} = 44.1 + \left[1.96 \times 10^3 - 7.44\ (.272 - \bar{\varepsilon}_p) \times 10^3\right]^{\frac{1}{2}} \qquad 0.012 < \bar{\varepsilon}_p < 1.2$$

$$\bar{\sigma} = 138\ (1 + 0.0962\ (\bar{\varepsilon}_p - 1.2)) \qquad 1.2 < \bar{\varepsilon}_p < \infty$$

where $\bar{\sigma}$ is again given in MN/m^2.

Fig. 30 shows the variation of the theoretical and experimental values of $\ell n(1/1-D)$ with pressure for the aluminum powder using an initial density of 0.80. There is agreement only over a limited range of pressures, from 76 to 276 MN/m^2. The linear portion of the experimental results only extends over this range and so again there is good agreement over the linear part of the curve.

The pressure-density data expressed directly in Fig. 31 show that this upper limit corresponds to a relative density of .975. Thus the model gives good agreement over the density range of 0.80 to 0.975.

7.2 OBSERVATIONS ON THE COMPACTION MODEL

The close agreement between the experimental and predicted values of $\ell n(1/1-D)$ against pressure in the second stage of compaction suggests that the proposed model provides an adequate description of the compaction behaviour of atomized iron or aluminum powder in this region. If the model is also valid for other materials, then several observations can be made.

One of the most important is that the slope of the $\ell n(1/1-D)$-pressure curve can now be accurately predicted by allowing for strain hardening in the theory. Previously, since the slope predicted by Torre was widely in error, investigators have resorted to empirical means of determining it, and there has been little justification for regarding it as a material constant. It now appears that the densification behaviour in the second stage of compaction is directly related to the mechanical properties of the material.

The strain hardening characteristics of the material are as important as its initial yield stress in determining the slope since very small amounts of strain hardening have an appreciable effect as shown in Fig. 2. Further, materials which exhibit a high degree of strain hardening show a greater linearity of $\ell n(1/1-D)$ against pressure than others.

Contrary to the suggestions of many investigators, strain hardening is not responsible for the curvature observed in the third stage of compaction.

It is interesting to consider the results of some other investigators in the light of this theory. Without the appropriate stress-strain data for each powder it is not possible to make quantitative comparisons, but a qualitative one is still worthwhile. Greenspan[24], for example, found that by pressing beryllium powder, annealing it and repressing to the same pressure, he obtained a higher density. This can be explained with the aid of Fig. 5; suppose the model initially became valid at $D_o = 0.6$ and that at the pressure considered it has increased to a density of 0.8; then, on repressing the stress-relieved compact, it would follow the upper curve of Fig. 5 instead of the lower and, consequently, a higher density would be achieved.

Bockstiegel[27] compacted a pure electrolytic iron powder and a carburized iron powder to investigate the effect of the powder ductility. He observed that the less ductile carburized powder (which might be expected to strain harden more rapidly) showed a slower and more linear increase of $\ell n(1/1-D)$ with pressure. This is the result predicted by the model.

Bockstiegel also investigated the effects of precompacting the pure electrolytic iron powder at 28, 296, 496 and 794 MN/m^2. He observed that precompacting at 28 MN/m^2 had no effect on the compaction behaviour. This follows from the theory for at this pressure the model has not yet become valid so that no effect would be expected. Compacting the other precompacted powders after a short annealing treatment produced a horizontal portion of the $\ell n(1/1-D)$-pressure graphs followed by the normal relationship, the slopes being a little less steep for the higher precompacting pressures and giving a greater density at a given pressure. Also, the transition from the horizontal occurred at a higher pressure for the higher precompacting pressure. This is as predicted from the model as explained above with reference to Greenspan's results. The horizontal portion exists since the model becomes valid for the low pressure range after the powder has been precompacted above a certain pressure. The precompaction pressure of 296 MN/m^2 is quite near the critical pressure at which the model becomes valid; material precompacted at this pressure follows the compaction behaviour of the virgin powder quite closely.

The curvature in the third stage of compaction still requires some explanation and some possible causes for it were examined. Unfortunately there is little published data on this stage and what there is concerns very few different materials. It would be useful to know at which pressure or density this stage of compaction begins for harder materials. The absence of data is no doubt due to the difficulty of achieving sufficiently high pressures to reach this stage with hard materials.

One effect which was not accounted for in the model is elastic recovery on release of the pressure. This would result in the hollow sphere expanding slightly, with a consequent decrease in density. An estimate of the effect of this can be obtained quite simply, however, as follows:

Consider the hollow sphere in the plastic condition with an external pressure P. Now consider a second hollow sphere of the same dimensions as this pressurized sphere and subject it to an external tension, T, numerically equal to the pressure P. Superimposing the action of T on the first sphere is equivalent to releasing the pressure, so by calculating the elastic strains produced in the second sphere (it is permissible to assume elastic behaviour since the sphere will go from compression to tension which effectively doubles the elastic range which has already been substantially increased by work hardening) it is possible to obtain the change in dimensions of the plastic sphere by elastic recovery.

The radial and circumferential stresses in the second sphere may be written

$$\sigma_\phi = \sigma_\theta = A + B/2r^3$$
$$\sigma_r = A - B/r^3$$

subject to the boundary conditions

$$\sigma_r = T \quad \text{at} \quad r = r_b \quad \text{(outside)}$$

and

$$\sigma_r = 0 \quad \text{at} \quad r = r_a \quad \text{(inside)}$$

Substituting these boundary conditions into the expressions for the stresses gives

$$\sigma_\phi = \sigma_\theta = \frac{Tr_b^3}{r_b^3 - r_a^3}\left(1 + \frac{r_a^3}{2r^3}\right)$$

and

$$\sigma_r = \frac{Tr_b^3}{r_b^3 - r_a^3}\left(1 - \frac{r_a^3}{r^3}\right)$$

The circumferential strain in the sphere may be thus written

$$\varepsilon_\theta = \frac{1}{E}\left(\sigma_\theta - \nu(\sigma_\theta + \sigma_r)\right)$$

i.e.

$$\varepsilon_\theta = \frac{Tr_b^3}{E(r_b^3 - r_a^3)}\left(1 - 2\nu + \frac{r_a^3}{r^3}(1+\nu)\right)$$

For an external pressure of 1250 MN/m^2, using the theoretical results obtained for Atoment 28 with $D_o = 0.85$

$$D = 0.97297$$

$$r_a^3 = 0.157464$$

$$r_b^3 = 5.8255$$

Using these values, the circumferential strains at the inside and outside due to elastic recovery can be calculated as

$$\varepsilon_{\theta_a} = 0.00656$$

$$\varepsilon_{\theta_b} = 0.00261$$

and the corrected value of relative density becomes

$$D' = 0.97265$$

Thus the density is decreased by less than 0.04% at 1250 MN/m^2; the effect of elastic recovery is therefore negligible.

Another suggestion is that any air trapped within the compact might have a significant effect at high densities. This can be investigated in terms of the model by calculating the pressure increase within the sphere as it is compressed.

The relative density of the hollow sphere can be written

$$D = \frac{V_m}{V_m + V}$$

where V_m is the volume of solid material and V is the internal volume of the sphere. Then the initial internal volume of the sphere, V_o, is given by

$$V_o = V_m\left(\frac{1}{D_o} - 1\right)$$

where D_o is the initial relative density. Similarly at any other relative density D, the internal volume of the sphere is given by

$$V = V_m\left(\frac{1}{D} - 1\right)$$

Hence

$$\frac{V_o}{V} = \frac{\frac{1}{D_o} - 1}{\frac{1}{D} - 1}$$

Assuming a constant temperature during compaction, it follows that

$$P'V = \text{const}$$

where P' is the internal pressure. Then the internal pressure P' at a relative density D is given in terms of the initial internal pressure, P'_o (atmospheric) by the expression

$$\frac{P'}{P'_o} = \frac{V_o}{V} = \frac{\frac{1}{D_o} - 1}{\frac{1}{D} - 1}$$

i.e.

$$P' = \frac{P'_o(\frac{1}{D_o} - 1)}{(\frac{1}{D} - 1)}$$

Taking $P'_o = 0.1$ MN/m^2 , $D_o = 0.6$ and $D = 0.99$

$$P' = \frac{0.1(1.66-1)}{(1.011-1)}$$

$$= 5 \text{ MN/m}^2$$

The effect of this internal pressure would be to raise the required external pressure for this relative density by an equal amount.

Thus even by assuming the air to be initially entrapped at a relative density of 60% (as opposed to 85% when the model becomes valid) this only alters the compaction pressure by about 5 MN/m^2 at 99% theoretical density compared to a required compacting pressure of over 1400 MN/m^2 for this density; this is clearly negligible. To alter the compaction pressure by 35 MN/m^2 under these conditions would require a density of 99.8% theoretical. Thus it appears that entrapped air cannot account for the curvature of the graph.

In all the previous calculations the relative densities have been based on a maximum density of 7.87 g/cm^3, the theoretical density of pure iron. But the question arises whether this is reasonable, since the density of conventional wrought iron is only 7.8 g/cm^3 and Moyer[74] only achieved a density of 7.81 g/cm^3 after a considerable amount of cold forging of iron powder preforms. Obviously the theoretical density of the fully compacted iron powder will depend on the alloy purity, its interstitial content, and on its microscopic defect density which may be influenced by the mode of powder consolidation. In order to determine whether the curvature observed in stage 3 could be due to errors in selecting the theoretical density, the calculations were repeated assuming the material of the model to be made of a 'solid' material with a density between 98% and 100% theoretical; the results were still expressed as a fraction of the theoretical density of pure iron. The results are shown in Fig. 32 together with the experimental results of Fig. 27. This modification does increase the curvature to some extent at high pressures as well as decreasing the slope slightly. Nonetheless, even with the

density of the sphere material taken as 98% theoretical (i.e. 7.71 g/cm) the observed curvature is still considerably less than that observed experimentally. Thus, while this might contribute to the curvature it is not the prime cause.

Another possible explanation is a change of mechanism in the compaction process. Up to about 95% theoretical density the porosity can be considered essentially macroscopic, and the model used to describe the densification behaviour should be adequate. But at very high densities, say 99%, the porosity is essentially microscopic and it is perhaps unreasonable to expect the macroscopic model to apply. Between these two regions one might expect the densification to be controlled by both macroscopic and microscopic effects.

7.3 METALLOGRAPHY AND MATERIAL PROPERTIES OF COMPACTS

7.3.1 Iron

Fig. 33 shows a sequence of micrographs of the iron powder compacted at different pressures. It is clear from Fig. 33a that the iron consists of a mixture of massive irregularly shaped particles and sponge-like fines, and the compaction sequence, with increasing pressure, is interpreted as:

(i) Compression and consolidation of the fines leading to point contact between the larger particles (Fig. 33b).

(ii) Plastic distortion in the surface regions of the larger particles at points of contact which produces convoluted and interlocking interparticle boundaries (Fig. 33c).

(iii) Bulk plastic flow which causes a gradual decrease in pore size with increasing pressure (Fig. 33d).

The green strength and hardness of the iron compacts are presented in Fig. 34 as a function of pressure. They show that consolidation occurs in this powder at pressures well below the initiation of stage 2 compaction, and therefore well below the point at which plastic flow and interparticle bonding have been presumed to occur. However, since both sets of data are influenced by the porosity and degree of interparticle bonding, they do not provide irrefutable evidence of plastic deformation. In contrast, the microhardness measurements shown in the same figure, obtained from large individual powder particles, show that the hardness of the powder material itself, and therefore the degree of plastic straining, increases progressively during compaction, even at pressures well within stage 1.

Further evidence of extensive plastic deformation during stage 1 compaction was obtained from the x-ray measurements. The variation of line widths with compaction pressure is shown in Fig. 22. The line widths increase rapidly with pressure at first and then tend to level off. There was a similar variation in line widths with increasing strain in the calibration samples. Combining these two shows the variation of strain in the material with pressure as in Fig. 35. There is an appreciable increase in strain with pressure, the rate of increase being greatest at low pressures. Even at relatively low pressures, e.g. 200 MN/m^2, the average strain is more than 5% which represents significant plastic deformation.

Other studies[75] have also shown that plastic deformation widens the diffraction lines up to a limiting value that is essentially unchanged

by further deformation. Thus if the low pressure region is not studied, or the powders are initially in a strained condition, it is quite possible that little line broadening would be observed as the compaction pressure is increased. This may have been the case with the study that Donachie and Burr[19] made on commercial copper powder.

Also shown in Fig. 35 is the variation of material flow stress with compaction pressure which was obtained from the x-ray measurements and calibration samples. As expected, the flow stress increases with compaction pressure. During stage 1, the mean flow stress of the powder is greater than the compaction pressure and hence the plastic deformation and resulting densification in this region is achieved by stress concentrations in the fines and at points of contact between larger particles, as suggested by the metallography. The mean flow stress and compaction pressure converge and become equal at about 300 MN/m^2, whereafter homogeneous or bulk plastic flow may occur in the compact. This pressure corresponds with the transition pressure from stage 1 to stage 2 as determined from Fig. 27.

It is interesting that this transition from local to homogeneous plastic flow occurs at a relative density of about 0.84. This is very close to the value of 0.85 which was earlier found to be the density at which the strain hardening hollow sphere model became valid for this material. By implication, this density was suggested to be where homogeneous plastic flow was initiated in the material.

7.3.2 Superalloy

Fig. 36 shows a sequence of microsections of the superalloy powders compacted at different pressures. In this material plastic deformation occurs at points of interparticle contact and causes the change in particle shape from spherical to polyhedral. This compaction took place at pressures below those required to produce a coherent compact and below the overall yield stress of the material, which suggests that it was entirely within stage 1. Thus Fig. 36 clearly refutes any suggestion that little deformation occurs within this stage.

Additional evidence of plastic deformation and strain hardening was obtained from the microhardness measurements. Fig. 37 shows that the hardness of the individual particles increases with compaction pressure from an initial value of about 370 VPN to about 500 VPN at 1400 MN/m^2.

7.3.3 Aluminum

Little detailed metallography was performed on the aluminum compacts as a function of compacting pressure, nor any mechanical tests, since all the aluminum extrusions were made on compacts pressed at the same pressure (551 MN/m^2). A sample compacted at this pressure was examined and this is described with the extrusion results in sections 7.6.2 and 7.6.3.

7.4 ON THE ROLE OF PLASTIC DEFORMATION IN METAL POWDER COMPACTION

It is clear from the observations of the previous section that while plastic deformation occurs throughout powder compaction and may be

essential to densification, it does not necessarily lead to consolidation. This appears to depend on the nature of the plastic flow and the particle geometry. In the iron and aluminum powders, consolidation is promoted by the presence of the porous fines which deform quite readily and appear to act as a binder for the larger particles. In addition, the irregular particle shape leads to asymmetric loading between particles, creating shear stresses, interparticle sliding and consequent frictional welding of freshly exposed surfaces. Green strength is therefore developed by a combination of mechanical interlocking and frictional welding. As a result, coherent compacts can be produced at pressures of about one third of the overall initial yield stress of the material.

In the superalloy powders the initial close packing arrangement of perfect spheres results in symmetrical point contact loading between particles and direct compressive stresses with little or no shearing and hence no sliding or frictional welding effect. The powder was also devoid of fines that could have acted as a binder and consequently coherent compacts could not be produced even at pressures approaching the bulk yield stress.

To illustrate the beneficial effect of the presence of fines in a powder, 15% by weight of fine carbonyl nickel powder was mixed with the superalloy before compaction and coherent compacts having a relative density of 91% were produced at a pressure of only 825 MN/m^2.

7.5 EXTRUSION OF IRON POWDER COMPACTS

7.5.1 Extrusion Pressure

Extrusion of the iron compacts did not occur at a steady run-out pressure, but exhibited stick-slip behaviour with two or three peaks as observed by Alexander and Quainton[2]. All the extrusion pressures quoted for iron in this section therefore refer to breakthrough pressures.

Although all the iron extrusions were cracked, this should not affect the relationship between the extrusion pressure and ratio, and it is possible to construct a plot of extrusion pressure versus logarithm of extrusion ratio (P_E vs ℓnR) in the usual way. This is shown in Fig.38. From the results at lower extrusion ratios shown on this figure it appears that the extrusion pressure for compacts at a given ratio increases with the compaction pressure. The difference is too large to explain entirely in terms of an increase in yield strength and is probably caused by the different porosities of the compacts.

The work done in extruding a billet is made up of three parts, namely:

(1) the work of homogeneous deformation

(2) the redundant work

(3) the work required to overcome friction at the die-billet interface.

The work of homogeneous deformation for a solid body is given by the expression

$$W = Y\ell nR \qquad (7.1)$$

for a non-work hardening material where Y is the yield stress and R the extrusion ratio. The redundant work is generally independent of R but depends on the die angle, and the friction is very small in hydrostatic extrusion. Thus the extrusion pressure for a solid body is usually proportional to the work of homogeneous deformation for a given die angle. The homogeneous work for a porous body can be approximated as follows:

Suppose the body has an initial density D_1 and a final density D_2 after a change in length from ℓ_1 to ℓ_2. Then the work of deformation is given by

$$W = \int_{\ell_1}^{\ell_2} YAD\,d\ell \qquad (7.2)$$

where A is the cross sectional area and Y is the yield stress. Since the volume of the solid material is constant,

$$AD\ell = \text{constant} = A_1D_1\ell_1 \qquad (7.3)$$

$$\therefore \quad AD = A_1D_1\ell_1/\ell \,. \qquad (7.4)$$

$\therefore$ if Y is constant, substituting equation (7.4) into (7.2) and integrating gives

$$W = YA_1D_1\ell_1 \ell n(\ell_2/\ell_1) \qquad (7.5)$$

If the extrusion pressure required for homogeneous deformation is P_H, then the work done can also be written

$$W = P_H A_1 \ell_1 \qquad (7.6)$$

Substituting equation (7.6) in (7.5)

$$P_H = YD_1 \ell n(\ell_2/\ell_1) \qquad (7.7)$$

But from equation (7.3)

$$\ell_2/\ell_1 = D_1A_1/D_2A_2 = D_1R/D_2 \qquad (7.8)$$

Substituting this into equation (7.7) produces the result

$$P_H = YD_1 \ell n(D_1R/D_2) \qquad (7.9)$$

The assumption of a constant yield stress in this derivation should introduce little error for the iron compacts since it is clear from Fig. 35 that the flow stress does not increase very much above a compaction pressure of about 400 MN/m^2.

Unfortunately, since all the iron extrusions were cracked, it was not possible to determine D_2. However, it should lie between D_1 and unity and so limits of P_H can be evaluated. The extrusion pressure is plotted against P_H in Fig. 39 for the same extrusions as in Fig. 38 using values of Y determined from Fig. 35. It is apparent that proportionality exists between extrusion pressure and the quantity $Y_oD_1 \ell n(D_1R/D_2)$ for iron compacts and that the density of a compact can therefore be important in determining its extrusion characteristics.

From Fig. 39 it appears that to achieve an extrusion ratio of 5, which Alexander and Quainton[2] found necessary to produce apparently sound products, would require an extrusion pressure of about 1650 MN/m^2.

Since this was very near the pressure capability of the system, and as shown in section 7.6 may not in fact give a sound product, no further extrusions were performed on the iron.

7.5.2 Crack Formation

The crack patterns in the extruded iron compacts followed the usual pattern found by other investigators for brittle materials, namely transverse cracking at low reduction ratios, changing to longitudinal cracking at higher ratios and then supposedly to sound products. Typical examples of longitudinal and transverse cracking are shown in Fig. 40; this is the normal way in which this behaviour is observed and shown, i.e. as a surface type effect. A more detailed examination of the crack patterns, however, might provide information that would ultimately lead to a better understanding of this type of cracking. Consequently, several of the cracked products were sectioned, mounted and polished to display the internal crack patterns.

Fig. 41 shows cross and longitudinal sections of products compacted at 1100 MN/m^2 and extruded through ratios of 1.78, 2.25, 2.78 and 3.36. The crack pattern at the low ratio is predominantly transverse while at the highest ratio is entirely longitudinal. The crack pattern has two components: (i) longitudinal surface cracks directed toward the centre of the product and (ii) transverse cracking (which tends to cut the product into discs) that changes to cone shaped cracking toward the centre. The depth to which the transverse cracking penetrates reduces as the reduction ratio is increased and the taper of the cone becomes smaller, until the transverse cracking has disappeared and the

cone taper becomes zero, i.e. purely longitudinal cracking is obtained. The radial penetration of the longitudinal surface cracks increases with extrusion ratio.

At even lower extrusion ratios, a central burst type of defect is obtained as shown in Fig. 42(a). The crack pattern in this case bulges in the direction of extrusion and thus has the opposite direction to those at higher ratios.

Little difference in the crack patterns was observed between extrusions produced from compacts of different pressures. Lower pressure compacts tended to show more transverse cracking at a given ratio, but the differences were too small to draw any definite conclusions.

Information about the deformation patterns occurring in these brittle compacts at low ratios is also of interest. Accordingly a method was developed to show this pattern. An iron compact was prepared in the normal way except that thin layers of aluminum powder were interspersed within the iron powder. After compaction, this resulted in thin aluminum discs bonded within the iron. The sample was machined and extruded as before, then sectioned and mounted. The longitudinal section is shown in Fig. 42(b); the boundary between the iron and aluminum represents the deformation of a plane perpendicular to the direction of extrusion.

No detailed studies of the deformation patterns were performed, but this might be a useful technique for doing so.

7.6 EXTRUSION OF ALUMINUM POWDER COMPACTS

7.6.1 Extrusion Pressure

All the aluminum extrusions, from reduction ratios of 2.25 to 7.60, produced apparently crack-free material (but see sections 7.6.2 and 7.6.4).

The extrusion pressures for these compacts generally exhibited a similar two peak effect to that observed for the iron and so the extrusion pressures used in this section are again breakthrough pressures. With an extrusion ratio of 7.6, however, only one peak was observed and extrusion was incomplete even after allowing the pressure to rise 25% above the initial breakthrough pressure. Only about 13 cm of product were obtained of which only 6 cm were at the full ratio. On removal of the billet from the die it was observed that there had been severe galling of the last few cm of product. A further extrusion was performed at this ratio after spraying the die with Teflon, but the same effect was observed. With an extrusion ratio of 9, galling occurred before the full reduction was achieved and no product of this reduction ratio was obtained.

Aluminum is always prone to galling and because of the high degree of strain hardening in these compacts the extrusion pressures are higher than usual which makes lubrication more difficult. Also, since the bonding in the unextruded compacts is weak, it is easier for material which tends to stick to the die to pull out from the billet. If higher reduction ratios are to be used for this material, lubricants other than simple MoS_2 or graphite grease will have to be used.

The relative densities of the aluminum compacts prior to extrusion were near unity (0.991) and all the compacts had the same powder yield strength since they were produced at the same pressure. Hence it was unnecessary to use equation (7.9) and the extrusion pressures were expressed as a function of ℓnR in the normal way. Fig. 43 shows this relationship together with that for wrought IS aluminum which was obtained for comparison. This latter relationship follows those of other investigators very closely; the constants a and n in equation (2.28) are 155 MN/m^2 and 0 compared with 154 and 0 obtained by Lowe and Goold[49] and 156 and 0 by Pugh[43]. The extrusion of the IS was relatively steady and therefore run-out pressures were used for this to enable direct comparison with the work of Lowe and Goold, and Pugh. The break-through pressures were about 3% higher.

A linear relationship between extrusion pressure and ℓnR was found for the aluminum compacts. This can be expressed as

$$P_E = 238\ \ell nR$$

where P_E is in MN/m^2. In terms of equation (2.28) this gives a = 238 and n = 0.

A much larger pressure is required to extrude these compacts than wrought material of a similar composition. This is because of the large amount of strain hardening that the compact receives during compaction, and the associated increase in flow stress. The ratio of extrusion pressures for the two materials is about 1.8 compared to a ratio of Vickers hardness of about 1.55. Comparison with the pressure-

hardness relationships of Pugh[48] or Lowe and Goold[49] does not provide any useful information as both of these have been found inaccurate for 99.5% pure aluminum.

7.6.2 Metallography of Extruded Material

Fig. 44 shows transverse sections of the aluminum compacts extruded at various ratios together with a section of the as-compacted material. No significant difference was observed between the outside and centre of the extrusions, and the sections shown are representative. There is little evidence of porosity in the as-compacted or extruded samples, and the deformation throughout the section appears relatively uniform. There is a decrease in the cross sectional area of the powder particles and grain structure as the extrusion ratio increases.

The longitudinal sections in Fig. 45 show that the powder particles and grain structure have been elongated, and the microstructures of those at higher ratios are very similar to that of a heavily deformed wrought aluminum structure.

Three small longitudinal cracks were observed in the transverse section of the sample extruded through a 2.25 reduction ratio. These were equispaced around the periphery and directed toward the centre, similar to the longitudinal cracking in the iron. The crack path is shown in Fig. 46 and follows the powder particle boundaries. There appears to be little bonding between particles in this region.

Macroscopic examination of this sample before polishing showed it to be apparently sound and the tensile sample machined from it

showed no evidence of cracking during the machining. It was only revealed by the electropolishing which demonstrates the importance of this type of examination in deciding the soundness of an extrude.

7.6.3 Mechanical Properties of Extruded Material

Results of the tensile tests and hardness measurements on the extruded material are shown in Figs. 47 and 48. Two tensile tests were performed for each extrusion ratio and the results presented are the mean values.

The Vickers hardness increases from 42.9 for the non-extruded material to 53.2 for an extrusion ratio of 2.25; for further increases in extrusion ratio the increase in hardness is more gradual rising to 56.4 at R = 7.6. This shows that the material is further strain hardened by the extrusion process but the extrusion ratio used does not have a large effect.

A similar pattern is observed with the ultimate tensile strength and true fracture stress; the uts increases from about 25 MN/m^2 as-compacted to 168 MN/m^2 at R = 2.25 and thereafter only rises to about 200 MN/m^2 at R = 7.6. The increase in fracture stress is greater, but the biggest increase occurs between the as-compacted sample and the lowest ratio extrusion.

The elongation and reduction of area results exhibit a very different pattern, however. The elongation only rises from near zero for the as-compacted sample to 0.8% at R = 2.25; even at R = 4.0, the elongation is only 6.6% compared with a maximum at R = 6.25 of 10.2%.

Similarly the reduction of area does not achieve values near the maximum until the extrusion ratio exceeds 5.

These results indicate that while most of the powder particle hardening occurs at the lower extrusion ratios, much higher reductions are necessary to create significant bonding in the material.

The ductility results at R = 7.6 are anomalous. The ductility should rise as the degree of bonding improves and then level off as the maximum bonding is achieved, or decrease slightly due to increased hardening. The decrease should not be as large as that observed, however, since most of the hardening occurs at lower reductions. This large decrease may be due to the galling that occurred at R = 7.6; this would result in greater deformation at the edge of the extrusion and less in the centre. Consequently the bonding in the centre would be inferior. Since the strength and hardness are not very dependent on reduction after R = 4.0, they would not be affected very much by this.

It is interesting to compare these results with those for wrought material of similar composition. IS aluminum extruded through ratios of 3.0 and 6.25 had ultimate tensile strengths of 137 and 157 MN/m^2 compared with a maximum for the extruded compacts of 200 MN/m^2. The elongations were much higher for the IS, however, being 29% and 26% compared with 10% for the extruded compact. Pugh[76] achieved a maximum strength of only 173 MN/m^2 for 99.5% pure aluminum at a reduction ratio of about 150; at higher ratios the strength decreased which Pugh attributed to recrystallization. The maximum Vickers hardness obtained was 51 compared with 56.4 for the present work.

7.6.4 Fractographic Examination of Tensile Specimens

Macroscopic examination of the fractured tensile specimens showed that the as-compacted sample and the one extruded at R = 2.25 broke on a plane perpendicular to the direction of loading. The specimens extruded at R = 6.25 broke at 45° to the loading direction and those at R = 4.0 and 5.06 exhibited a combination of the two types of fracture, with a shear lip and flat centre section. The specimens extruded at R = 7.6 showed a very pronounced shear face with a small flat centre section indicating poorer bonding in this region.

Low power observation in the scanning electron microscope revealed longitudinal radial cracks in the specimens extruded at R = 2.25 and 4.0 as shown in Fig. 49. These are very similar to those observed in the electropolished section for R = 2.25.

Although these products appeared sound initially, the stresses arising in the extrusion probably prevented bonding in these areas and consequently they are very weak and open up when loaded or attacked by the electropolishing. Thus a simple macroscopic examination is not sufficient to determine the soundness of a product. In view of these results it is possible that the sound iron product obtained by Alexander and Quainton[2] may not have been sound and that much higher extrusion ratios would be necessary.

Transmission and scanning electron micrographs of the tensile fracture surface of the as-compacted aluminum are shown in Fig. 50. The surface is composed of individual powder particles. There is little evidence of bonding in this surface; powder particles have been

deformed to produce mating surfaces but little interparticle bonding has occurred. The transmission picture in particular shows the high degree of conformity obtained, with small particles being forced into cavities of the larger particles, but shows the absence of any welding on the large powder surfaces. In the scanning pictures the original shape of the powder particles is still evident (compare Fig. 21).

Fig. 51 (a) and (b) show part of the tensile fracture surface of the sample extruded at R = 2.25. The large powder particle in (a) is surrounded by smaller particles and their original shape is still evident to some extent. The fracture is still principally interparticle. The same large particle at higher magnification in (b) exhibits some evidence of bonding. The ridge along the top indicates that it was welded to other particles and the bonded region has necked down to fracture; the microvoid coalescence along this ridge provides further evidence of this. The ridges perpendicular to the main one do not show this microvoid coalescence and are probably where the large particle was extruded into crevices between adjacent particles.

Considerably more bonding is exhibited by the fracture surfaces of the specimen extruded at R = 4.0 shown in Fig. 51 (c) and (d). Although the original powder particles can still be distinguished and the fracture is still interparticle, there is evidence of tearing in (c) which indicates bonding between particles. Further evidence of tearing occurs in (d), along side ridges between particles; unlike those of Fig. 51 (b), these ridges occur between faces of particles instead of being ridges forced into crevices between smaller particles, and

are probably sites of intermittent welding between particles which have necked during testing. There is further evidence of microvoid coalescence in (d) along the top ridges, and a few examples of dimples occurring.

These dimples may be compared with those occurring in the fracture surface of wrought IS aluminum shown in Fig. 52. This shows a surface typical of a very ductile failure. The dimples are very large and the surrounding material has necked down to very thin sections.

A similar feature is seen on the fracture surface of the compact extruded at R = 5.06 shown in Fig. 53 (a). This shows a single powder particle that has necked and fractured like a miniature tensile sample, and the large dimple is of a similar type to those in Fig. 52. The fracture here was through the particle and the ends of this particle must have been securely bonded to the remainder of the material for this to have occurred. There are more side ridges on this particle and evidence of tearing of these ridges. Another large fractured particle is shown in Fig. 53 (b) and it appears that intraparticle fracture only occurs on the larger particles at this extrusion ratio. Many smaller particles can be seen around the larger one and the fracture surface there seems to have followed the powder particle boundaries.

For an extrusion ratio of 6.25, however, intraparticle fracture occurs in much smaller particles as shown in Fig. 53 (c) and (d). There are many more dimples and a network of very thin sections similar to those occurring in the wrought material. There is still some tendency

for the particles to neck and fracture individually, however, and original particle boundaries can be seen in some areas, but the majority of the surface is well bonded.

7.7 ON THE DEVELOPMENT OF BONDING IN COMPACTS BY HYDROSTATIC EXTRUSION

From the results of the previous two sections it is apparent that it is possible to create metallurgical bonds in compacted aluminum at room temperature by the process of hydrostatic extrusion.

The bonding mechanism is interpreted as a frictional welding effect. Material is extruded into crevices between particles thereby exposing fresh, uncontaminated surfaces; also, different extrusion rates between particles caused by different constraints and varying amounts of strain hardening between large and small particles promote a shearing tendency between surfaces which again exposes fresh surfaces which can then weld.

At the lower extrusion ratios, bonding occurs principally on the ridges extruded into crevices, but as the extrusion ratio is increased intermittent welding between surfaces begins to occur. Larger particles, having a larger surface for bonding to occur on, are more firmly anchored within the material and consequently are the first to show intraparticle fracture. Increasing the extrusion ratio further results in intra-particle fracture occurring in progressively smaller particles as the overall degree of interparticle bonding improves.

It appears that an extrusion ratio of about 6.25 is necessary for good bonding of aluminum. A further increase in extrusion ratio

would probably increase the bonding a little as there is still some interparticle fracture at R = 6.25; some regions of the sample extruded at R = 7.6 did show improved bonding but there were areas of poor bonding also, probably due to the galling as explained above. Thus the effect of the increased ratio is not certain. Higher extrusion ratios may not lead to better ductilities, however, as the material is in a very hardened condition and any improvement in bond strength may be offset by decreasing ductility of the particles themselves.

Since apparently sound aluminum products can be obtained at lower ratios than for iron (2.25 compared with 4.7 found by Alexander and Quainton[2]) it is probable that ratios higher than 6.25 would be necessary to promote good bonding in the iron. For stronger and more brittle materials even higher extrusion ratios may be necessary.

The use of back pressure or double reduction dies is not likely to help either; although sound products may be produced at lower ratios using these methods, a high extrusion ratio is still required to get good bonding. The cracking that occurs is caused by the bond strength being insufficient to withstand the stress system set up in the extrusion. Back pressure extrusion and double reduction dies merely alter the stress pattern so that there is less stress on the interparticle bonds; the poor bonding still exists.

As a method for producing useful material, the process appears to be limited by the very high pressures that would be required for high strength materials. Besides the inherently high initial strengths of these materials, the strain hardening which occurs during compaction makes extrusion more difficult and the need for high extrusion ratios compounds the problem.

8 CONCLUSIONS

Equipment for high pressure isostatic compaction and hydrostatic extrusion has been designed, built and pressure tested to 1400 MN/m^2.

A numerical technique for calculating the usable internal pressure in a tapered pressure vessel set has been developed which accounts for the elastic-plastic expansion of a work-hardening liner material in an elastic container. It has been shown that the product of the coefficient of friction between the liner and container and the effective liner length is the most important design consideration once the materials and diameter ratios have been chosen. Using this technique, it has been shown that for the equipment used, a pressure of 1600 MN/m^2 can be achieved without causing the container to yield or making the equivalent liner bore strain exceed 0.5%.

The $\ell n(1/1-D)$ versus pressure curves for Atomet 28 iron powder and Alcoa grade 1202 aluminum powder were found to exhibit the three characteristic regions observed by other investigators for a variety of materials. The 713 LC superalloy powder could not be consolidated at pressures up to 1400 MN/m^2.

Contrary to the suggestions of previous investigators it has been shown that extensive plastic deformation can occur during the first stage of compaction. The transition from stage 1 to stage 2 compaction occurs when the pressure exceeds the current bulk yield stress of the material, i.e. when plastic flow becomes homogeneous

instead of local. At this point the compaction model of a hollow plastic sphere subject to external pressure becomes valid.

It has been demonstrated that by incorporating the strain hardening characteristics of the material in this model, the compaction behaviour in the second stage can be accurately predicted. However, the strain hardening characteristics of the material do not cause the curvature observed in the third stage of compaction. This is thought to be governed by a mechanism concerned with the closing of microscopic defects and pores.

Although plastic deformation always occurs during consolidation, it does not cause it. Consolidation is seen as a result of a combination of mechanical interlocking and associated frictional welding created by surface shear deformation resulting from asymmetric loading. Thus it is difficult to achieve consolidation in spherical powders even after considerable plastic deformation.

The porosity of a compact can be important in determining its extrusion characteristics, more porous compacts requiring a lower extrusion pressure; an expression has been derived relating these two quantities.

It has been shown that Alcoa grade 1202 aluminum powder isostatically compacted at 551 MN/m^2 can be hydrostatically extruded to give apparently crack-free products at extrusion ratios of 2.25 and above. However, at extrusion ratios below about 5, the products develop longitudinal cracking when tested in tension. An extrusion ratio of 6.25 is sufficient to cause a high degree of bonding in the aluminum

and to give ultimate tensile strengths of 200 MN/m^2 and reductions of area of 30%. Wrought material of similar composition has a strength of only 173 MN/m^2 after extrusion through a reduction ratio of 150. The substantial increase in strength over the wrought material is attributed to the high degree of strain hardening imparted to the material during compaction.

The bonding mechanism is interpreted as a frictional welding effect where material is extruded into crevices between particles exposing fresh material, or where different extrusion rates between particles promote shearing between them which again exposes fresh, uncontaminated surfaces which can then weld.

It is thought that the extrusion ratio required to cause bonding will be higher for stronger and more brittle materials.

Although it has been shown that hydrostatic extrusion can successfully be used to consolidate powder to bar material, the method is limited by the very high pressures that would be needed to use the process for those materials of commercial interest. This high pressure requirement is due both to the high strengths of these materials, which further increase during compaction, and to the higher extrusion ratios that would be necessary to promote bonding.

REFERENCES

1. J.M. Alexander and L.B. Dove, "A Preliminary Investigation of the Isostatic Compaction and Hydrostatic Extrusion of Iron Powder", Annals of the CIRP, Vol.19 (1971), p.29.

2. Private communication from J.M. Alexander and D.R. Quainton, "On the Isostatic Compaction and Hydrostatic Extrusion of Iron Powder", McMaster University Engineering Report No. ME/71/SM/REP/2, (1971).

3. E.E. Walker, "The Compressibility of Powder", Trans. Faraday Soc., Vol.19 (1923), p.83.

4. M.Y. Balshin, "Theory of Compacting" (in Russian) Vestnik Metalloprom, Vol.18 (1938), p.124.

5. I. Shapiro and I.M. Kolthoff, "The Compressibility of Silver Bromide Powders", J. Phys. Colloid. Chem., Vol.51 (1947), p.483.

6. P.E. Wretblad and J. Wulff, "Sintering", Powder Metallurgy (ed. J. Wulff), p.45 (1942), American Society for Metals.

7. K. Konopicky, "Paralletitat der Gesetzmassigkeiten in Keramik und Pulvermetallurgie", Radex-Rundschau, Vol.141 (1948), p.141.

8. L.F. Athy, "Density, Porosity and Compaction of Sedimentary Rocks", Bull. Am. Assocn. Petrol. Geologists, Vol.14 (1930), p.1.

9. G.B. Smith, "Compressibility Factor. Development of a General Formula", Metal Ind., Vol.72 (1948), p.427.

10. M.Yu. Balshin, Poroshkovaya Metallurgiya, (1948), Mashgiz, Moscow.

11. C. Torre, "Theorie und Verhalten der Zussammengepressten Pulver", Berg-Huttenmann, Monatsh. Montan. Hochschule Leoben, Vol.93 (1948), p.62.

12. C.E. Van Buren and H.H. Hirsch, "Hydrostatic Pressing of Powders", Powder Metallurgy (ed. W. Leszynski) p.403 (1961), Interscience Publishers.

13. R.W. Heckel, "Density-Pressure Relationships in Powder Compaction", Trans. Metall. Soc. AIME, Vol.221 (1961), p.671.

14. R.W. Heckel, "An Analysis of Powder Compaction Phenomena", Trans. Metall. Soc. AIME, Vol.221 (1961), p.1001.

15. R.W. Heckel, "A Normalized Density-Pressure Curve for Powder Compaction", Trans. Metall. Soc. AIME, Vol.224 (1962), p.1073.

16. A.N. Nikolaev, "Relationship Between Pressure and Density of Compacts from Metal Powders", Poroshkovaya Metallurgiya, Vol.9 (1962), p.3.

17. A.R. Cooper and L.E. Eaton, "Compaction Behaviour of Several Ceramic Powders", J. Am. Ceramic Soc., Vol.45 (1962), p.97.

18. G.A. Meerson, "Some Problems of Powder Compacting", Poroshkovaya Metallurgiya, Vol.11 (1962), p.3.

19. M.J. Donachie and M.F. Burr, "Effects of Pressing on Metal Powders", J. Metals, Vol.15 (1963), p.849.

20. M.F. Burr and M.J. Donachie, "Effects of Pressing on Copper Powders", Trans. ASM, Vol.56 (1963), p.863.

21. I. Shapiro, "Fundamental Studies of Compressibilities of Powders", Tech. Doc. Rep. No. ASD TDR-63-147, U.S. Department of Commerce, (1963).

22. N.F. Kunin and B.D. Yurchenko, "Regularities in the Compacting of Powders of Different Materials", Poroshkovaya Metallurgiya, Vol.18 (1963), p.3.

23. N.F. Kunin and B.D. Yurchenko, "On a Rational Equation of Pressing Metal Powders", Poroshkovaya Metallurgiya, Vol.20 (1964), p.3.

24. J. Greenspan, "High Pressure Isostatic Pressing and Pressureless Sintering of Some Metal Powder Compacts", Metals for the Space Age, (ed. F. Benesovsky) p.163 (1964), Vienna (Springer).

25. K. Kawakita and Y. Tsutsumi, "An Empirical Equation of State for Powder Compression", Japanese J. App. Phys., Vol.4 (1965), p.56.

26. K. Kawakita and Y. Tsutsumi, "A Comparison of Equations for Powder Compression", Bull. Chem. Soc. of Japan, Vol.39 (1966), p.1364.

27. G. Bockstiegel, "The Porosity-Pressure Curve and its Relation to the Pore Size Distribution in Iron Powder Compacts", Modern Developments in Powder Metallurgy, (ed. H.H. Hausner) p.155 (1966), Plenum Press, N.Y.

28. I.D. Radomysel'skii and N.I. Shcherban', "Certain Regularities of Pressing Two-Component Cermet Materials", Poroshkovaya Metallurgiya, Vol.32 (1966), p.45.

29. W.R. Morgan and R.L. Sands, "Isostatic Compaction of Metal Powders", Metallurgical Review, 134, Vol.14 (1969), p.85.

30. V.S. Savin, N.B. Ukhina and N.A. Fedotov, "Equation of Pressing of Nickel Powders", Poroshkovaya Metallurgiya, Vol.74 (1969), p.11.

31. A.G. Yurchenko, L.I. Pugina and N.I. Shcherban', "Densification of Two-component Materials in Cold Pressing", Poroshkovaya Metallurgiya, Vol.77 (1969), p.19.

32. E.M. Petrova, N.I. Shcherban' and V.M. Sleptsov, "Densification Behaviour of Fe, Co, and Ni Powders with Additions of Zirconium, Niobium and Molybdenum Carbide Powders", Poroshkovaya Metallurgiya, Vol.79 (1969), p.7.

33. G.A. Meerson, A.F. Islankina, V.N. Mel'nikov, and L.D. Gol'man, "Hydrostatic Pressing of Steel Powders", Poroshkovaya Metallurgiya, Vol.79 (1969), p.13.

34. I.D. Radomysel'skii and G.G. Serdyuk, "Shaping of Metal Powders - a Survey", Poroshkovaya Metallurgiya, Vol.85 (1970), p.10.

35. G.A. Il'in and L.D. Gol'dman, in: Powder Metallurgy, Transactions of the Ninth All-Union Conference on Powder Metallurgy (in Russian), p.42 (1968), Riga.

36. G.A. Meerson, N.I. Rasskazov and V.P. Chulkov, "Experimental Investigation of the Compaction Process of Powder Materials", Poroshkovaya Metallurgiya, Vol.85 (1970), p.21.

37. P.A. Boiko and N.I. Shcherban', "Densification of Nickel-Carbide Composites", Poroshkovaya Metallurgiya, Vol.94 (1970), p.23.

38. V.P. Severdenko and V.N. Iosifov, "Pressing of Compacts from Aluminum Granules", Poroshkovaya Metallurgiya, Vol.96 (1970), p.24.

39. R.M. Koerner and F.J. Quirus, "High Density P/M Compacts Utilizing Shear Stresses", Int. J. Powder Metallurgy, Vol.7 (1971), p.3.

40. R.M. Koerner, "Triaxial Compaction of Metal Powders", Powder Metallurgy International, Vol.3 (1971), p.186.

41. J. Robertson, "Method of and Apparatus for Forming Metal Articles", British Patent No. 19356, October 14, 1893.

42. P.W. Bridgman, Studies in Large Plastic Flow and Fracture, (1952), McGraw-Hill, London & N.Y.

43. H.Ll.D. Pugh, "Hydrostatic Extrusion", Mechanical Behaviour of Materials Under Pressure, (ed. H.Ll.D. Pugh), p.391 (1970), Elsevier, Amsterdam, London, N.Y.

44. B.I. Beresnev, L.F. Vereshchagin, Yu. N. Ryabinin and L.D. Livshits, Some Problems of Large Plastic Deformation of Metals at High Pressures, (1960), Akad, Nauk, SSSR; translated by V.M. Newton, (1963), MacMillan, N.Y.

45. T.E. Davidson and D.P. Kendall, "The Design of High Pressure Containers and Associated Equipment", Mechanical Behaviour of Materials Under Pressure, (ed. H.Ll.D. Pugh), p.54 (1970), Elsevier, Amsterdam, London, N.Y.

46. H.Ll.D. Pugh, "Applications of Static High Pressure to the Forming of Metals - Hydrostatic Extrusion", Metal Deformation Processing, Vol.11 (1966), DMIC Report No.226.

47. H.Ll.D. Pugh and K. Ashcroft, "Hydrostatic (Ramless) Extrusion of Metals by Liquid Pressure", Symposium of the Physics and Chemistry of High Pressures, (1962), London Society of Chemical Industries, p.163.

48. H.Ll.D. Pugh, Bulleid Memorial Lectures, (1965), University of Nottingham.

49. B.W.H. Lowe and D. Goold, "An Account of Some Recent Experimental Work on the Hydrostatic Extrusion of Non-Ferrous Metals", Proc. Inst. Mech. Eng., Vol. 182 (1967-68), part 3c, p.197.

50. A.H. Low and C.J. Donaldson, "An Investigation of Speed Instability in Hydrostatic Extrusion", National Engineering Laboratory Report, No.289, East Kilbride, Glasgow (1967).

51. B.I. Beresrev, L.F. Vereshchagin, Yu.N. Ryabinin, "Conditions of Extrusion and Variation of the Mechanical Properties of Metals in their Extrusion by a High-Pressure Fluid", Inzh-fiz. Zh., Vol.3 (1960), p.43.

52. A. Bobrowsky and E.A. Stack, "Final Report on an Investigation of Fluid Extrusion of Metals", NASA contract NASW-742, (1965).

53. R.J. Fiorentino, A.M. Sabroff and F.W. Boulger, "Development of Manufacturing Capabilities of the Hydrostatic Extrusion Process", Interim Report, Batelle Memorial Institute, Project 8-198, Contract AF 33(615) - 1390, February, 1965.

54. R.J. Fiorentino, A.M. Sabroff and F.W. Boulger, "Investigation of Hydrostatic Extrusion", Final Report, Batelle Memorial Institute, Contract AF 33(600) - 43328, January, 1965.

55. R.J. Fiorentino, B.D. Richardson, A.M. Sabroff and F.W. Boulger, "New Developments in Hydrostatic Extrusion", ASTME-CIRP Int. Conf. on Manufacturing Technology, Ann Arbor, Michigan (1967), p.941.

56. R.J. Fiorentino, J.C. Gerden, W.R. Hansen, A.M. Sabroff and F.W. Boulger, "Development of the Manufacturing Capabilities of the Hydrostatic Extrusion Process", Interim Engineering Progress Report IR-8-198 (V and IV) Batelle Memorial Institute (1966).

57. A.H. Low, "Some Effects of Varying the Pressurizing Speed in Hydrostatic Extrusion", National Engineering Laboratory Report No.358, East Kilbride, Glasgow, (1968).

58. R.J. Fiorentino, B.D. Richardson and A.M. Sabroff, "Hydrostatic Extrusion of Brittle Materials - Role of Die Design and Residual Stress Formation", Metal Forming, Sept. 1969, p.243.

59. K. Osakada, N. Shiraishi and M. Oyane, "Residual Stresses in Hydrostatically Extruded Copper Rod", J. Inst. Metals, Vol.99 (1971), p.341.

60. A. Bobrowsky, "Hydrostatic Extrusion of Metal Powders", New Methods for the Consolidation of Metal Powders (ed. H.H. Hausner), p.195, (1967), Plenum Press, New York.

61. N.R. Gardner, A.D. Donaldson and F.M. Yans, "The Extrusion of Metal Powders", New Methods for the Consolidation of Metal Powders (ed. H.H. Hausner), p.169 (1967), Plenum Press, New York.

62. Ye.D. Martynov, B.I. Beresnev, A.V. Kocherov, D.K. Bulychev, K.P. Rodionov, Yu.N. Ryabinin and M.V. Mal'tsev, "Effect of Hydroextrusion on the Mechanical Properties of Molybdenum", Fiz. Metal. Metalloved, Vol.23 (1967), p.1044.

63. G.A. Mochalov, Ye.D. Martynov, B.I. Beresnev, A.I. Yevstyukhin, K.P. Rodionov, D.K. Bulychev and Yu.N. Ryabinin, "Mechanical Properties of Molybdenum after Hydroextrusion", Fiz. Metal. Metalloved, Vol.25 (1968), p.357.

64. G.A. Mochalov, Ye.D. Martynov, B.I. Beresnev, A.I. Yevstyukhin, K.P. Rodionov, D.K. Bulychev and Yu.N. Ryabinin, "Mechanical Properties of Hydroextruded Molybdenum after Annealing", Fiz. Metal. Metalloved, Vol.25 (1968), p.529.

65. D.K. Bulychev, B.I. Beresnev, M.G. Gaydukov, Ye.D. Martynov, K.P. Rodionov and Yu.N. Ryabinin, "Possibility of Closing up Pores and Cracks in Metals in the Process of Plastic Deformation under High Hydrostatic Pressure", Fiz. Metal. Metalloved, Vol.18 (1964), p.437.

66. B.I. Beresnev, D.K. Bulychev, M.G. Gaydukov, Ye.D. Martynov, K.P. Rodionov and Yu.N. Ryabinin, "Closing of Pores and Cracks in Copper due to High-Pressure Hydroextrusion", Fiz. Metal. Metalloved, Vol.18 (1964), p.778.

67. W.R.D. Manning, "Overstrain of Tubes by Internal Pressure", Engineering, Vol.159 (1945), p.101 and p.183.

68. P.V. Marcal, "Note on Elastic-Plastic Thick Cylinder with Internal Pressure in Open and Closed-End Condition", Int. J. Mech. Sci., Vol.7 (1965), p.841.

69. P.V. Marcal, "Stiffness Method for Elastic-Plastic Problems", Int. J. Mech. Sci., Vol.7 (1965), p.229.

70. J.M. Alexander and J.S. Gunasekera, "On the Geometrically Similar Expansion of a Hole in a Thin Infinite Plate", Proc. R. Soc. Lond., Vol.A326 (1972), p.361.

71. F.P. Beer and E.R. Johnston, Mechanics for Engineers, Vol.1 (1956), McGraw-Hill, N.Y.

72. S.E. Babb, "The Measurement of Hydrostatic Pressure", Mechanical Behaviour of Materials Under Pressure, (ed. H.Ll.D. Pugh), p.119 (1970), Elsevier, Amsterdam, London, N.Y.

73. H.Ll.D. Pugh, "Redundant Work and Friction in the Hydrostatic Extrusion of Pure Aluminum and an Aluminum Alloy", J. Mech. Eng. Sci., Vol.6 (1964), p.362.

74. K.H. Moyer, "The Effect of Density on Impact Properties of Iron P/M Forgings", Metals Engineering Quarterly, August 1972, p.34.

75. F.E. Haworth, "Energy of Lattice Distortion in Cold-Worked Permalloy", Phys. Rev., Vol.52 (1937), p.613.

76. H.Ll.D. Pugh, "Hydrostatic Extrusion", National Engineering Laboratory Report No.416, East Kilbride, Glasgow, (1969).

	lbf/in^2	kgf/cm^2	bar	atm	$tonf/in^2$ (USA)	$tonf/in^2$ (British)	MN/m^2
1 lbf/in^2	1	0.0703070	0.689476	0.0680460	0.5×10^{-3}	0.446427×10^{-3}	0.0689476
1 kgf/cm^2	14.2233	1	0.980662	0.967841	7.11168×10^{-3}	6.34969×10^{-3}	0.0980662
1 bar	14.5038	1.01972	1	0.986923	7.25189×10^{-3}	6.47488×10^{-3}	0.1
1 atm	14.6959	1.03323	1.01325	1	7.34798×10^{-3}	6.56067×10^{-3}	0.101325
1 $tonf/in^2$(USA)	2000	140.614	137.895	136.092	1	0.892854	13.7895
1 $tonf/in^2$(British)	2240	157.488	154.443	152.423	1.12000	1	15.4443
1 MN/m^2	145.038	10.1972	10	9.86923	7.25189×10^{-2}	6.47488×10^{-2}	1

APPENDIX: Interrelationship Between Various Pressure Units

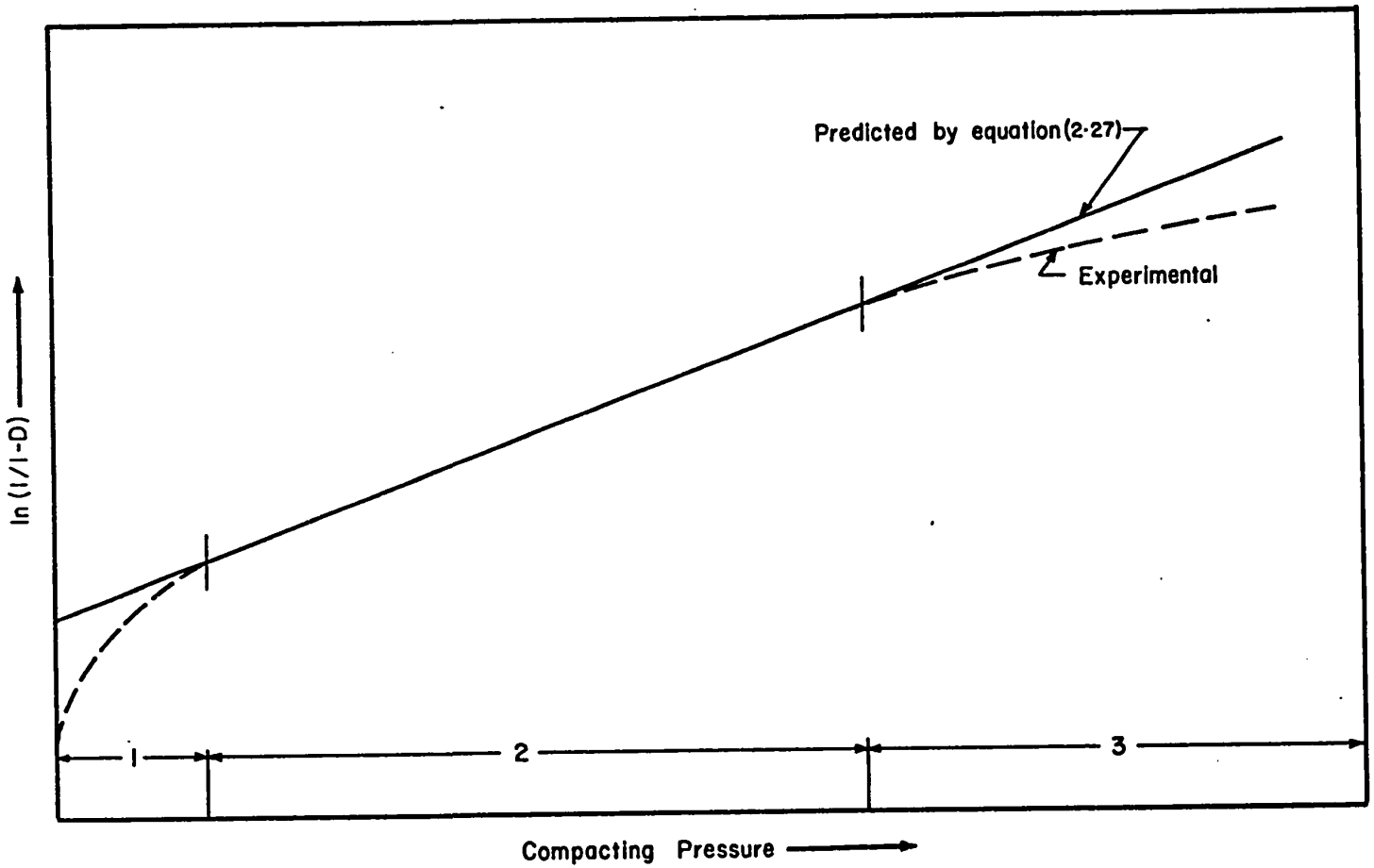

FIG. 1 TYPICAL EXPERIMENTAL DEVIATIONS FROM PREDICTIONS OF EQUATION (2·27)

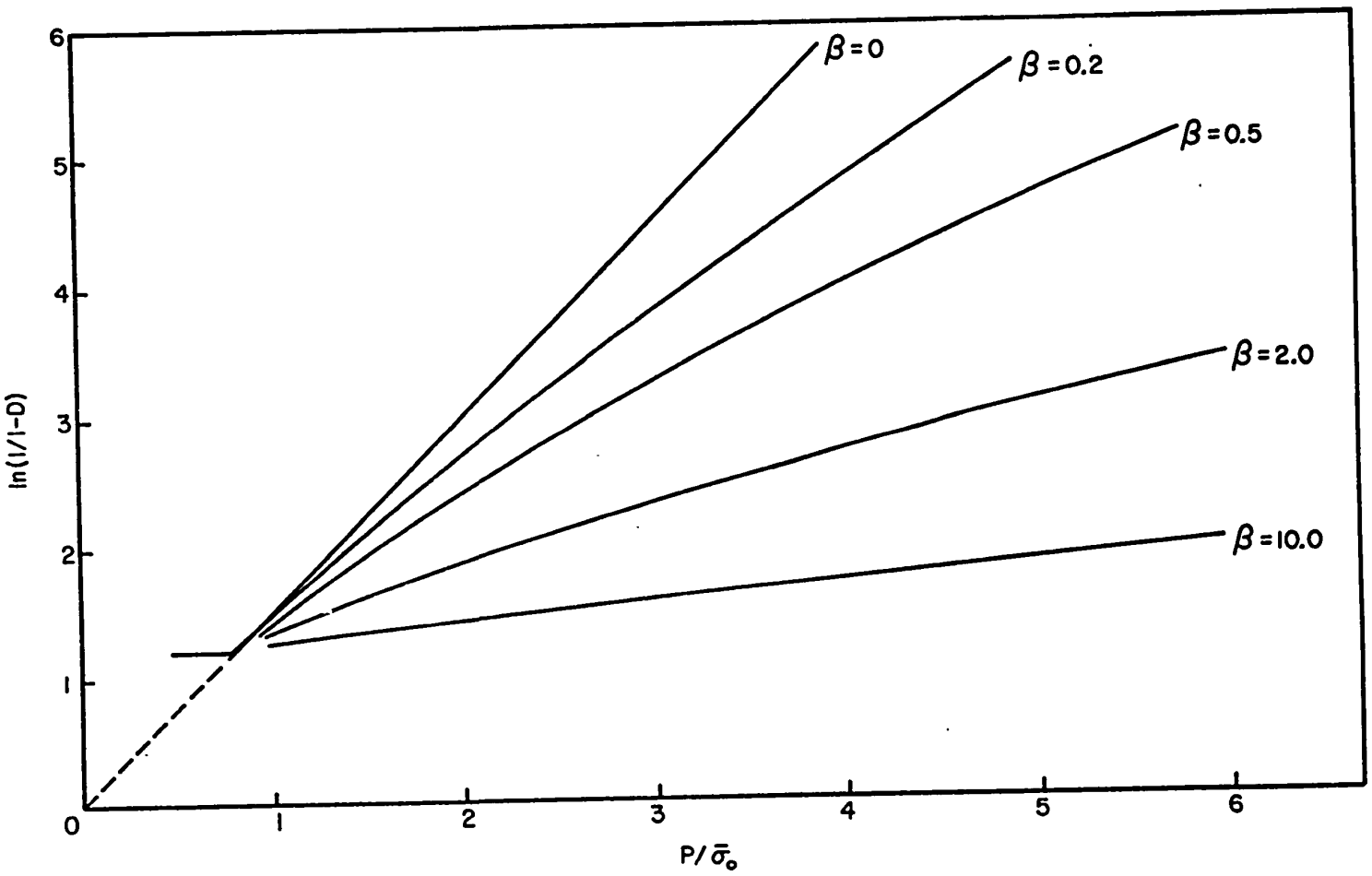

FIG. 2 EFFECT OF DIFFERENT DEGREES OF LINEAR STRAIN HARDENING ON Ln (1/1-D) VERSUS $P/\bar{\sigma}_o$ FOR $D_o=0.7$. THE STRESS-STRAIN CURVES USED ARE GIVEN BY $\bar{\sigma}=\bar{\sigma}_o(1+\beta\bar{\epsilon}_p)$

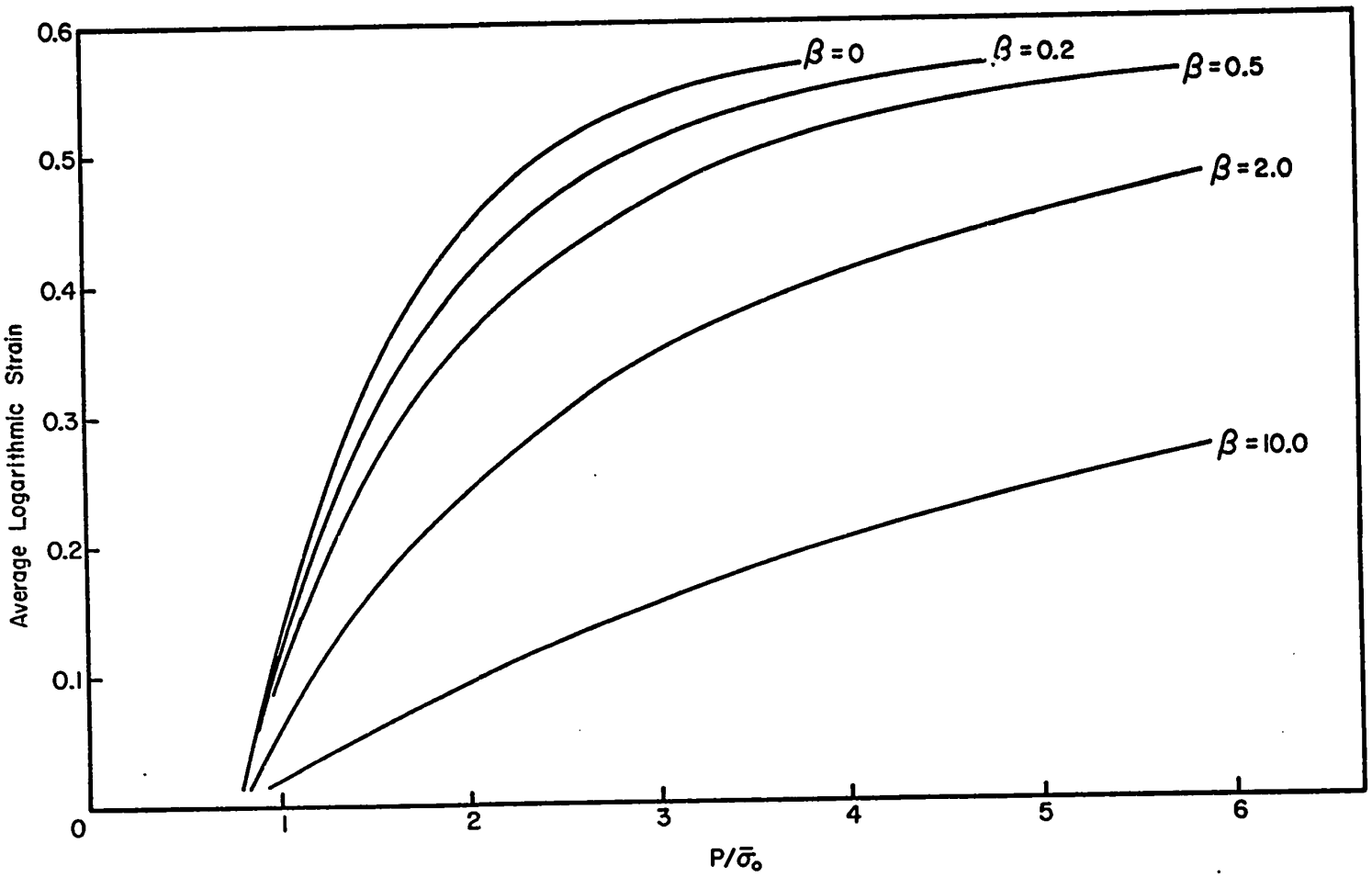

FIG. 3 EFFECT OF DIFFERENT DEGREES OF LINEAR STRAIN HARDENING ON STRAIN VERSUS $P/\bar{\sigma}_o$ FOR $D_o = 0.7$. THE STRESS-STRAIN CURVES USED ARE GIVEN BY $\bar{\sigma} = \bar{\sigma}_o(1+\beta\bar{\epsilon}_p)$

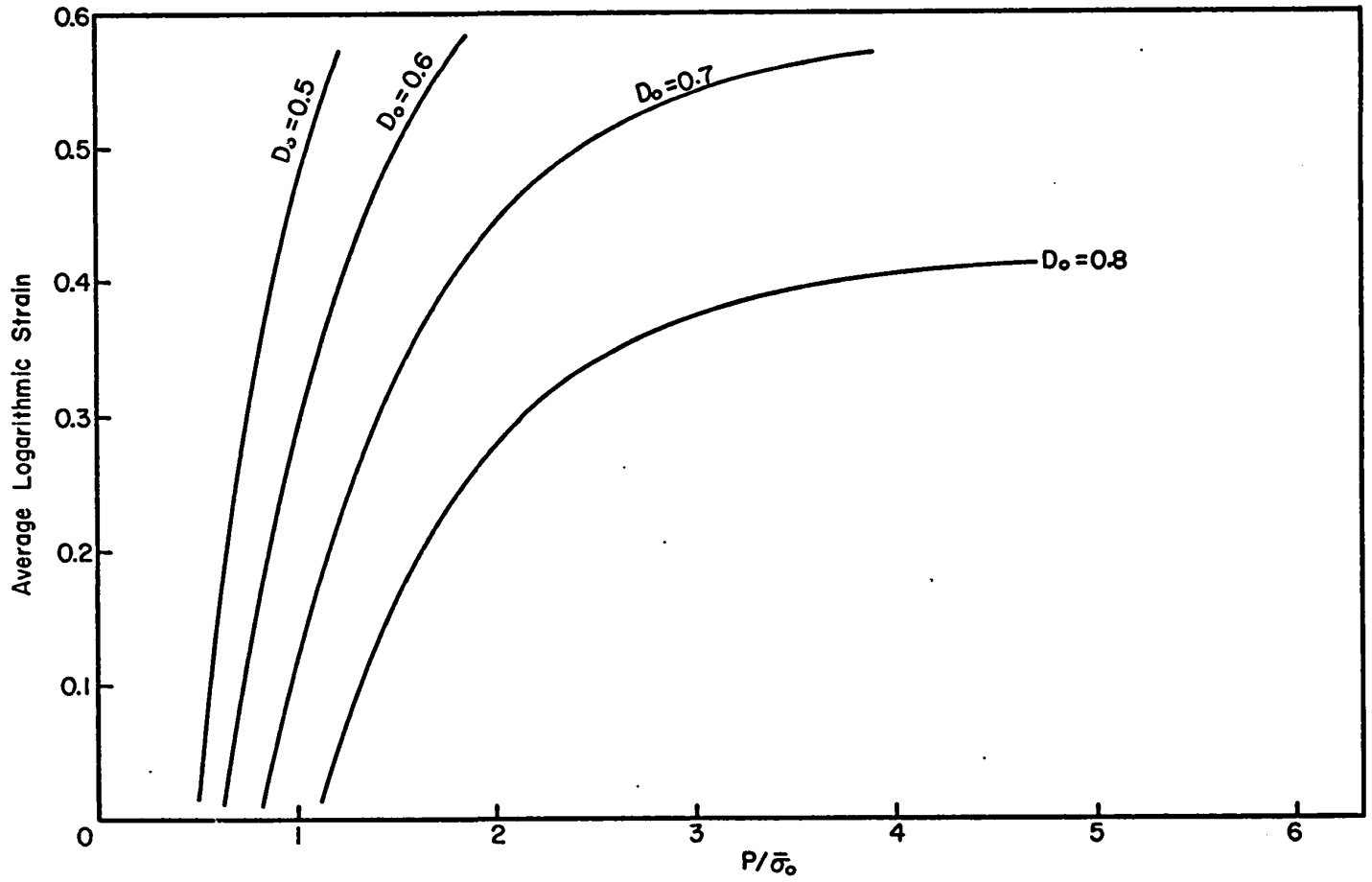

FIG. 4 EFFECT OF D_o ON STRAIN VERSUS $P/\bar{\sigma}_o$ USING STRESS-STRAIN CURVE $\bar{\sigma} = \bar{\sigma}_o$

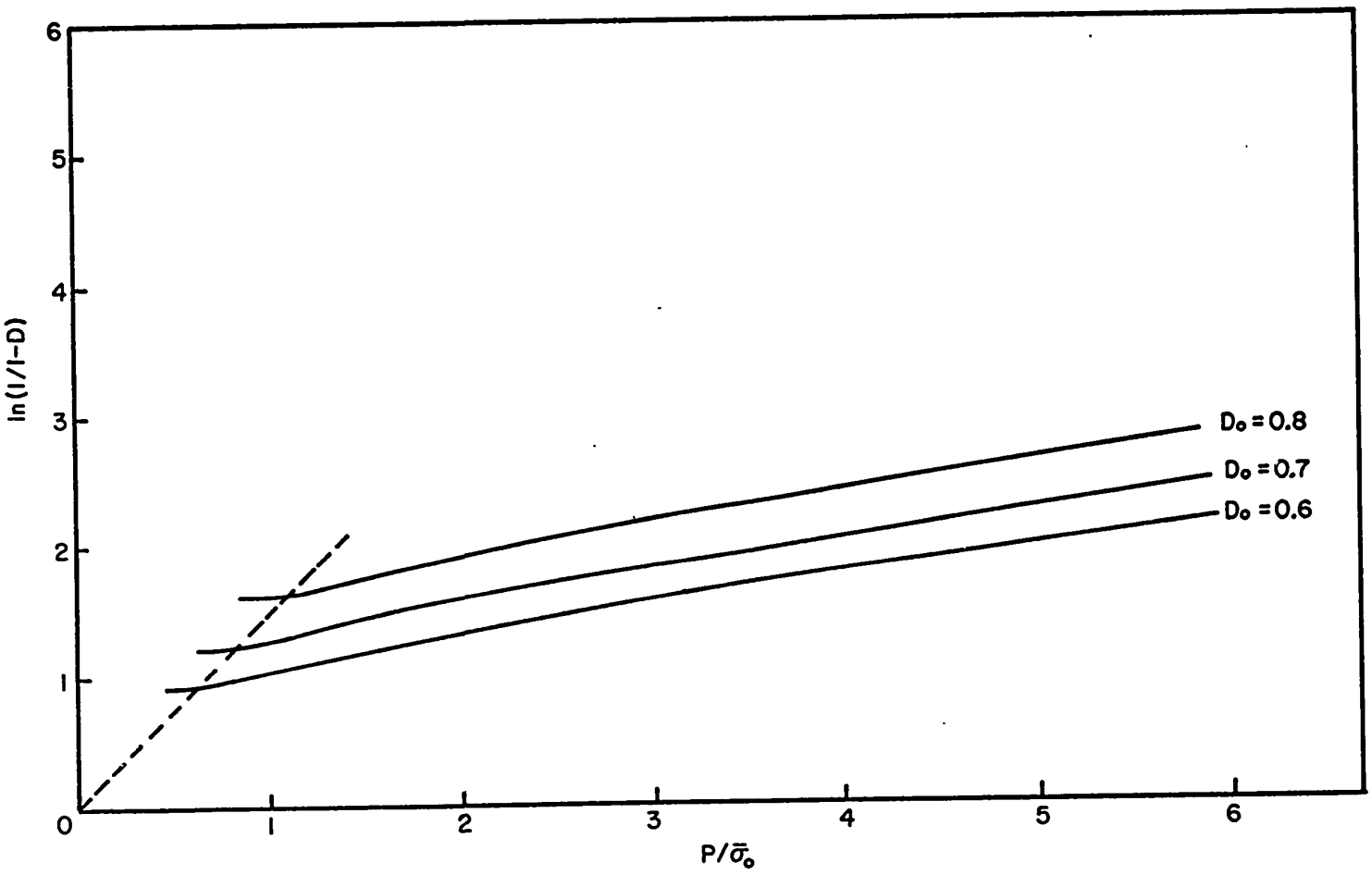

FIG. 5 EFFECT OF D_o ON Ln(1/1-D) VERSUS $P/\bar{\sigma}_o$ USING STRESS-STRAIN CURVE $\bar{\sigma} = \bar{\sigma}_o(1+5\bar{\epsilon}_p)$

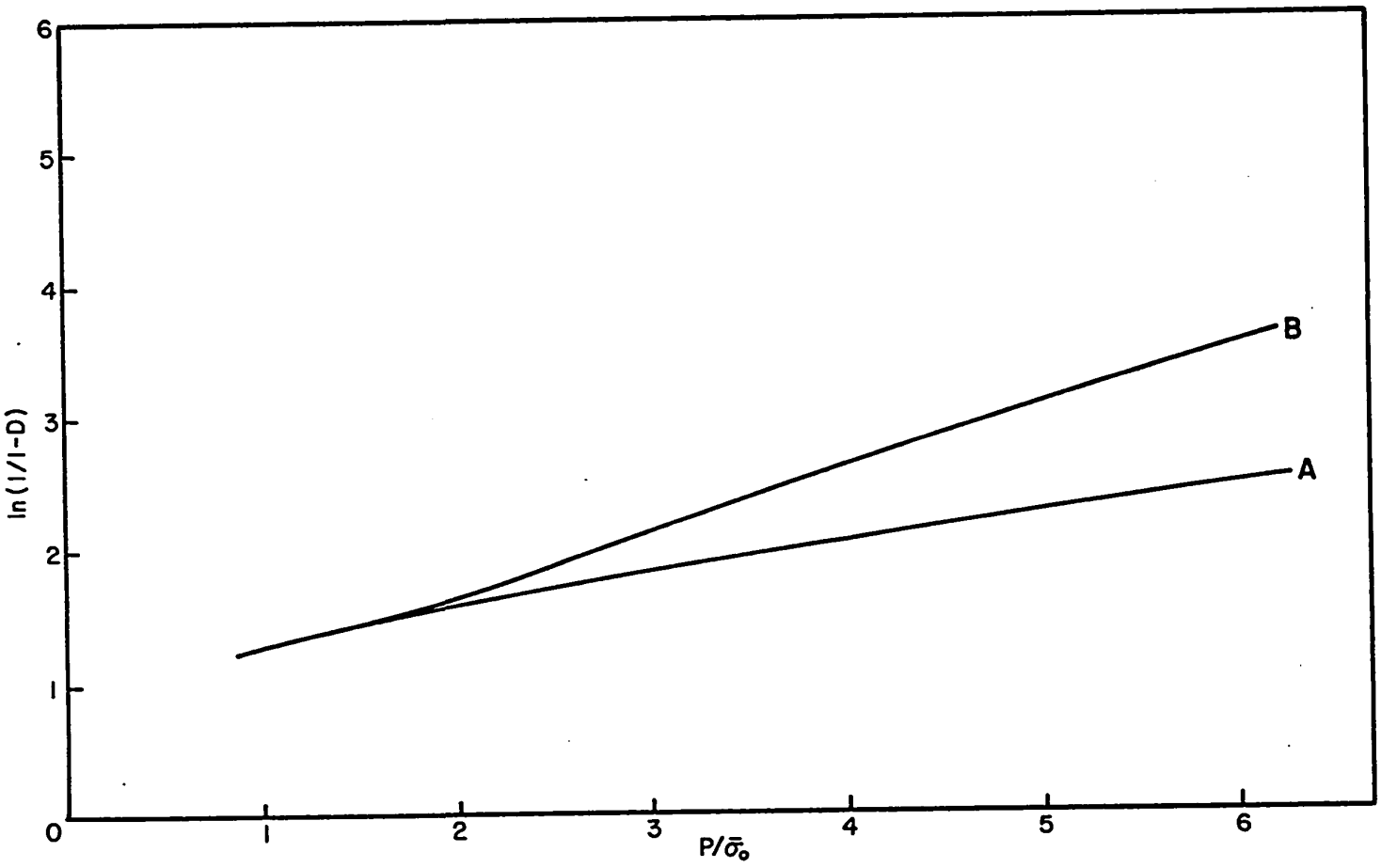

FIG. 6 EFFECT OF STEPPED STRESS-STRAIN CURVE ON Ln(1/1-D) VERSUS $P/\bar{\sigma}_o$ FOR $D_o = 0.7$. THE STRESS-STRAIN CURVES USED ARE GIVEN BY (A) $\bar{\sigma} = \bar{\sigma}_o(1 + 5\bar{\epsilon}_p)$ AND (B) EQUATION (3·19)

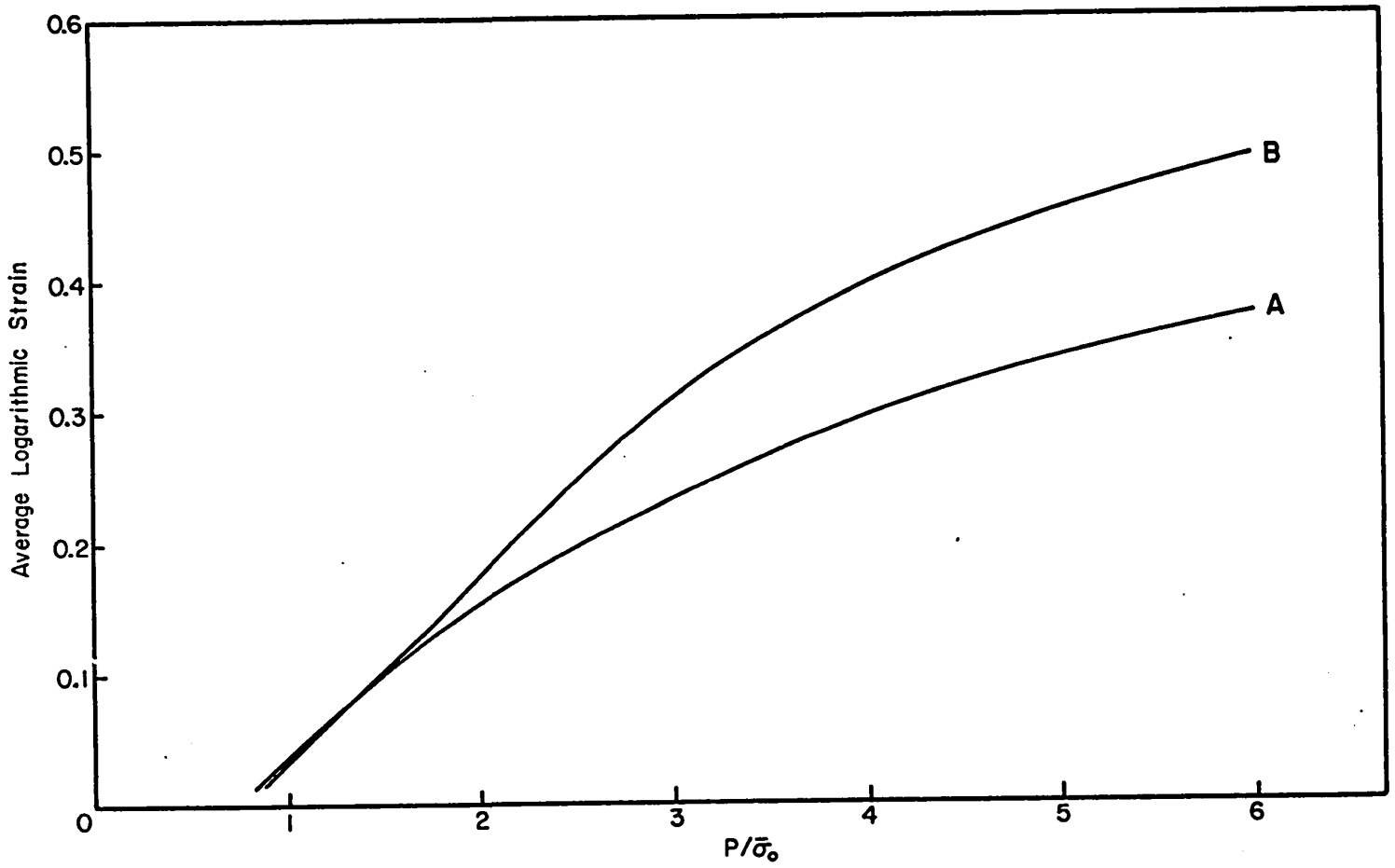

FIG. 7 EFFECT OF STEPPED STRESS-STRAIN CURVE ON STRAIN VERSUS $P/\bar{\sigma}_o$ FOR $D_o = 0.7$. THE STRESS-STRAIN CURVES USED ARE GIVEN BY (A) $\bar{\sigma} = \bar{\sigma}_o(1 + 5\bar{\epsilon}_p)$ AND (B) EQUATION (3·19)

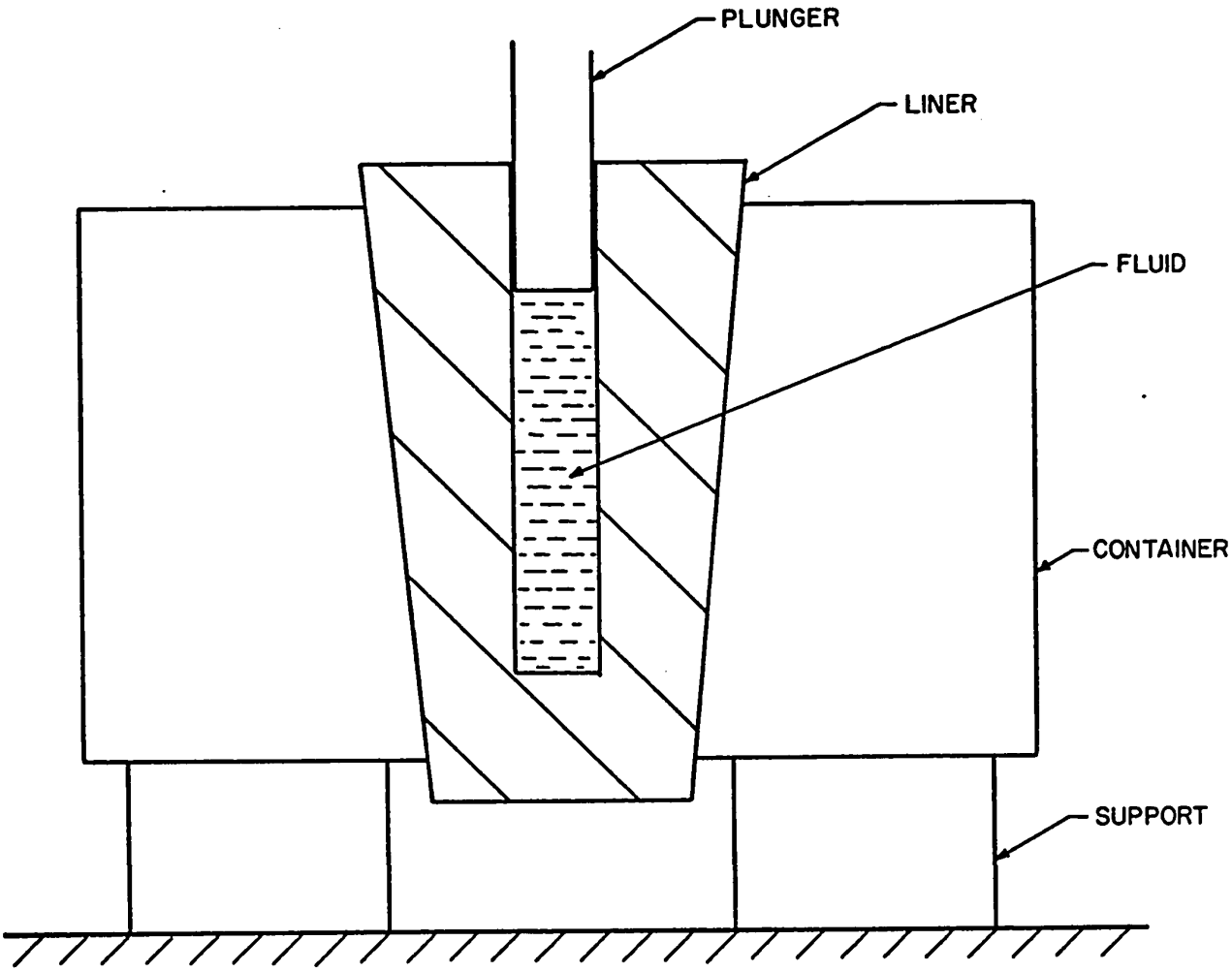

FIG. 8 TAPERED PRESSURE VESSEL SET

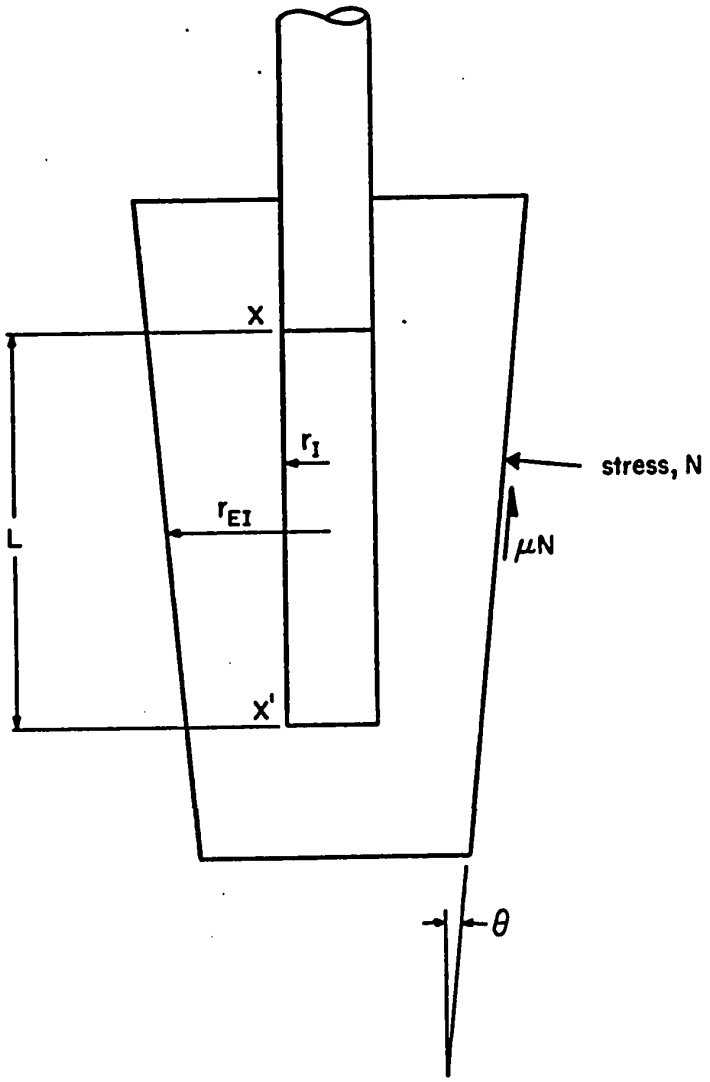

FIG. 9 FORCES ON LINER

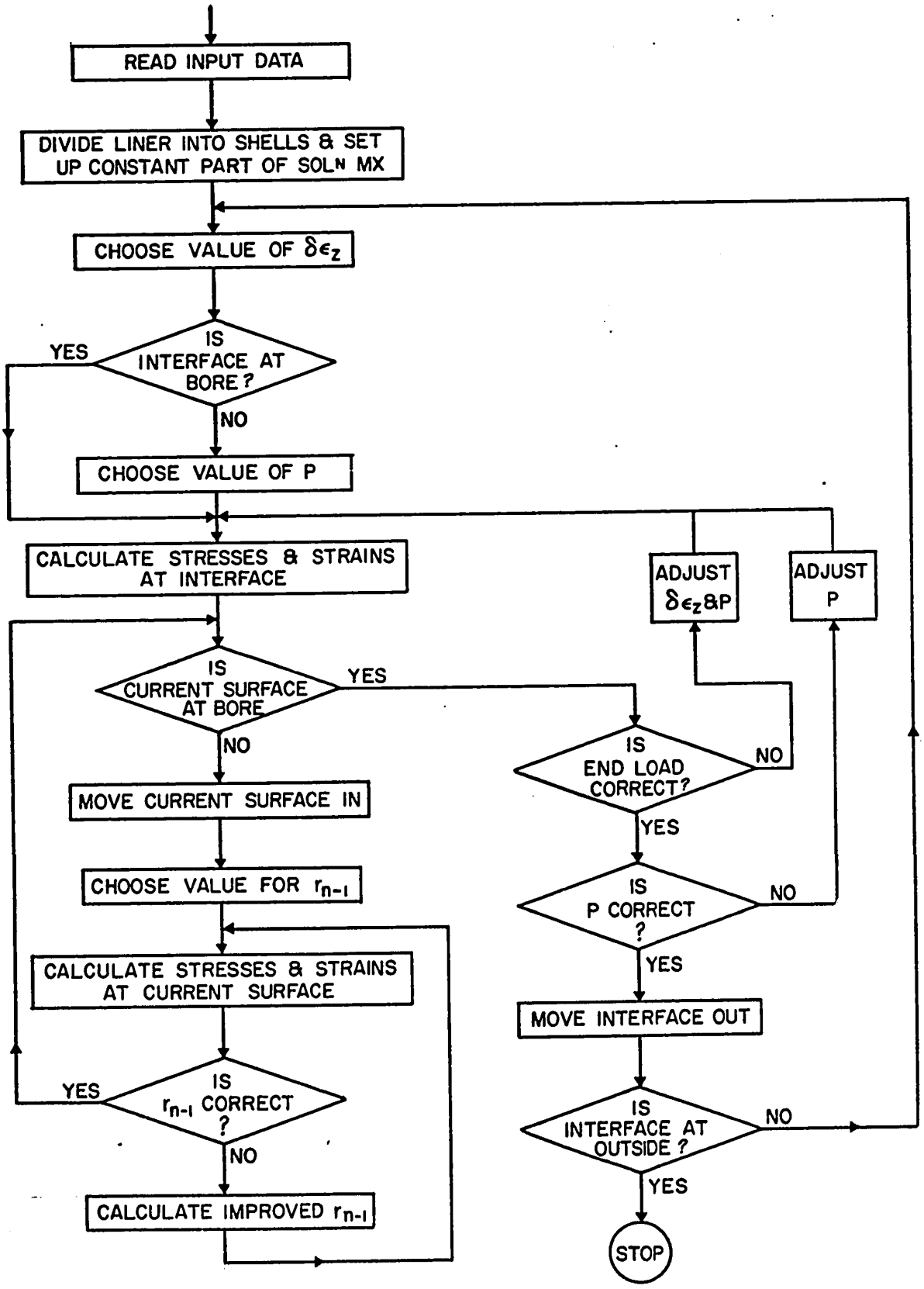

FIG. 10 FLOW CHART OF NUMERICAL METHOD

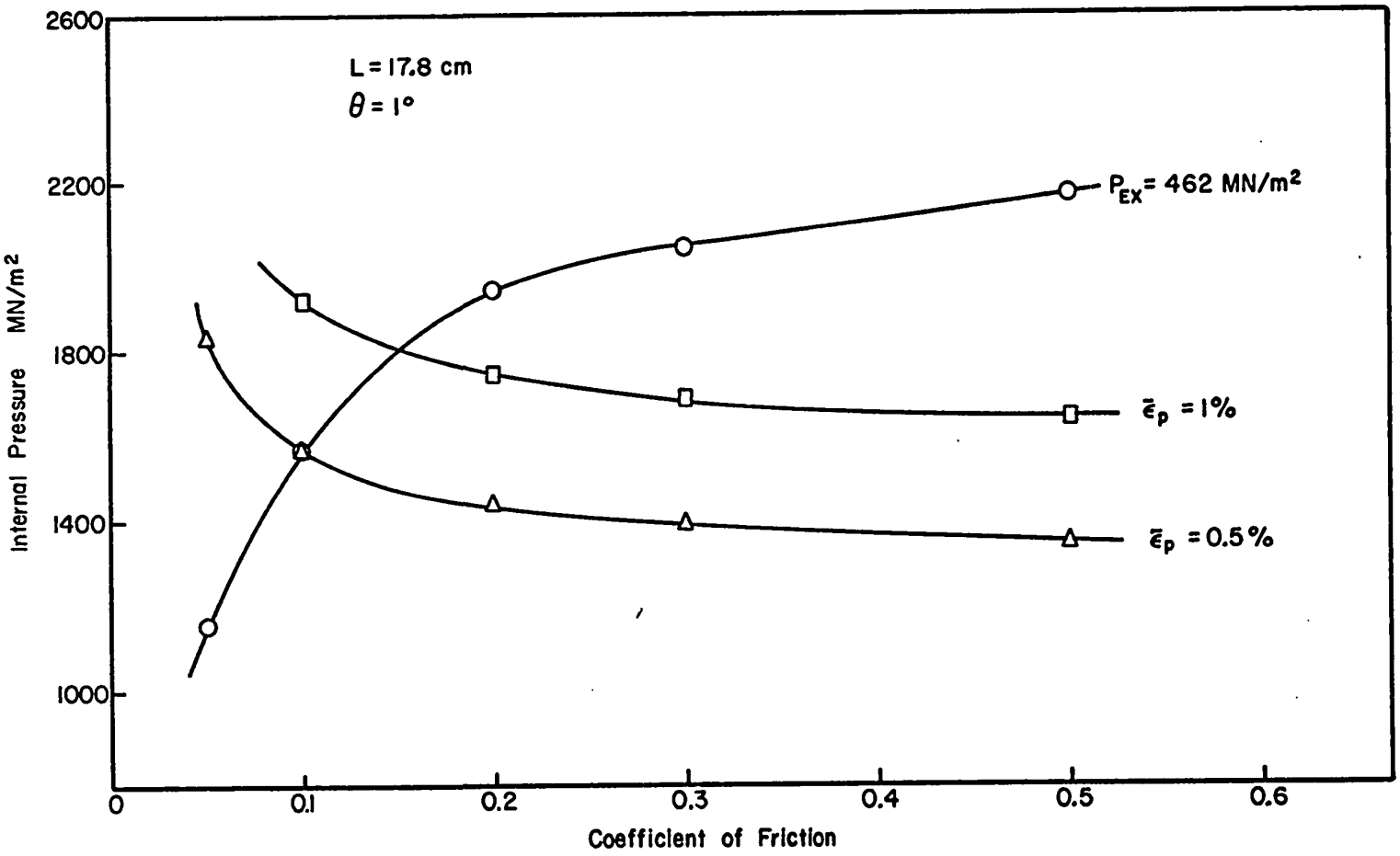

FIG. 11 VARIATION OF INTERNAL PRESSURE WITH COEFFICIENT OF FRICTION

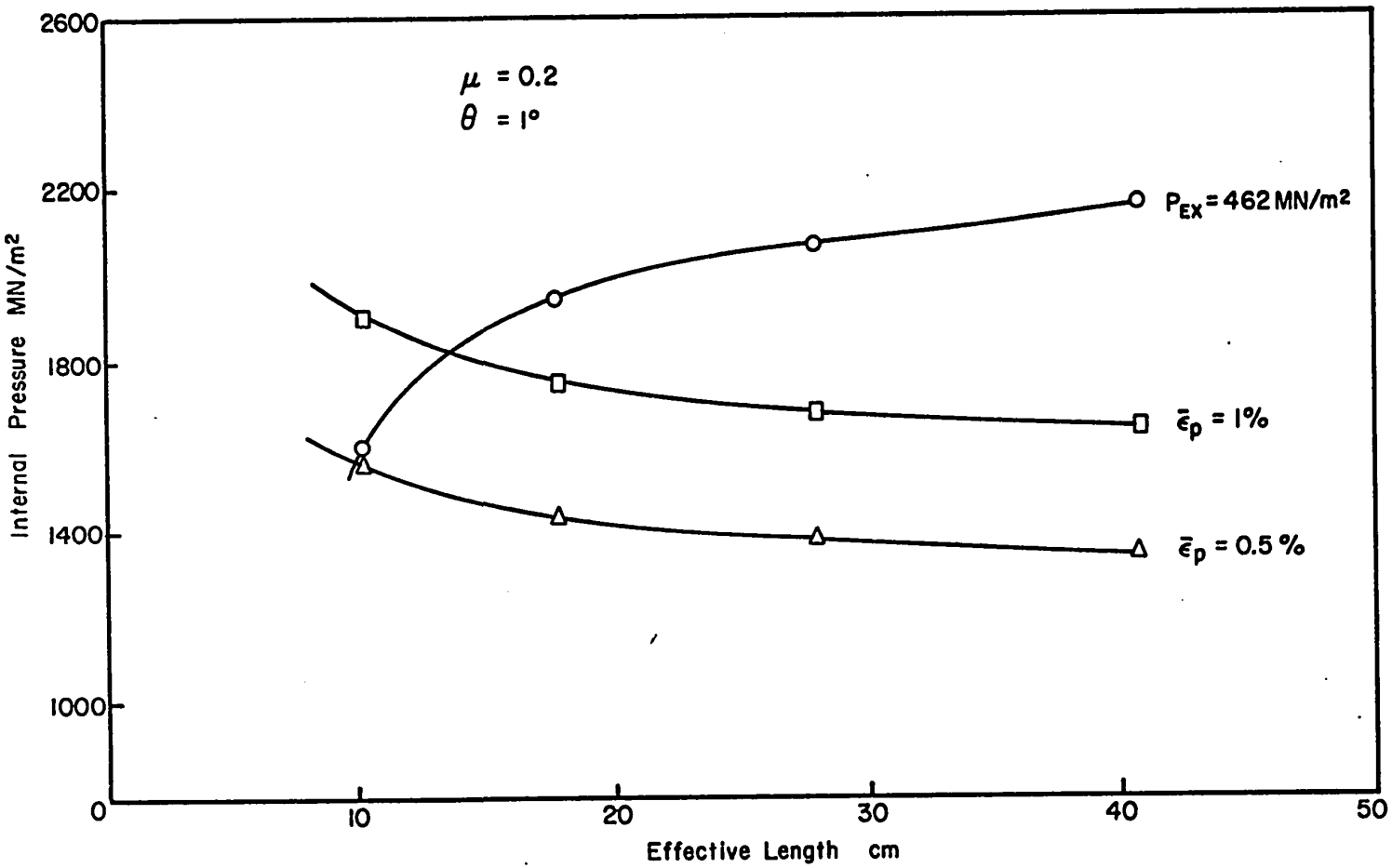

FIG. 12 VARIATION OF INTERNAL PRESSURE WITH EFFECTIVE LINER LENGTH

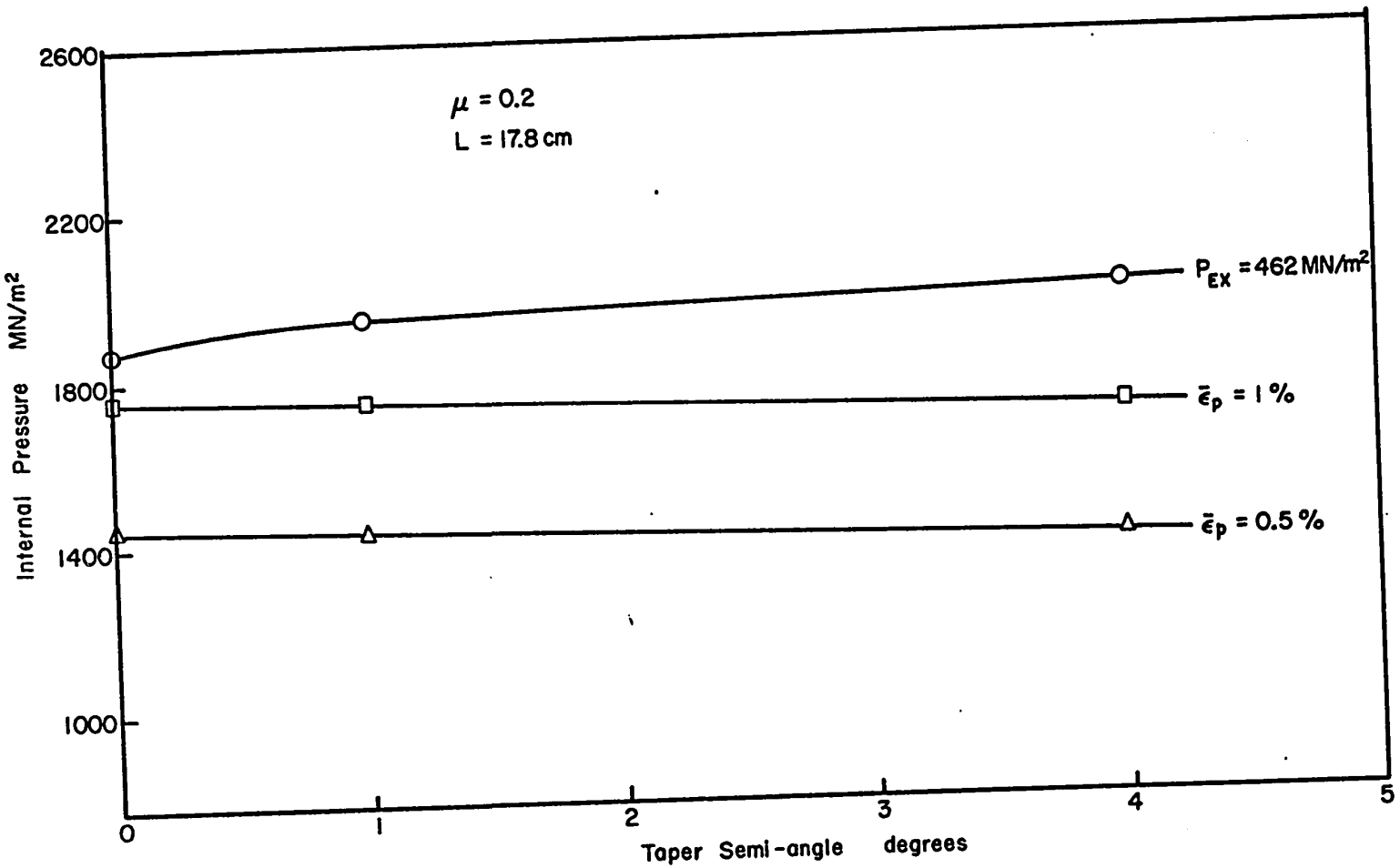

FIG. 13 VARIATION OF INTERNAL PRESSURE WITH TAPER SEMI-ANGLE

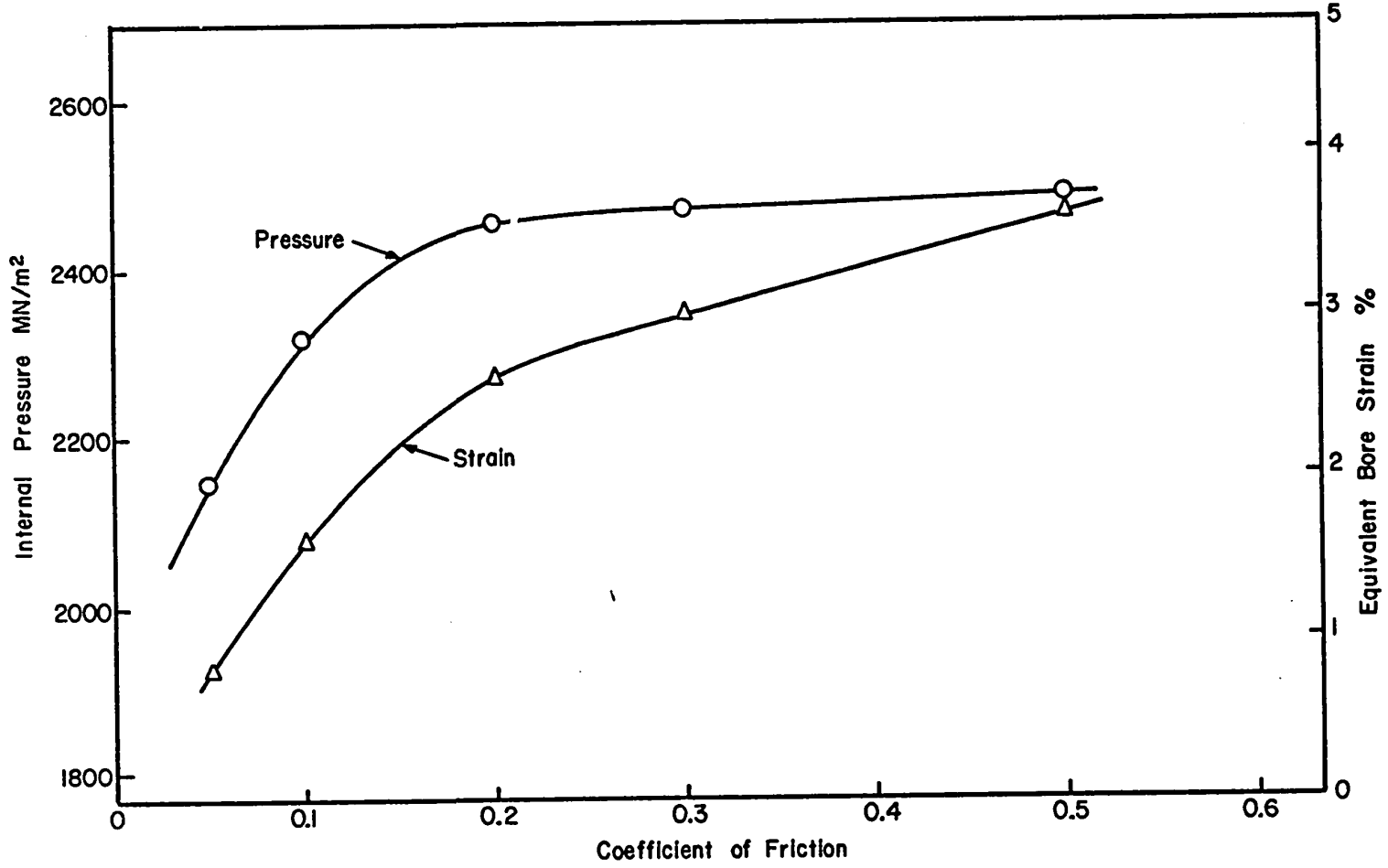

FIG. 14 VARIATION OF LIMITING EQUIVALENT BORE STRAIN WITH COEFFICIENT OF FRICTION

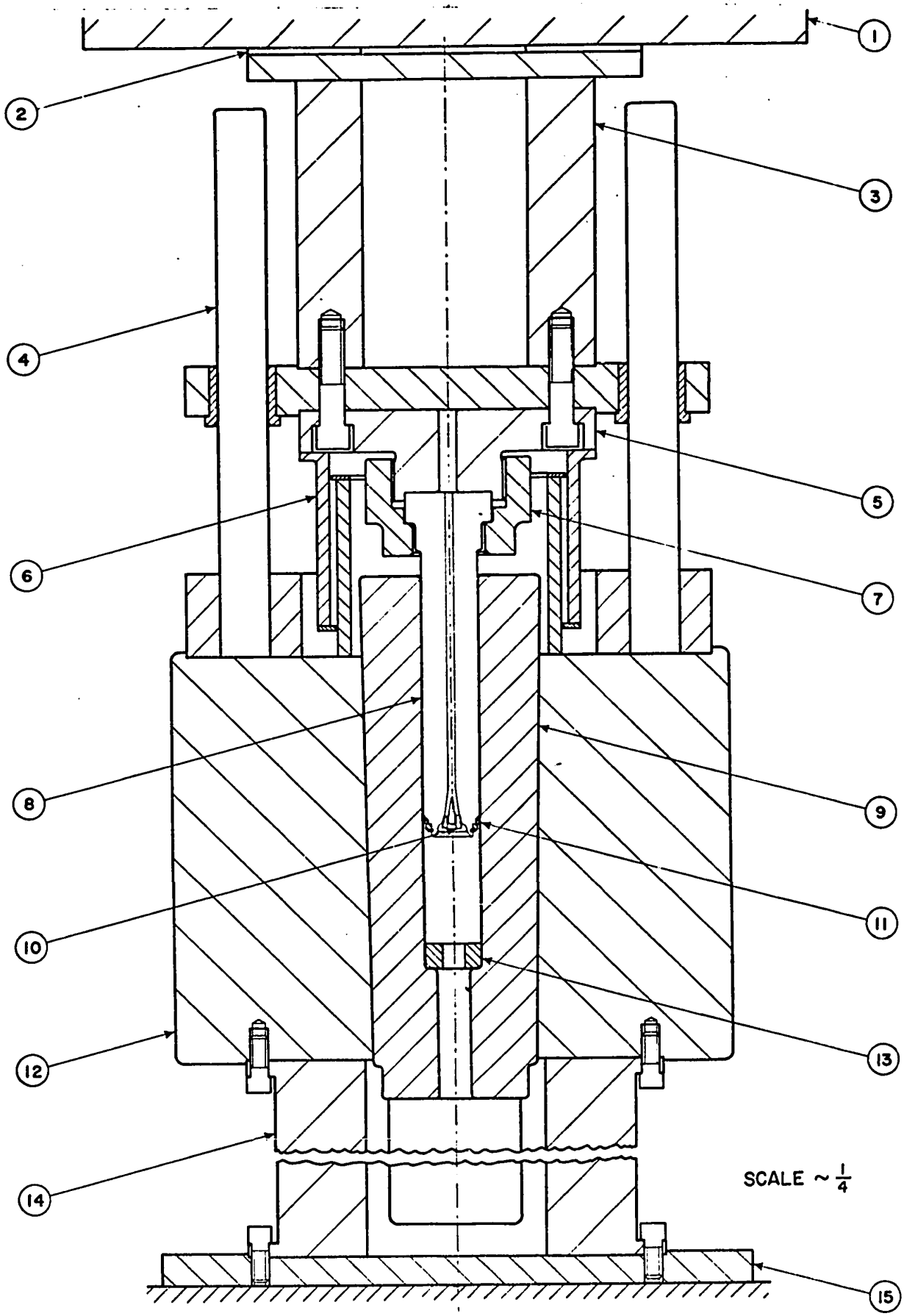

FIG. 15 CROSS SECTION OF INITIAL DESIGN OF COMPACTION AND EXTRUSION APPARATUS

KEY TO FIGURE 15

1. Top platen of press
2. Lead gasket
3. Press attachment bolster
4. Die set
5. Plunger retaining plate
6. Plunger safety jacket
7. Plunger retaining nut
8. Plunger
9. Liner
10. Terminals for manganin coil
11. O-ring seals
12. Container
13. Maximum hardness pad
14. Stool
15. Baseplate

Machine to final size all over.
Polish
Vacuum harden to 62R_C
Final polish

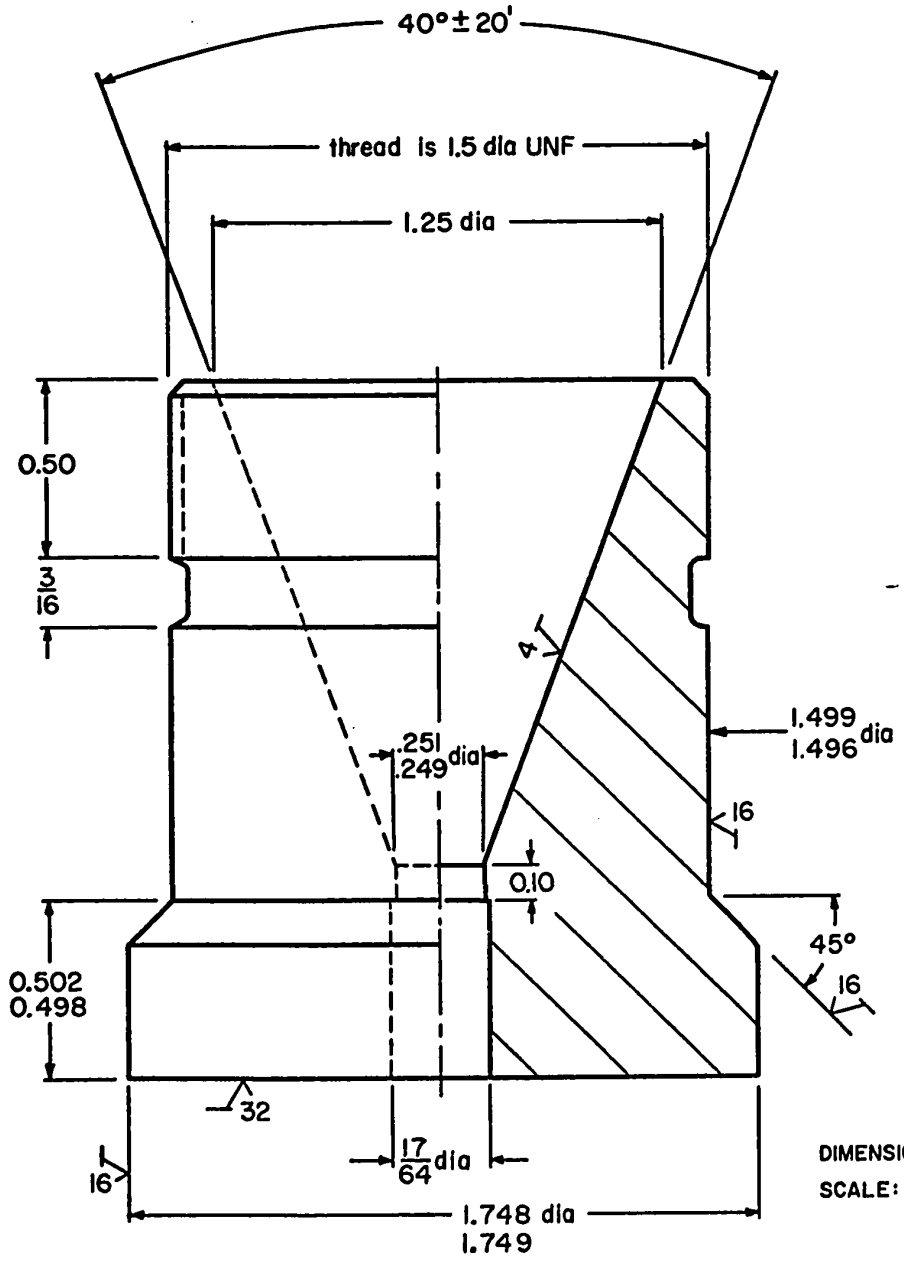

DIMENSIONS IN INCHES
SCALE: X2

FIG. 16 EXTRUSION DIE

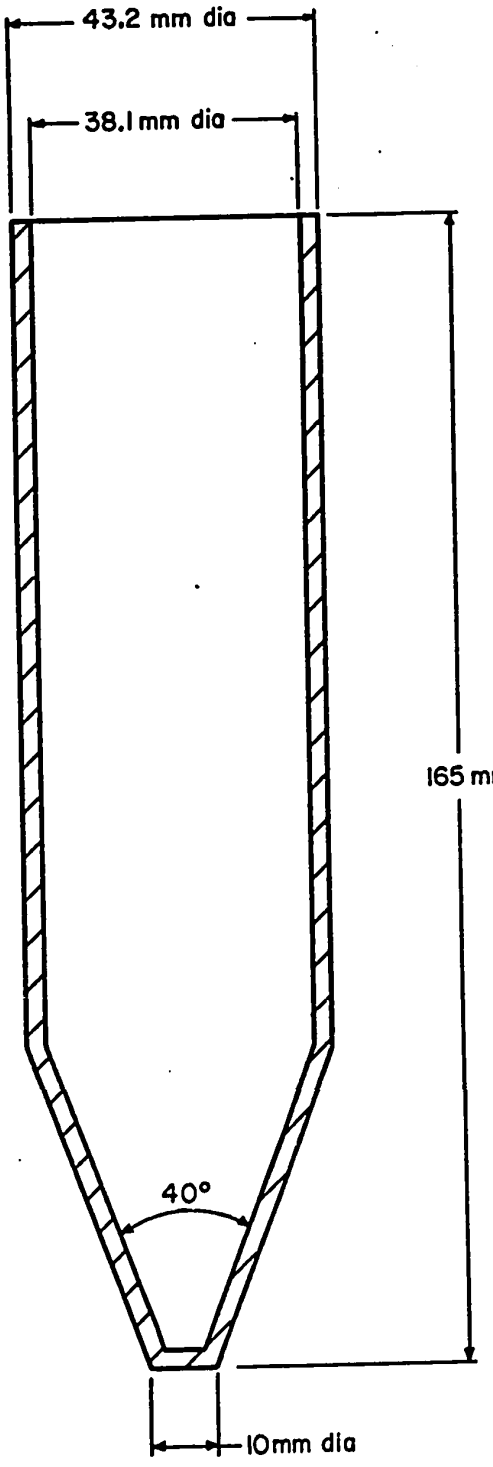

MOULDED FROM
FLEXANE 95

SCALE: FULL SIZE

FIG. 17 COMPACTION BAG

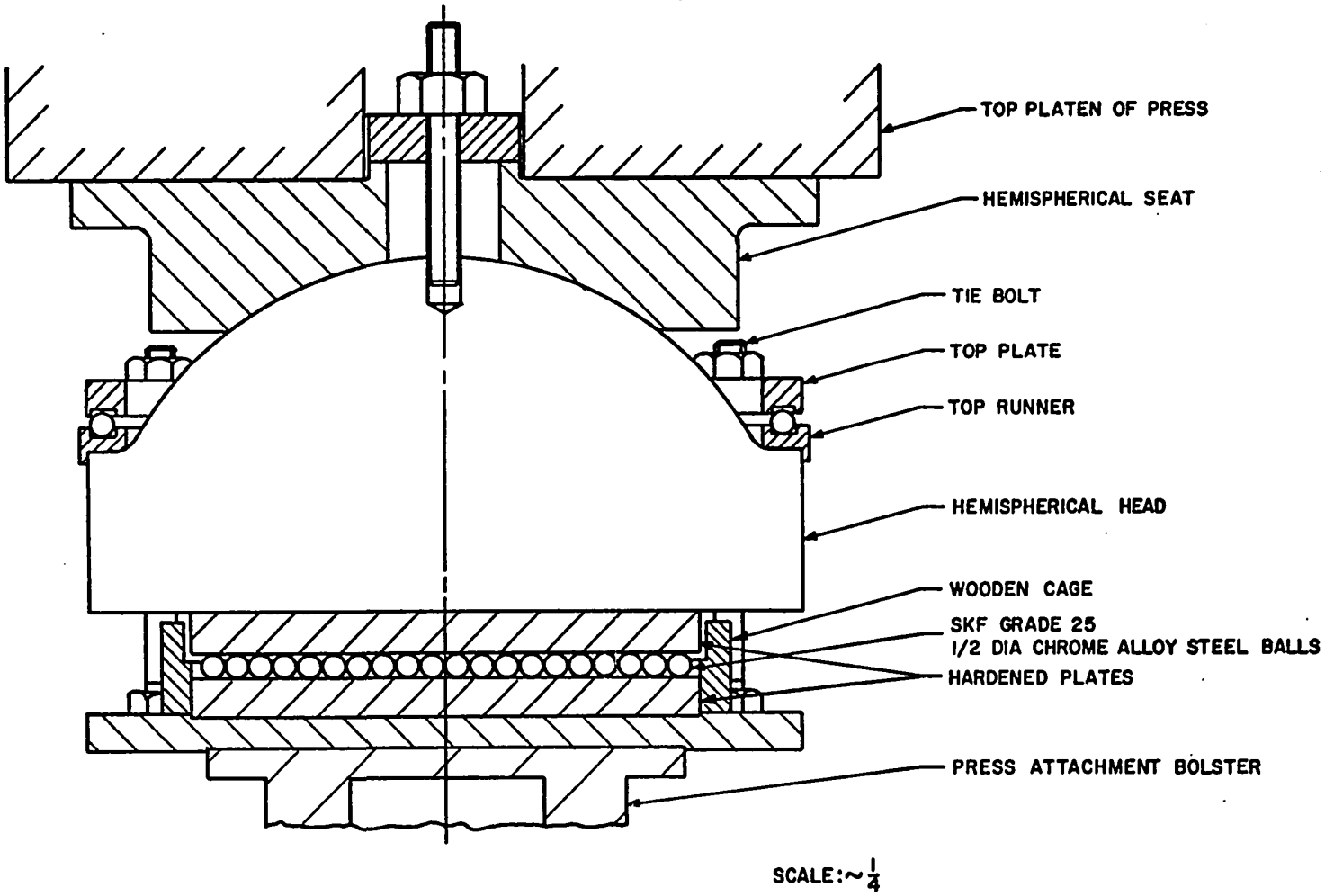

FIG. 18 MODIFIED PRESS ATTACHMENT ASSEMBLY

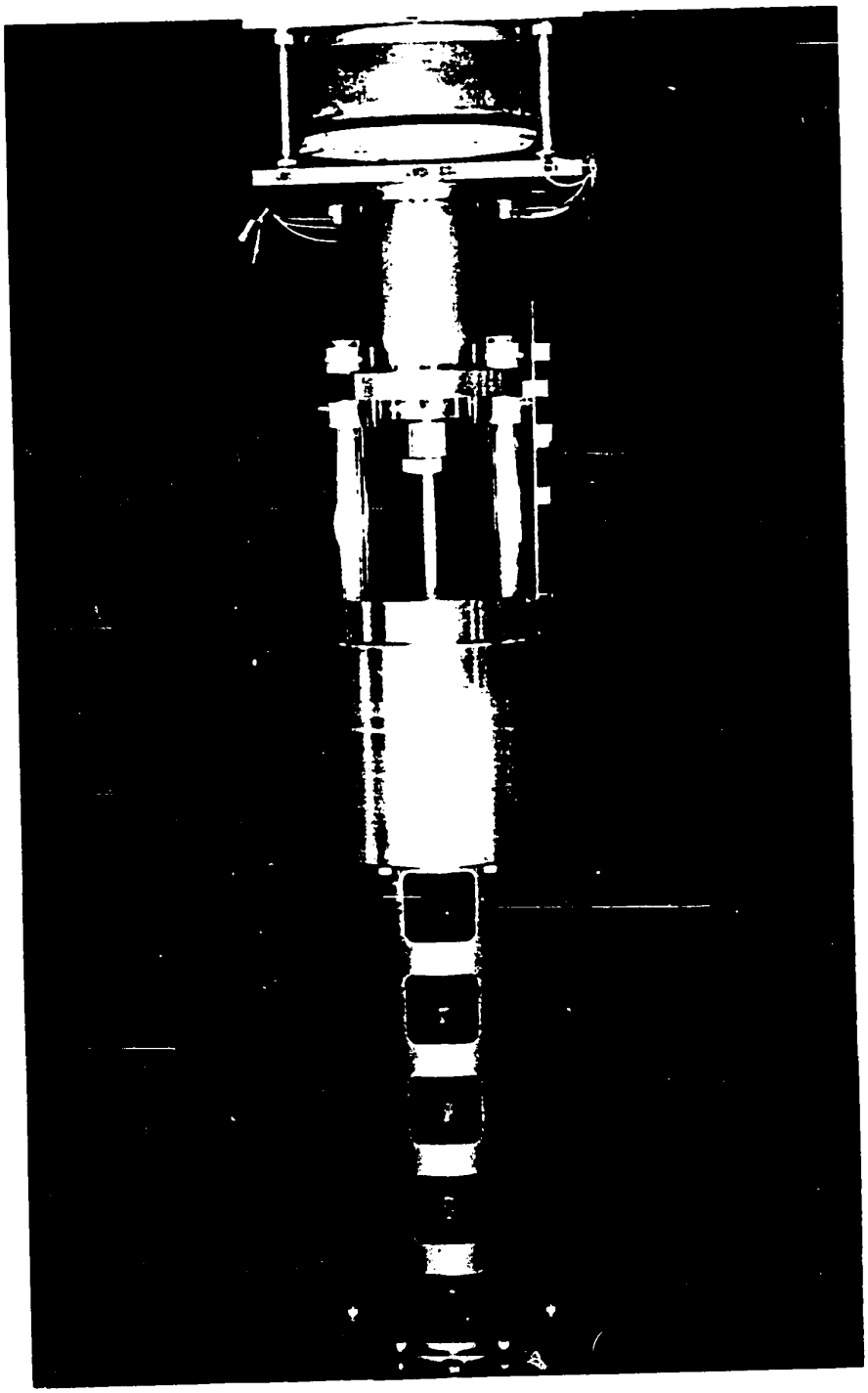

FIG. 19 COMPLETED COMPACTION AND EXTRUSION EQUIPMENT

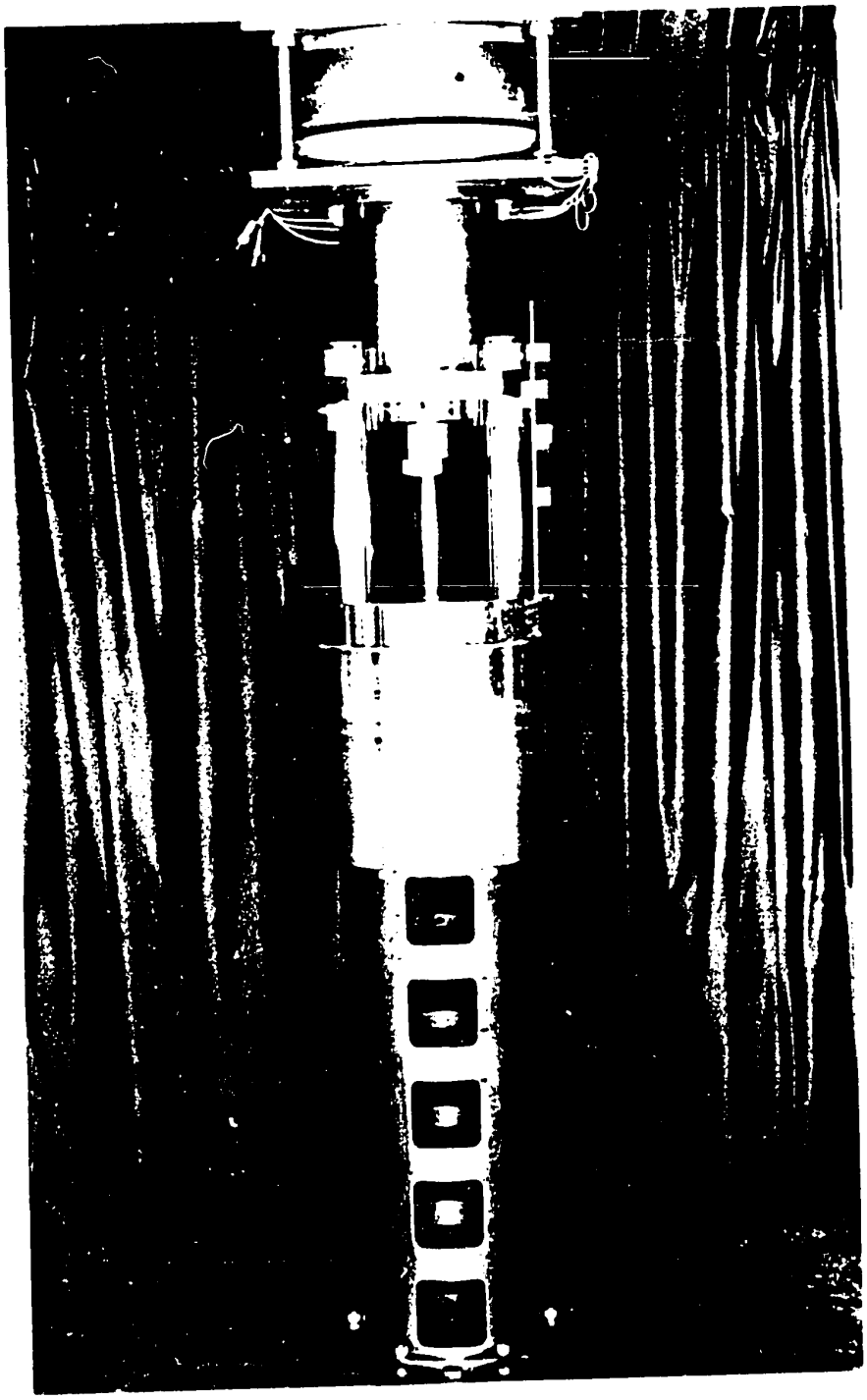

FIG. 19 COMPLETED COMPACTION AND EXTRUSION EQUIPMENT

(a) ATOMET 28

Atomized iron powder

Initial yield strength ~ 210 MN/m^2

Hardness ~ 90 VPN

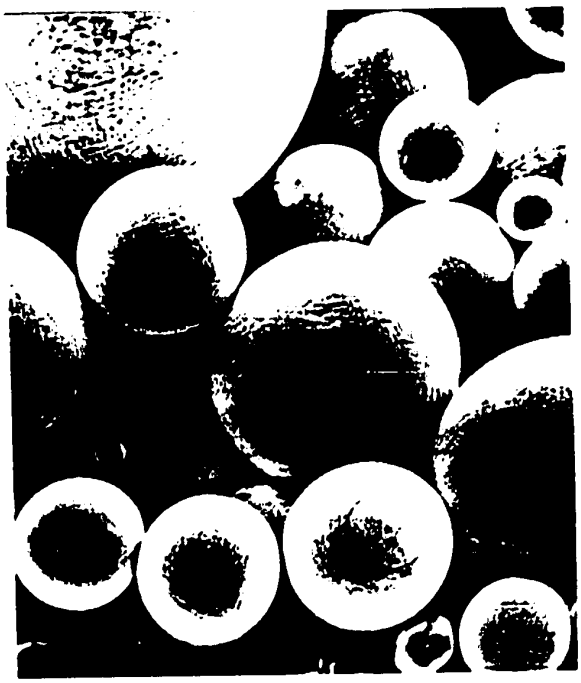

(b) INCO 713LC

Argon atomized nickel base superalloy

Initial yield strength ~ 1000 MN/m^2

Hardness ~ 375 VPN

FIG. 20 SCANNING ELECTRON MICROGRAPHS OF AS-RECEIVED IRON AND SUPERALLOY POWDERS

ALCOA 1202

Atomized aluminum powder

Initial yield strength ~ 35 MN/m^2

Hardness ~ 24 VPN

Typical composition (%)

Al	99.4
Al_2O_3	.3
Fe	.15
Si	.07
other metallics each	.01

FIG. 21 SCANNING ELECTRON MICROGRAPHS OF AS-RECEIVED ALUMINUM POWDER

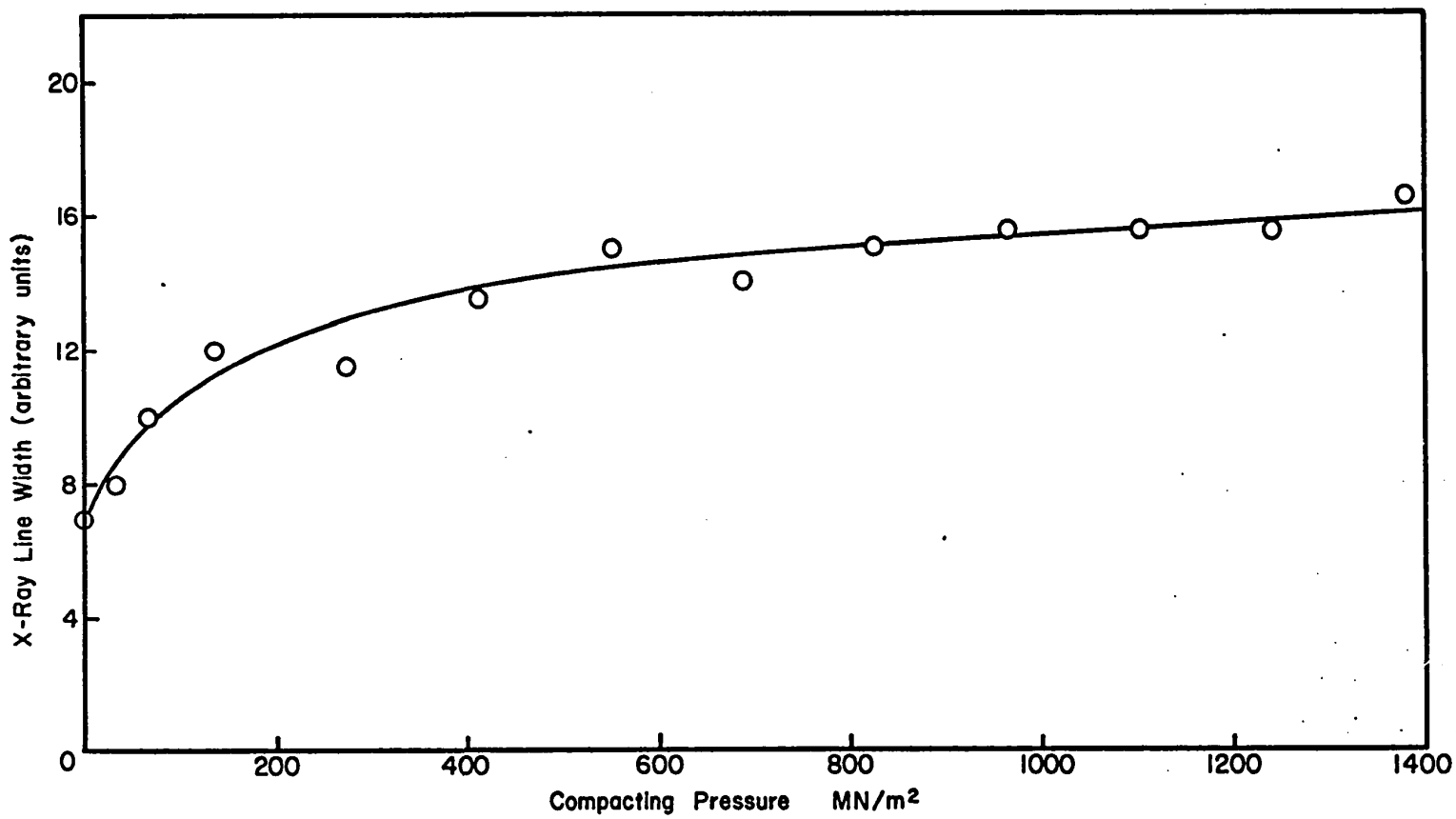

FIG. 22 VARIATION IN X-RAY LINE WIDTH WITH COMPACTING PRESSURE FOR IRON COMPACTS

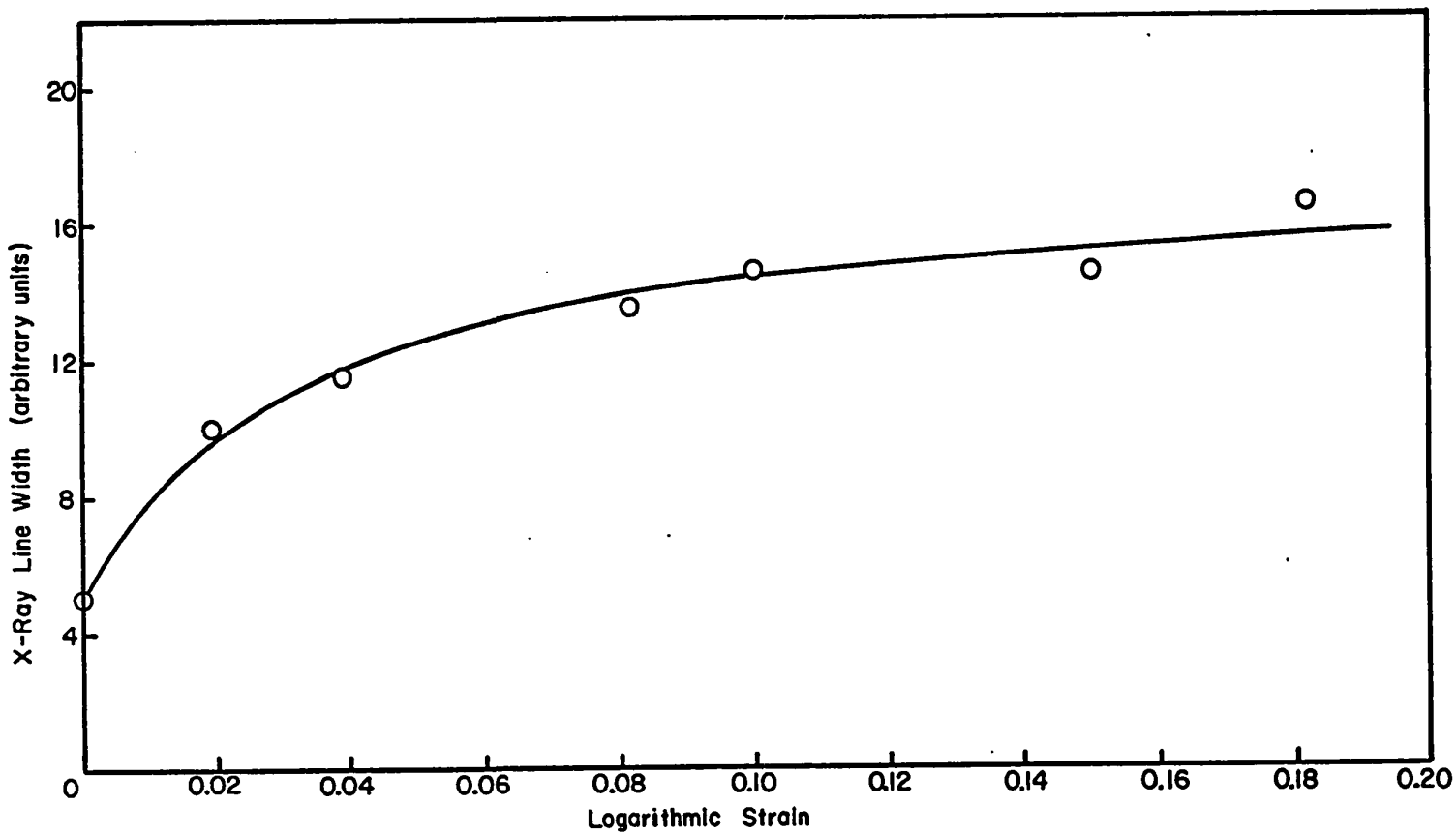

FIG. 23 VARIATION IN X-RAY LINE WIDTHS WITH STRAIN FOR THE CALIBRATION SAMPLES

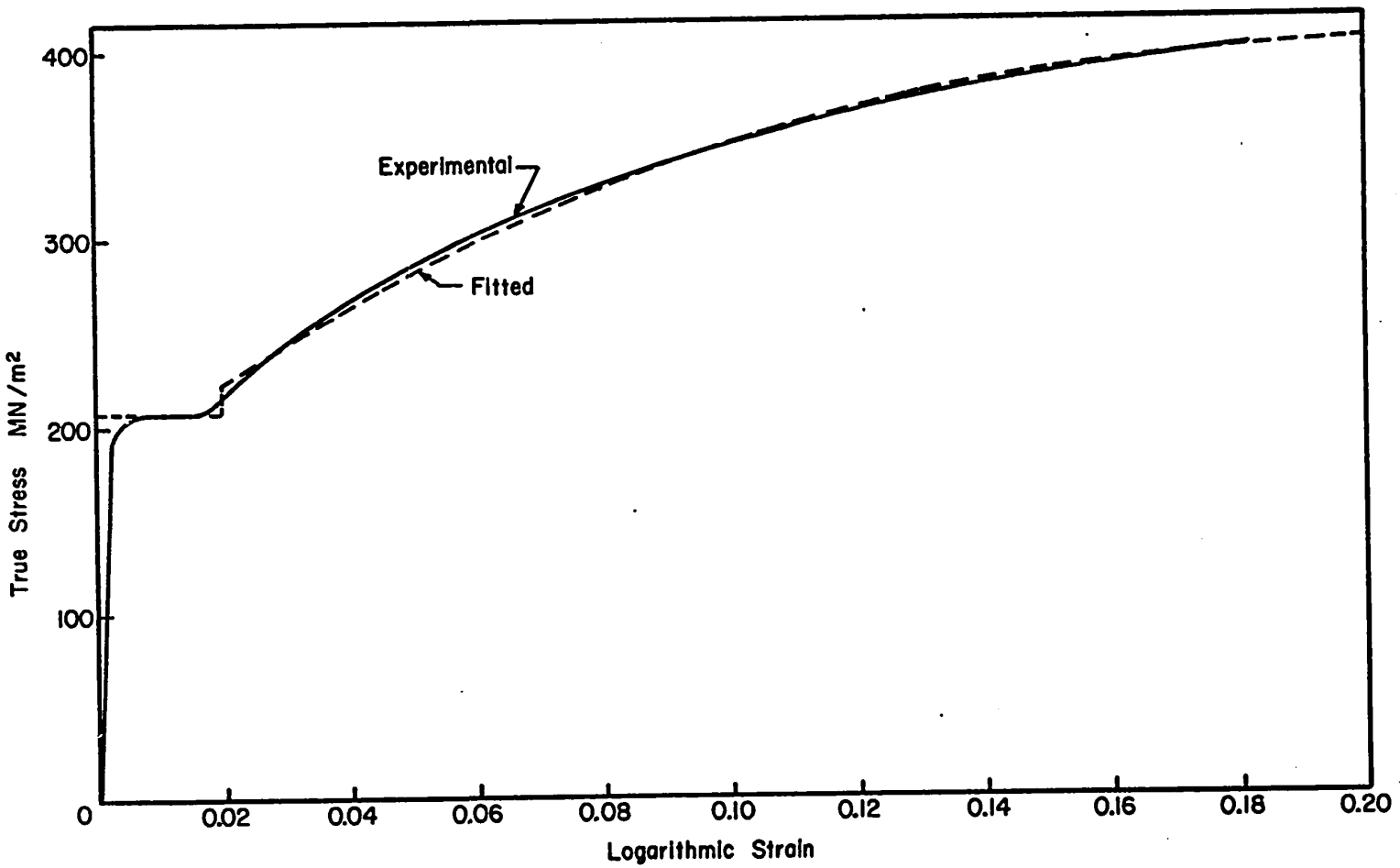

FIG. 24 EXPERIMENTAL AND FITTED STRESS-STRAIN CURVES FOR SINTERED ATOMET 28 IRON POWDER COMPACT

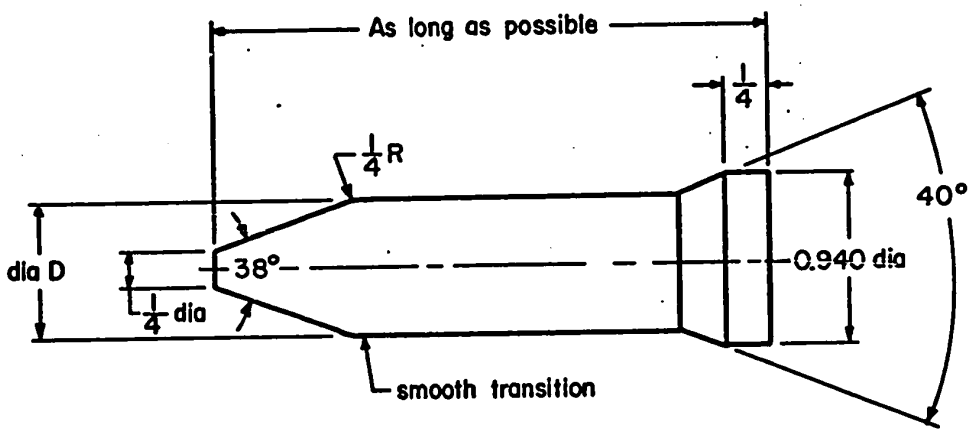

ALL DIMENSIONS IN INCHES

(a) BILLET FOR IRON COMPACTS

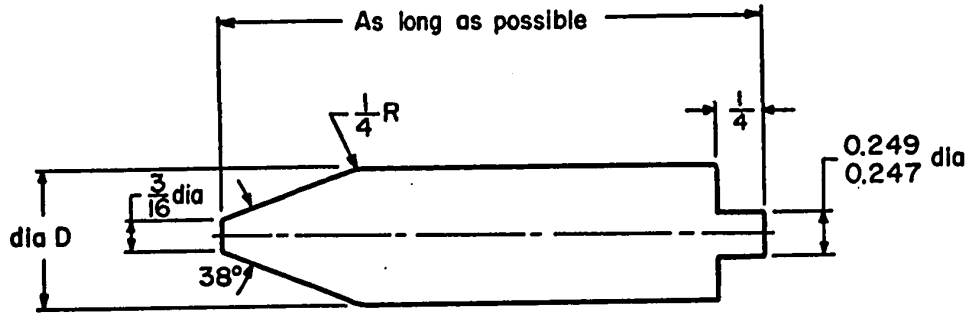

ALL DIMENSIONS IN INCHES

(b) BILLET FOR ALUMINUM COMPACTS

FIG. 25 HYDROSTATIC EXTRUSION BILLETS

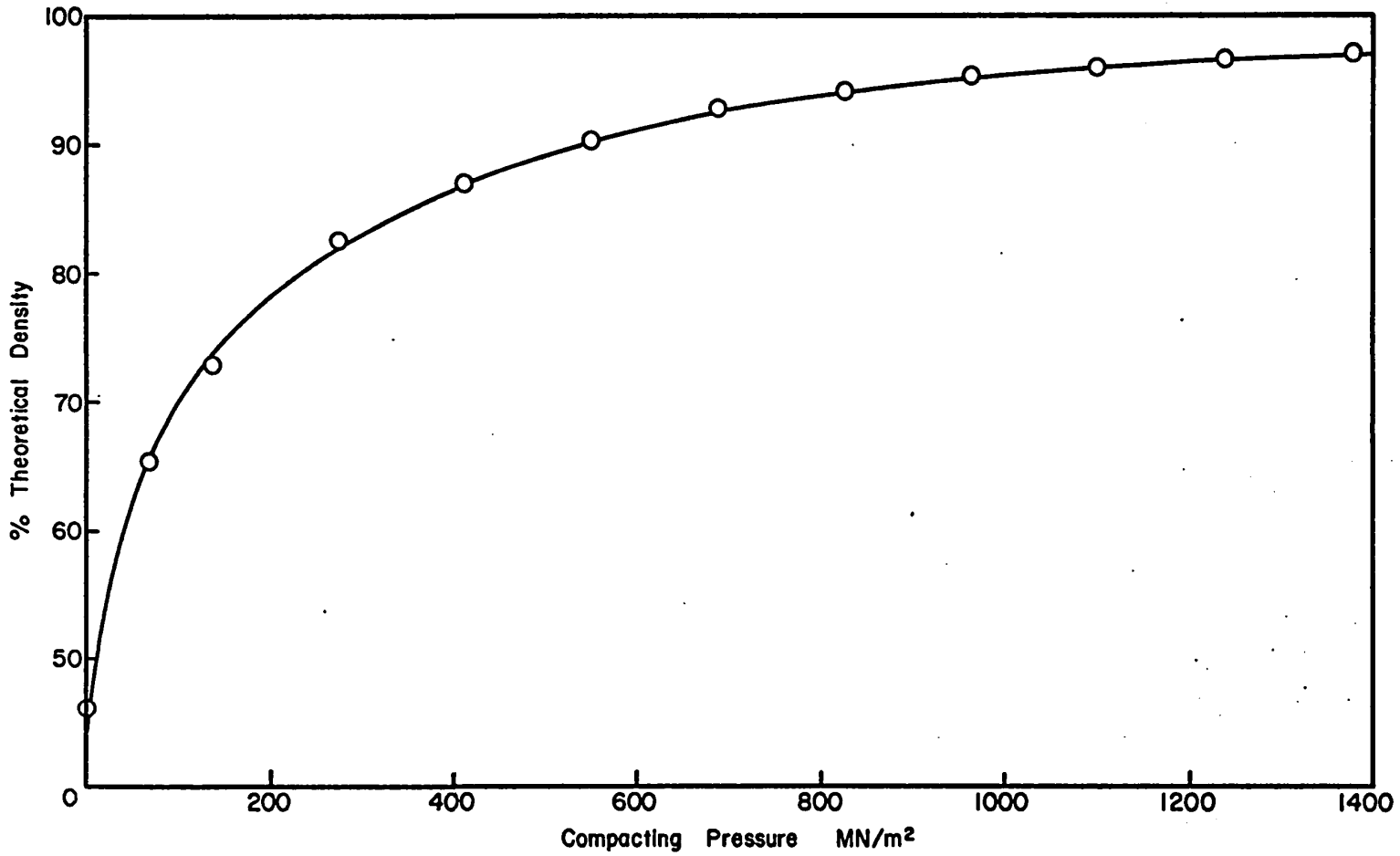

FIG. 26 EXPERIMENTAL PRESSURE-DENSITY DATA FOR ATOMET 28 IRON POWDER EXPRESSED DIRECTLY

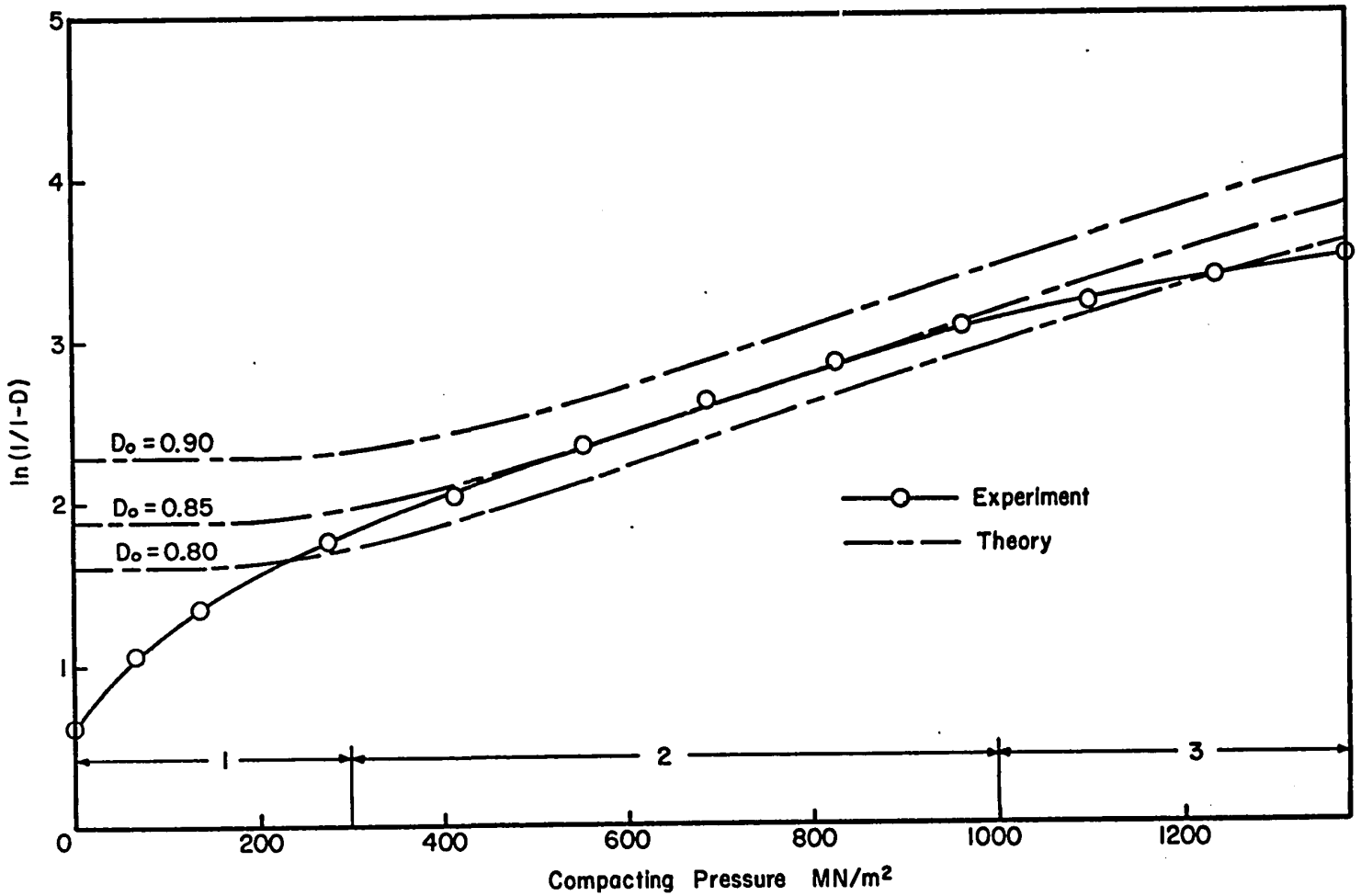

FIG. 27 COMPARISON OF EXPERIMENTAL AND PREDICTED VALUES OF Ln(1/1-D) FOR ATOMET 28 IRON POWDER USING DIFFERENT VALUES OF D_o

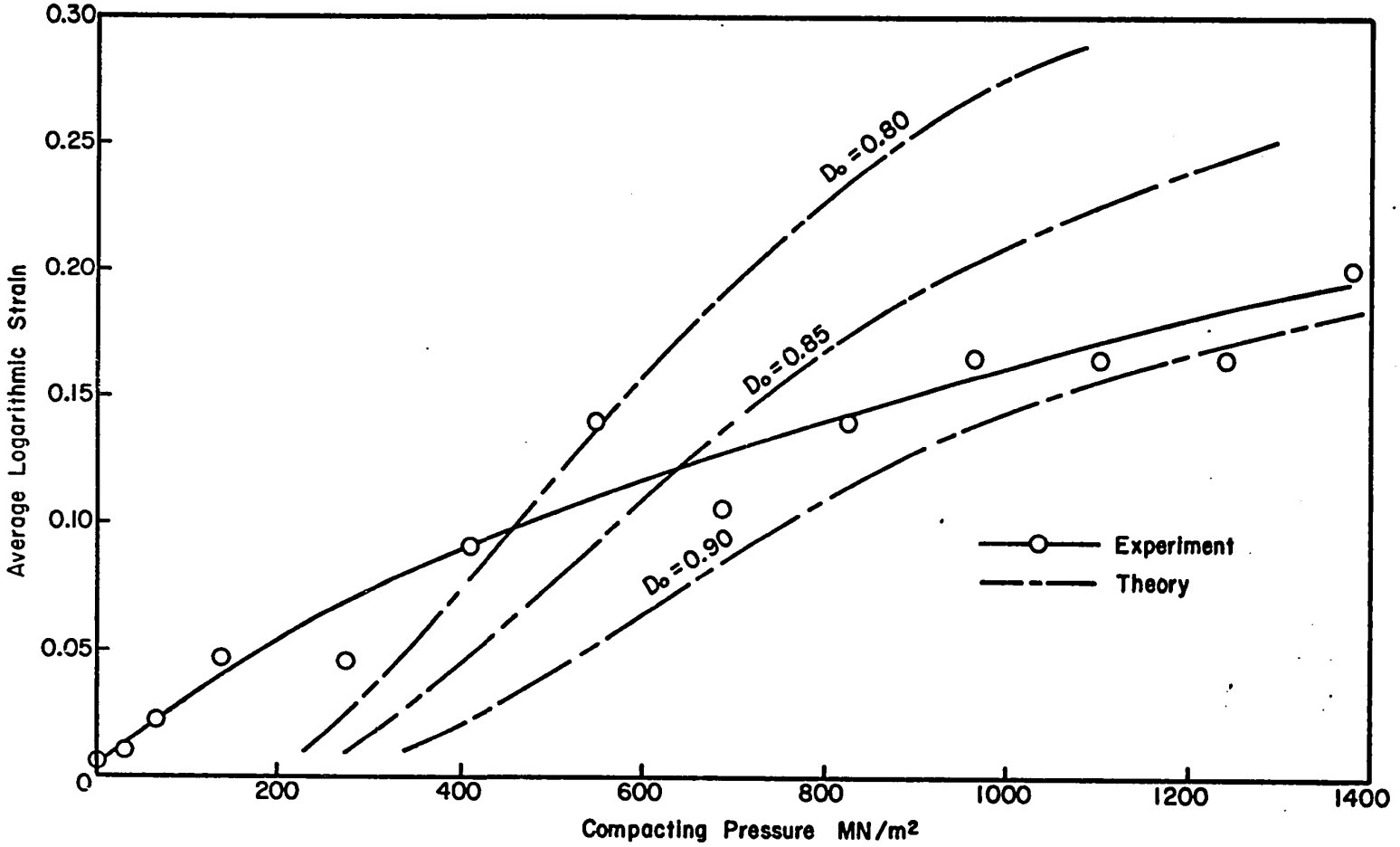

FIG. 28 COMPARISON OF EXPERIMENTAL AND PREDICTED VALUES OF STRAIN FOR ATOMET 28 IRON POWDER USING DIFFERENT VALUES OF D_o

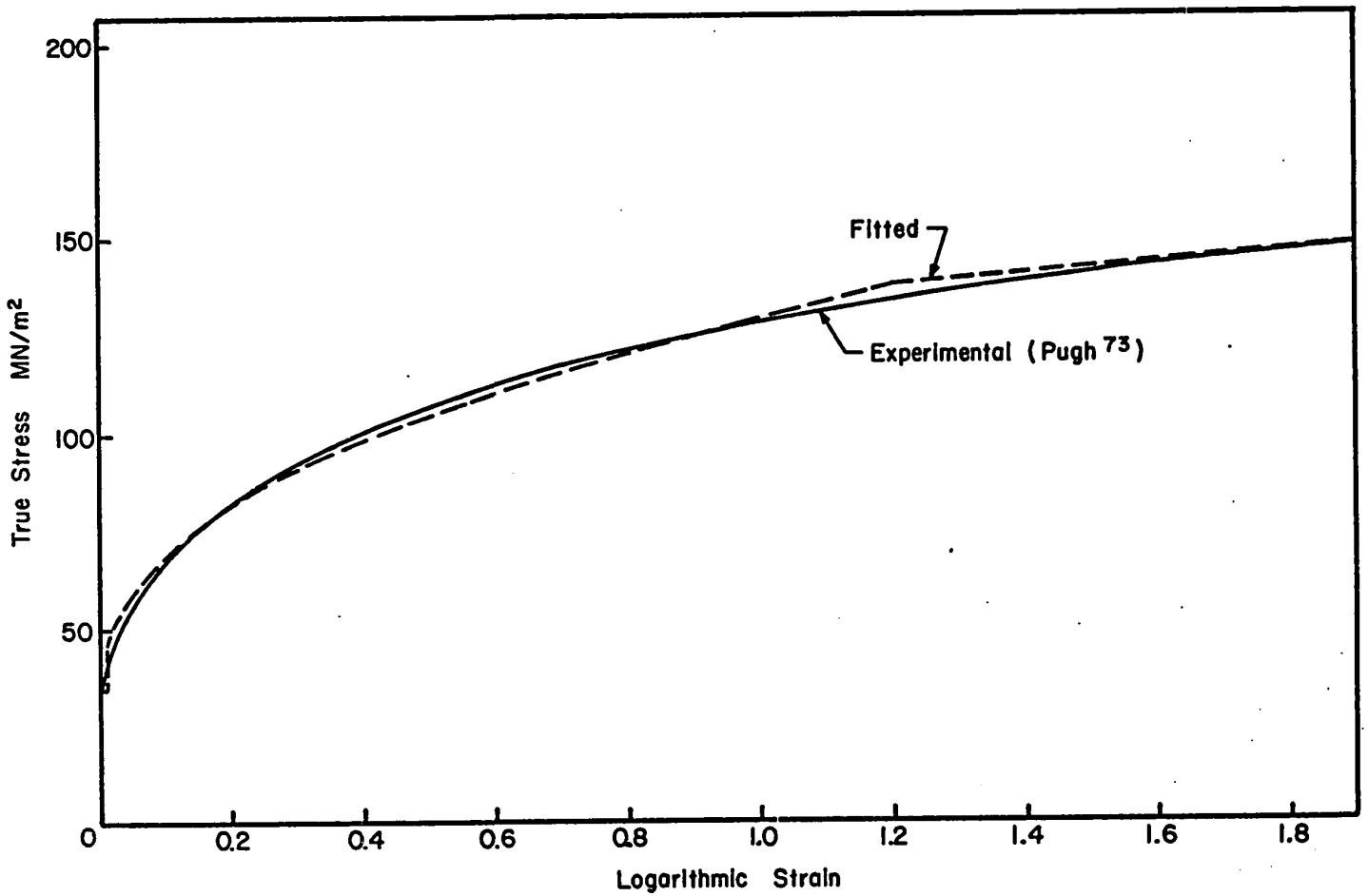

FIG. 29 EXPERIMENTAL AND FITTED STRESS-STRAIN CURVES FOR 99.5 % PURE ALUMINUM

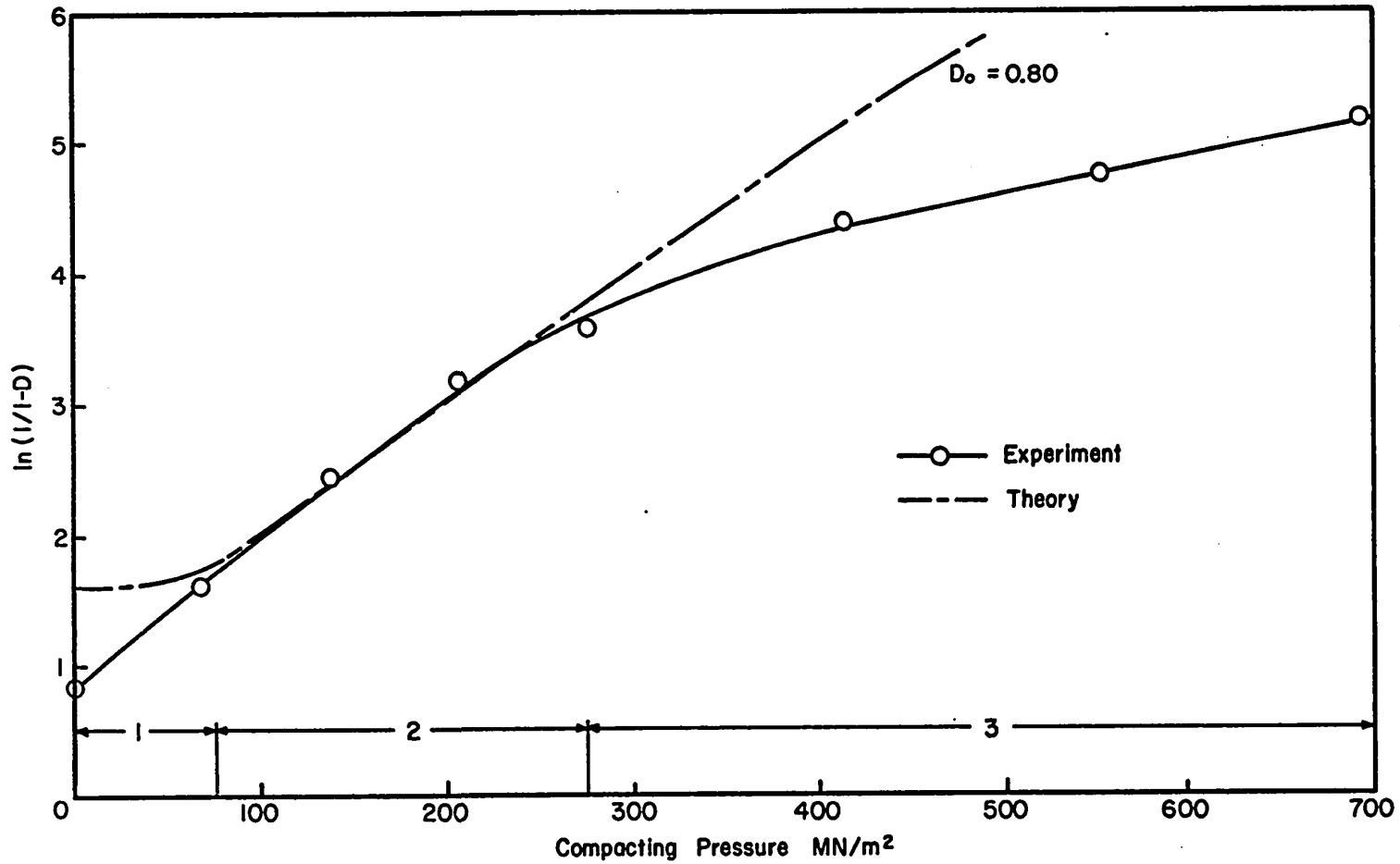

FIG. 30 COMPARISON OF EXPERIMENTAL AND PREDICTED VALUES OF Ln(1/1-D) FOR ALCOA GRADE 1202 ALUMINUM POWDER

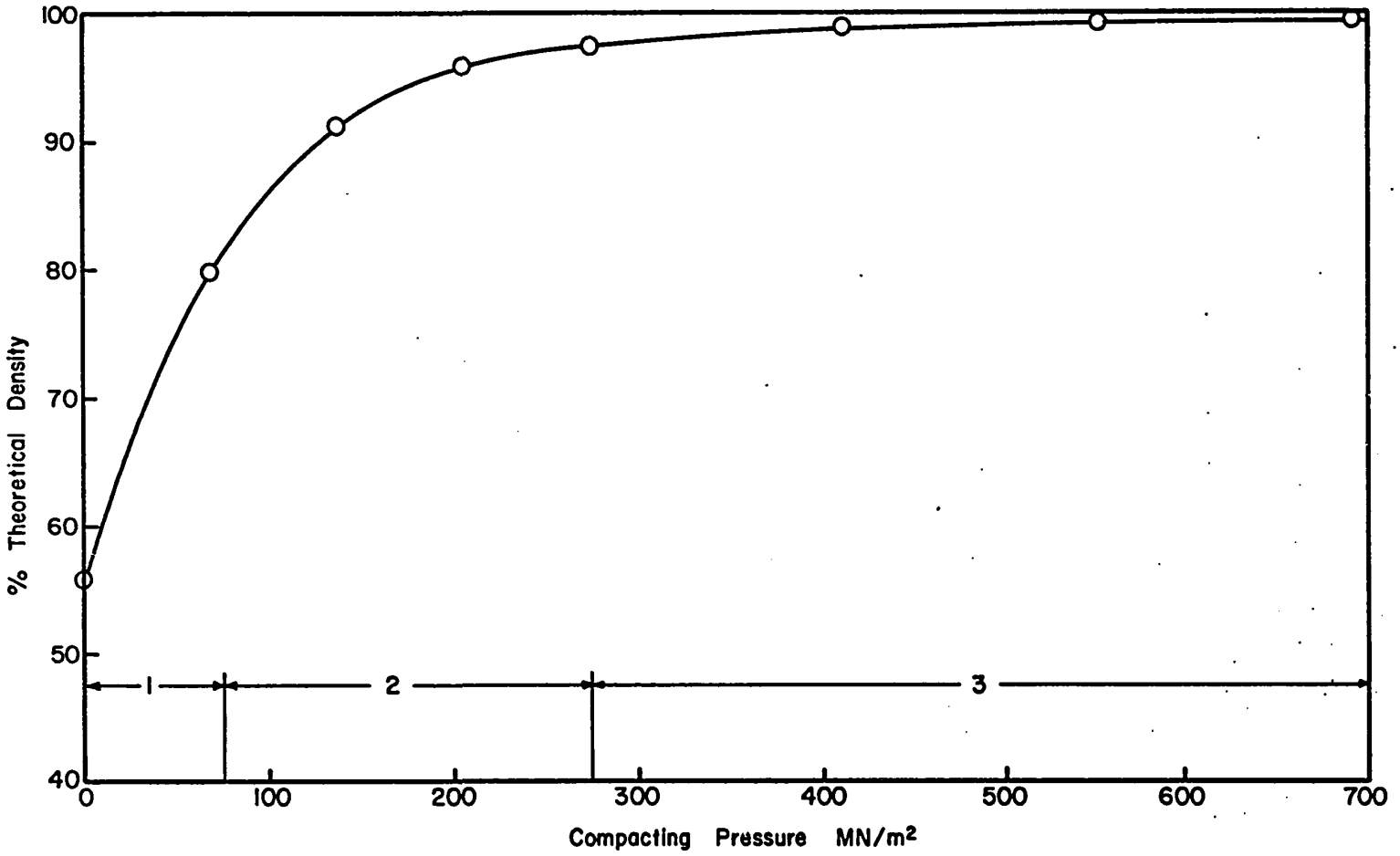

FIG. 31 EXPERIMENTAL PRESSURE-DENSITY DATA FOR ALCOA GRADE 1202 ALUMINUM POWDER EXPRESSED DIRECTLY

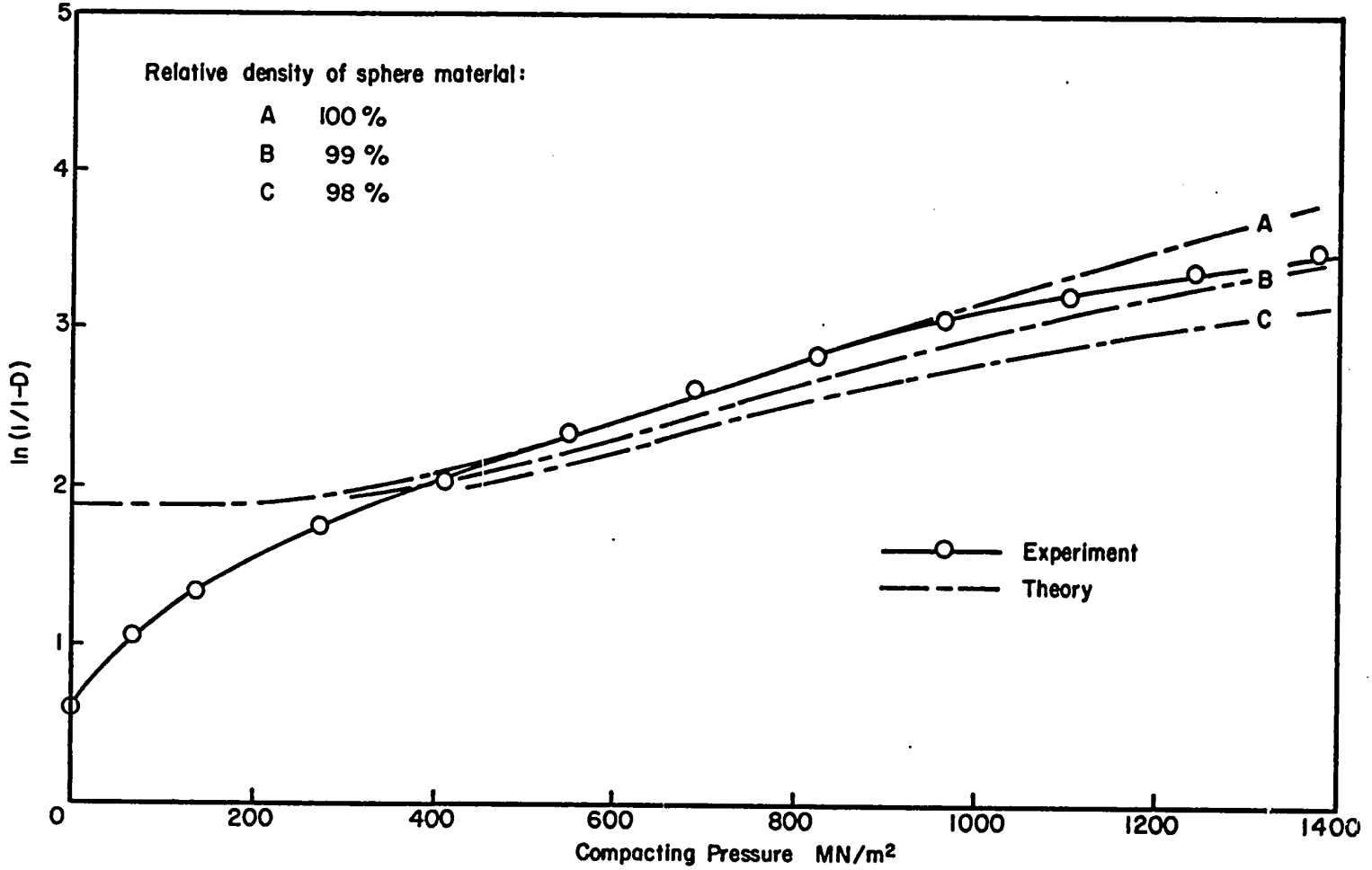

FIG. 32 EFFECT OF VARYING DENSITY OF SPHERE MATERIAL ON NUMERICAL PREDICTIONS OF Ln(1/1-D) FOR ATOMET 28 IRON POWDER USING $D_o = 0.85$

(a) 138 MN/m² unetched

(b) 415 MN/m² unetched

(c) 690 MN/m² etched 2% nital

(d) 1100 MN/m² etched 2% nital

FIG. 33 MICROSECTIONS OF ATOMET 28 IRON POWDER ISOSTATICALLY COMPACTED AT DIFFERENT PRESSURES

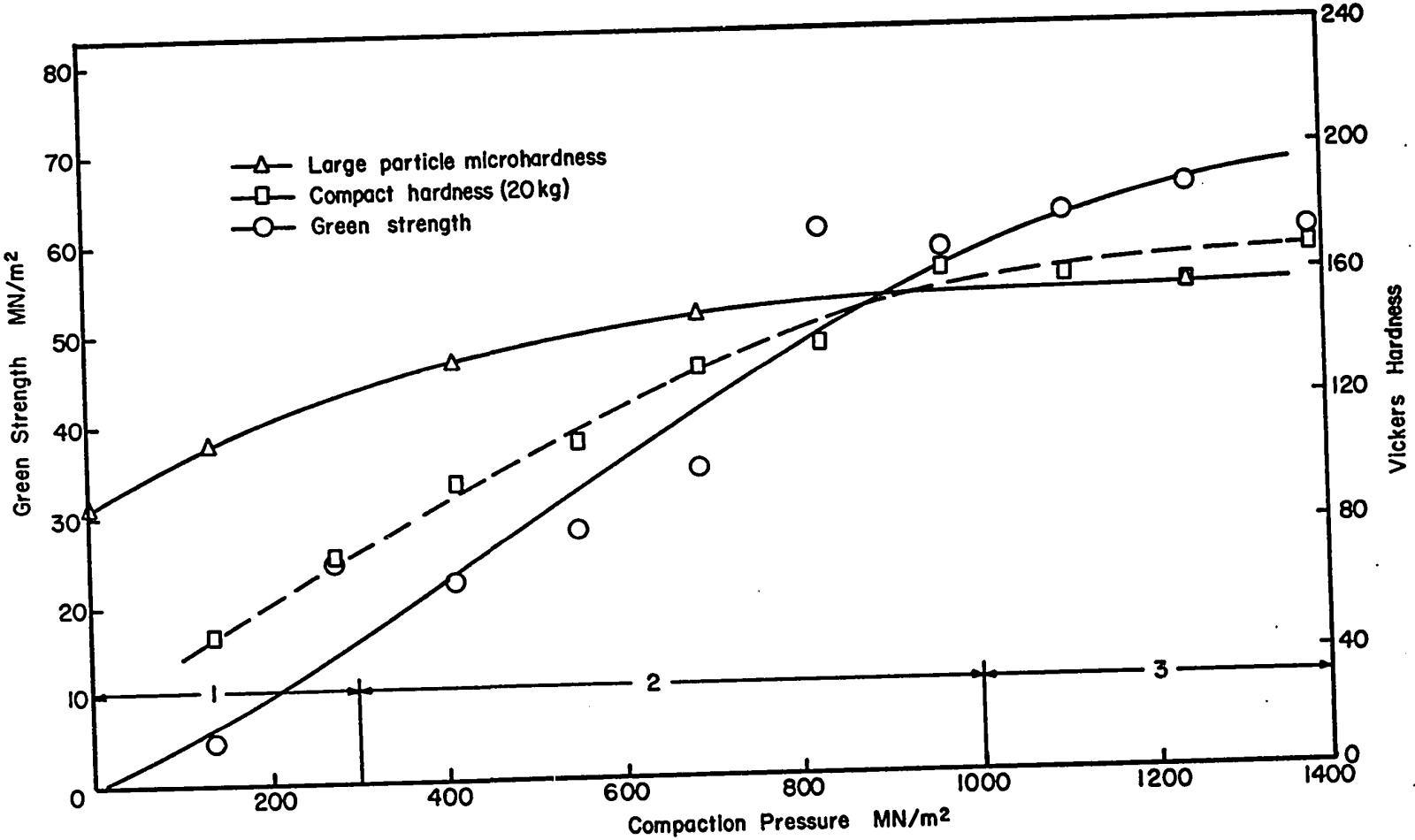

FIG. 34 VARIATION OF STRENGTH AND HARDNESS OF ATOMET 28 IRON COMPACTS WITH COMPACTING PRESSURE

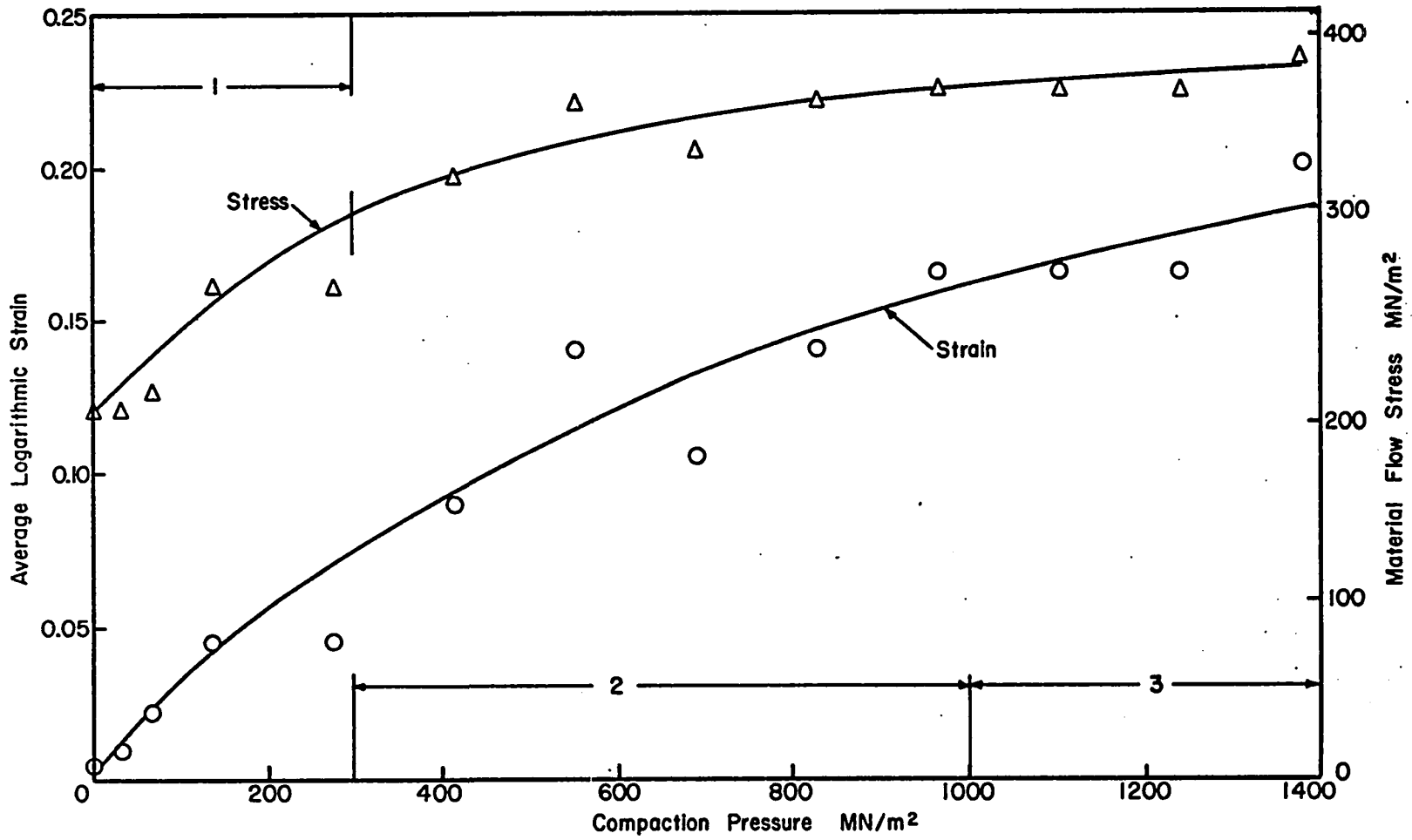

FIG. 35 VARIATION OF STRAIN AND FLOW STRESS OF ATOMET 28 IRON POWDER WITH COMPACTING PRESSURE

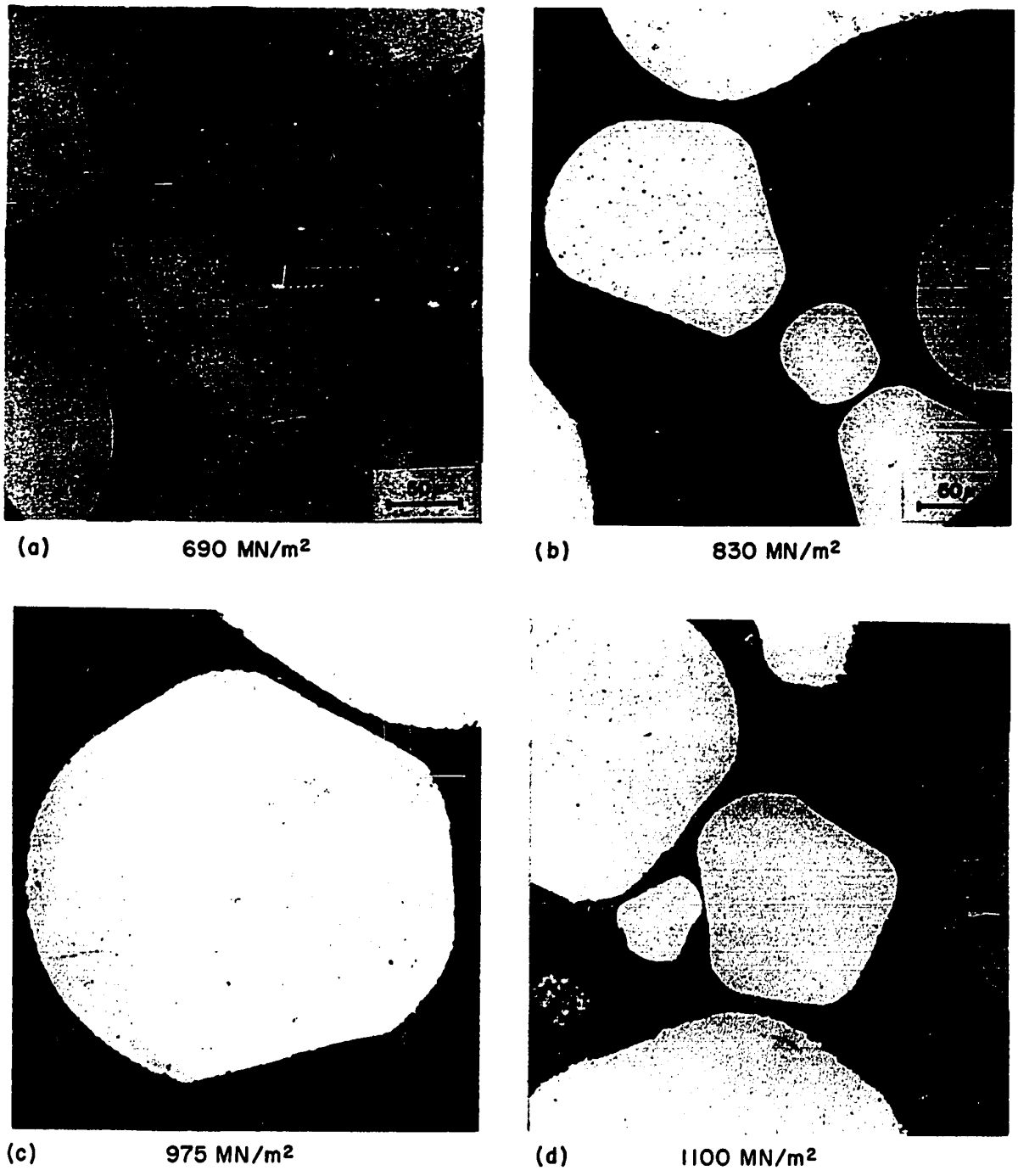

FIG. 36 MICROSECTIONS OF INCO 713 LC POWDER ISOSTATICALLY COMPACTED AT DIFFERENT PRESSURES

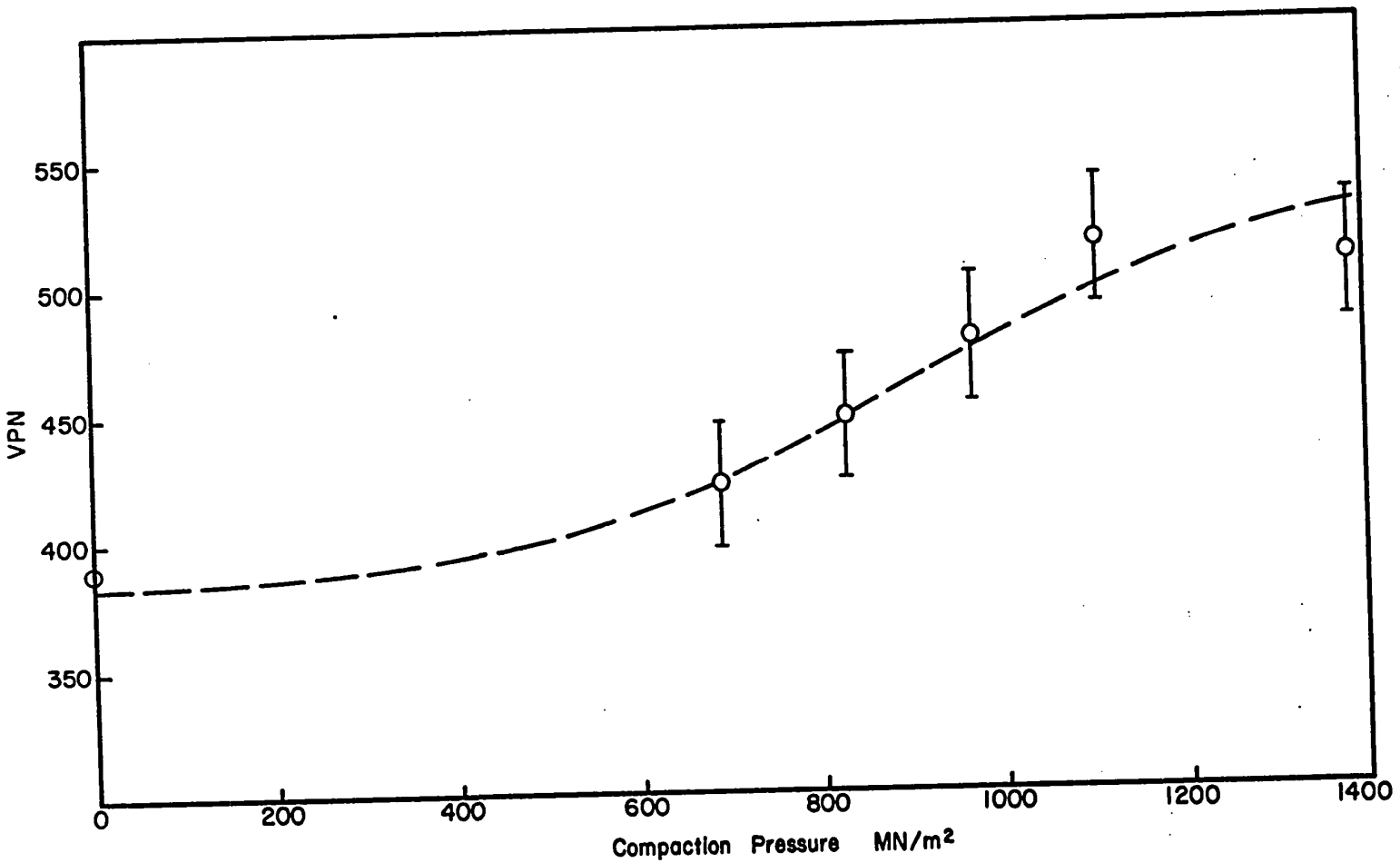

FIG. 37 VARIATION OF PARTICLE HARDNESS WITH COMPACTING PRESSURE FOR INCO 713LC POWDER

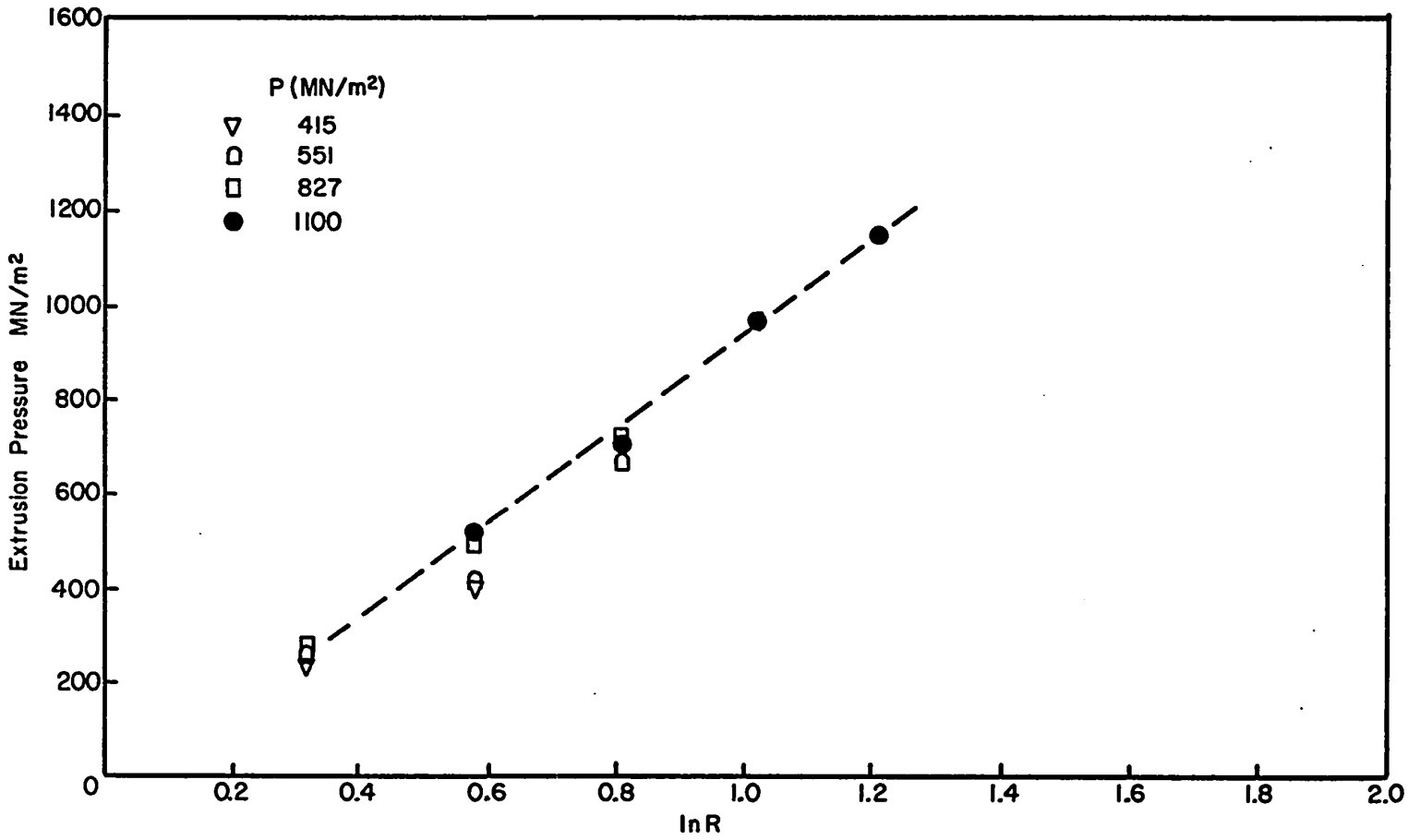

FIG. 38 EXTRUSION PRESSURE VERSUS LnR FOR IRON COMPACTED AT DIFFERENT PRESSURES

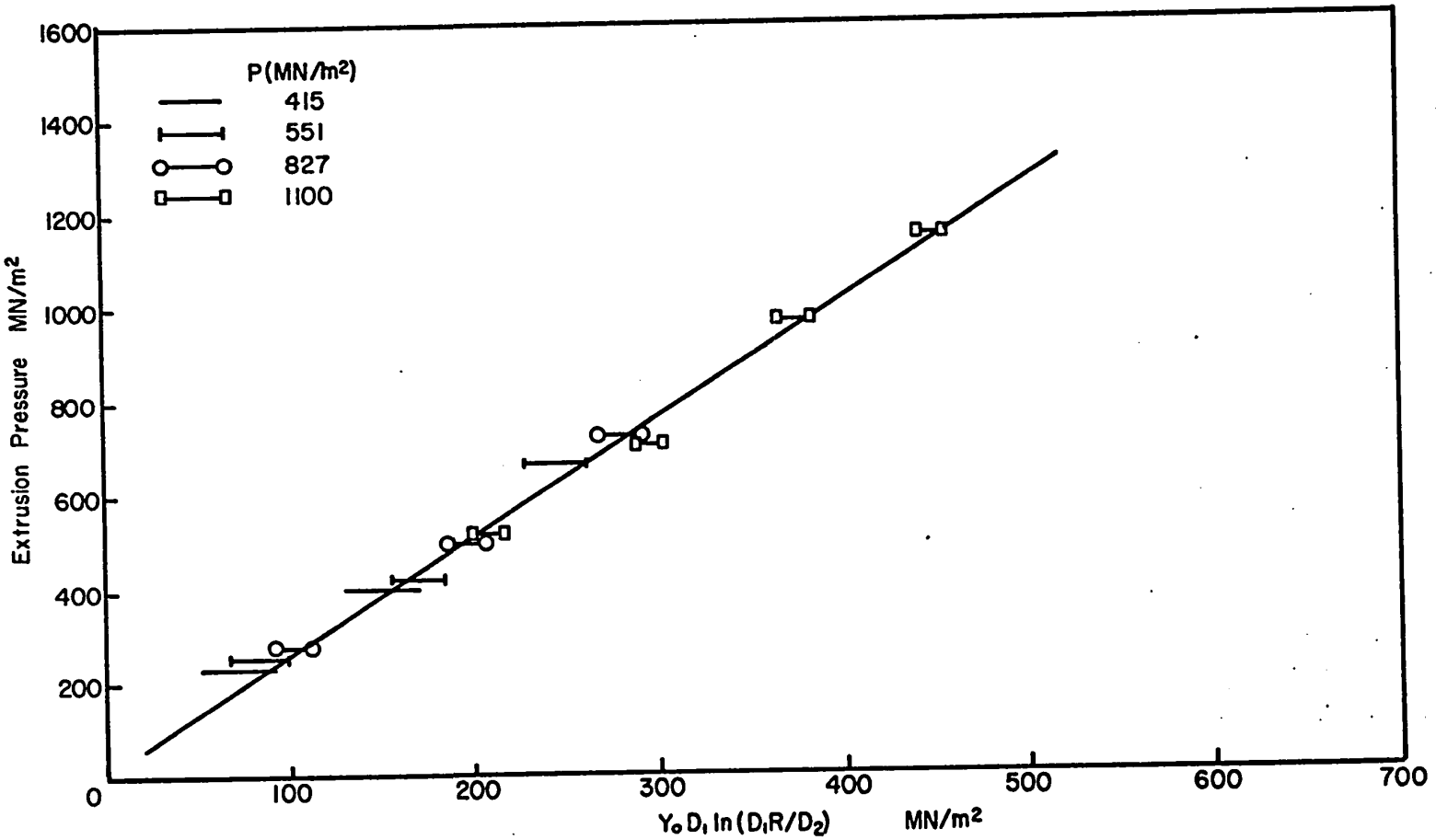

FIG. 39 EXTRUSION PRESSURE VERSUS $Y_o D_1 Ln(D_1R/D_2)$ FOR IRON COMPACTS

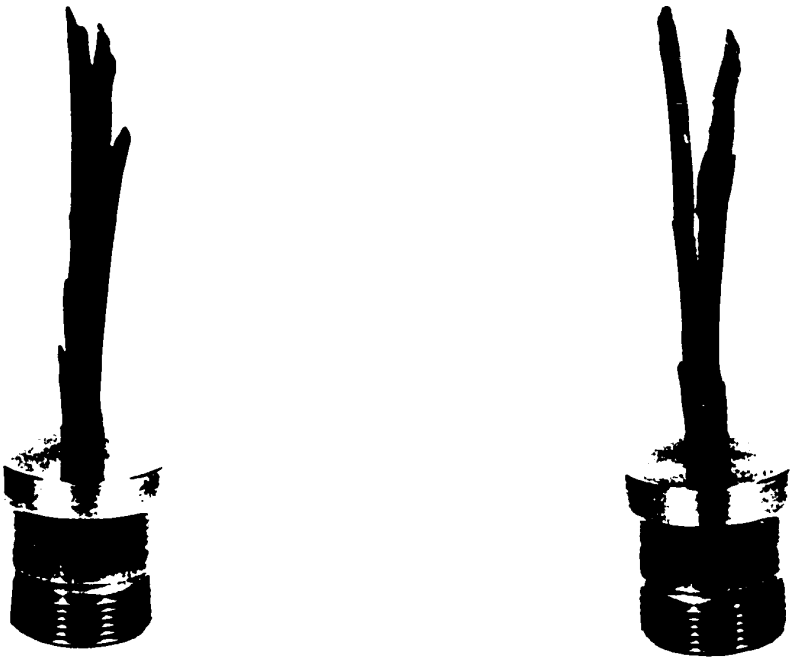

R = 3.36, P = 1100 MN/m²

R = 2.25, P = 827 MN/m²

FIG. 40 SURFACE CONDITION OF IRON POWDER EXTRUSIONS

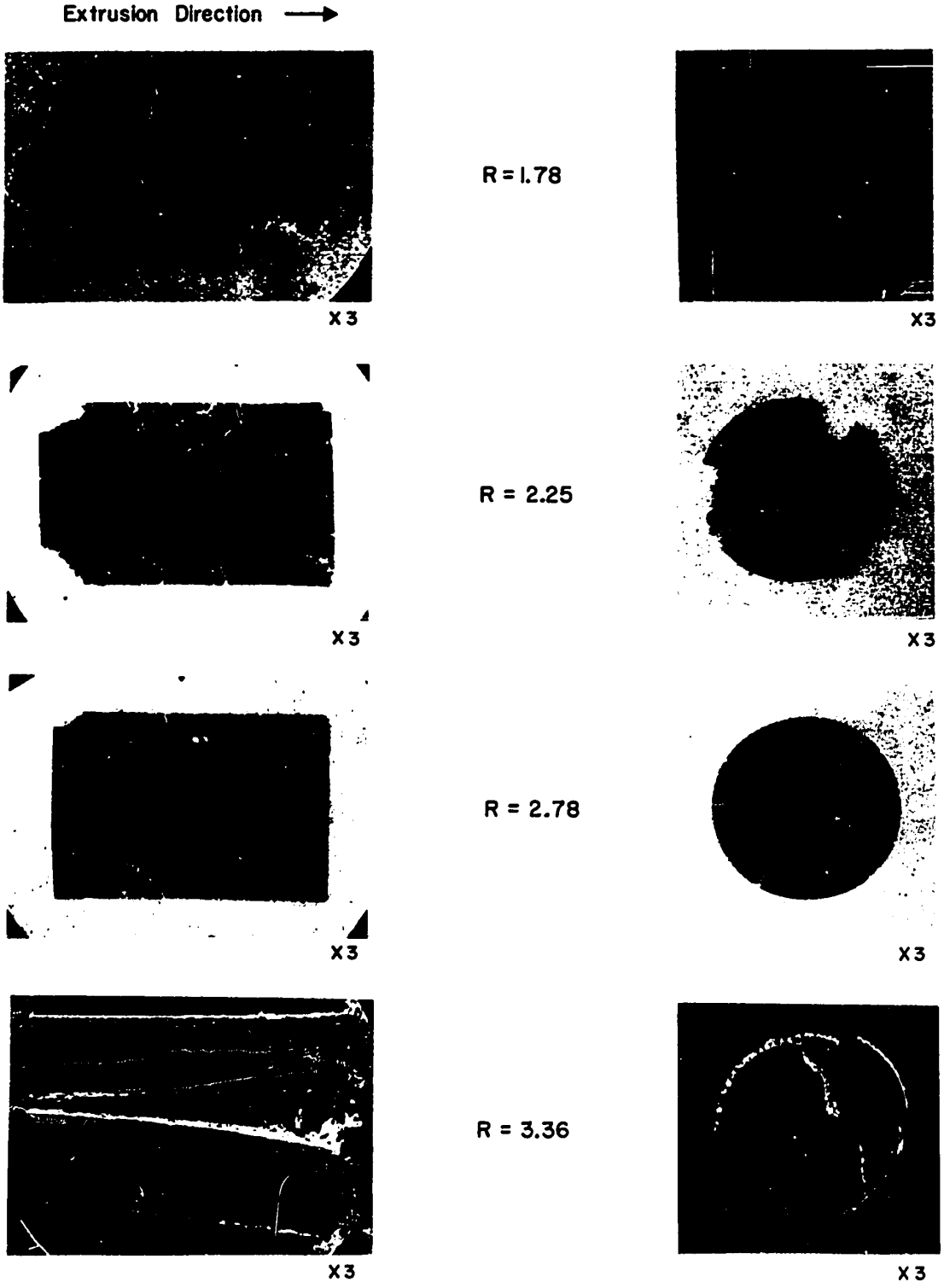

FIG. 41 LONGITUDINAL AND TRANSVERSE SECTIONS OF IRON POWDER EXTRUSIONS COMPACTED AT 1100 MN/m² SHOWING CRACK PATTERNS

Extrusion Direction ⟶

FIG. 42 (a) CENTRAL BURST TYPE DEFECT
P = 827 MN/m², R = 1.36

Extrusion Direction ⟶

FIG. 42(b) DEFORMATION PATTERN IN EXTRUDED IRON COMPACT
P = 551 MN/m² , R = 1.78

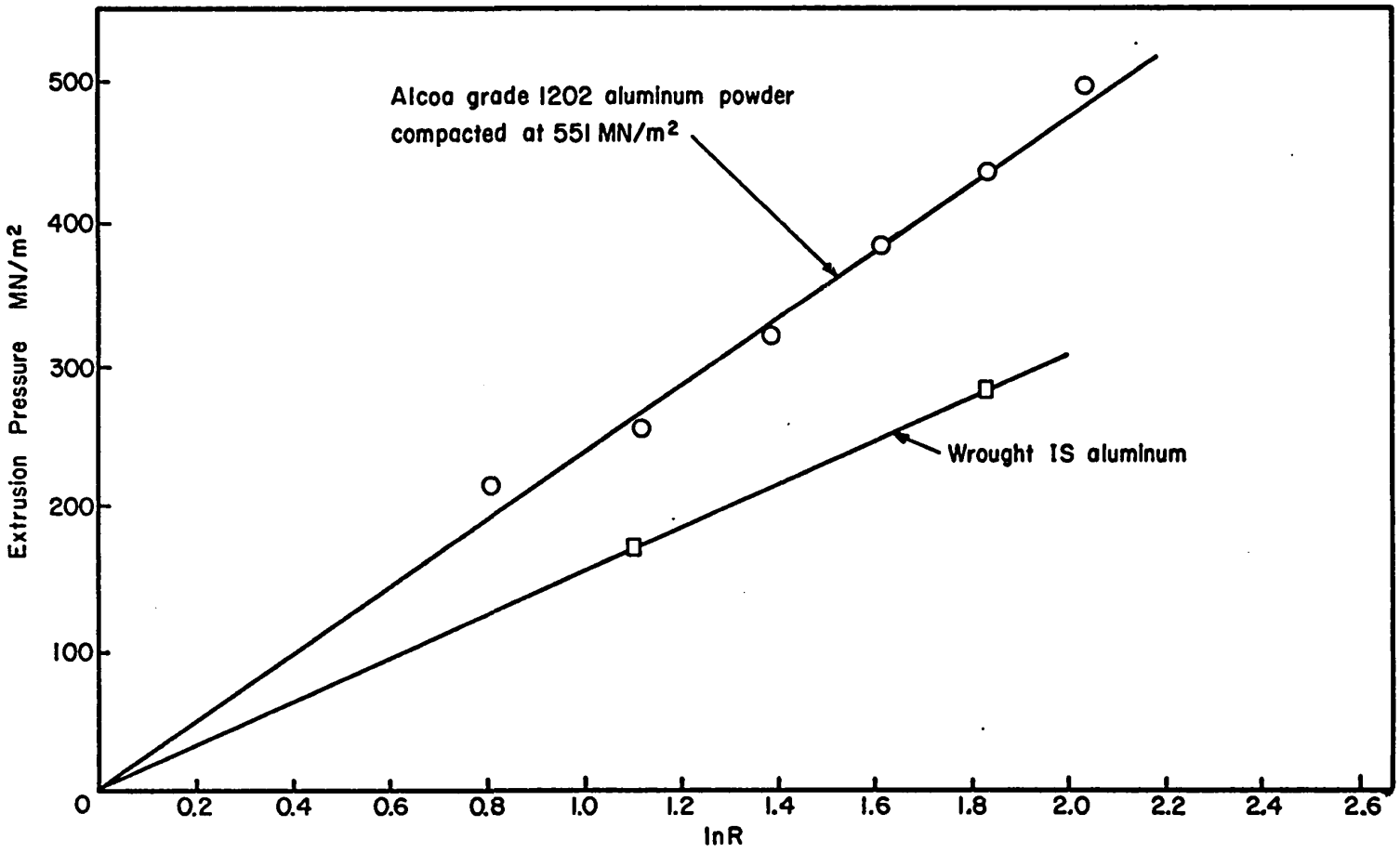

FIG. 43 EXTRUSION PRESSURE VERSUS LnR FOR ALUMINUM

As Compacted

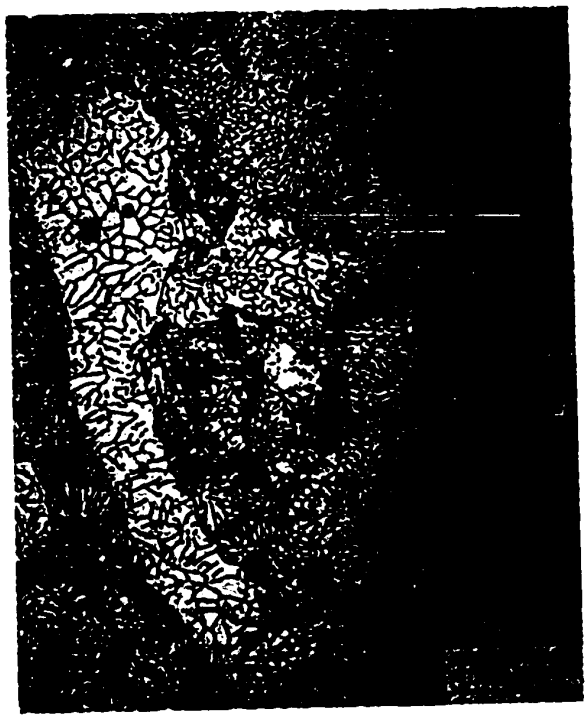

R = 2.25

R = 4.0

R = 6.25

FIG. 44 CROSS SECTIONS OF EXTRUDED ALCOA GRADE 1202 ALUMINUM POWDER COMPACTED AT 551 MN/m²

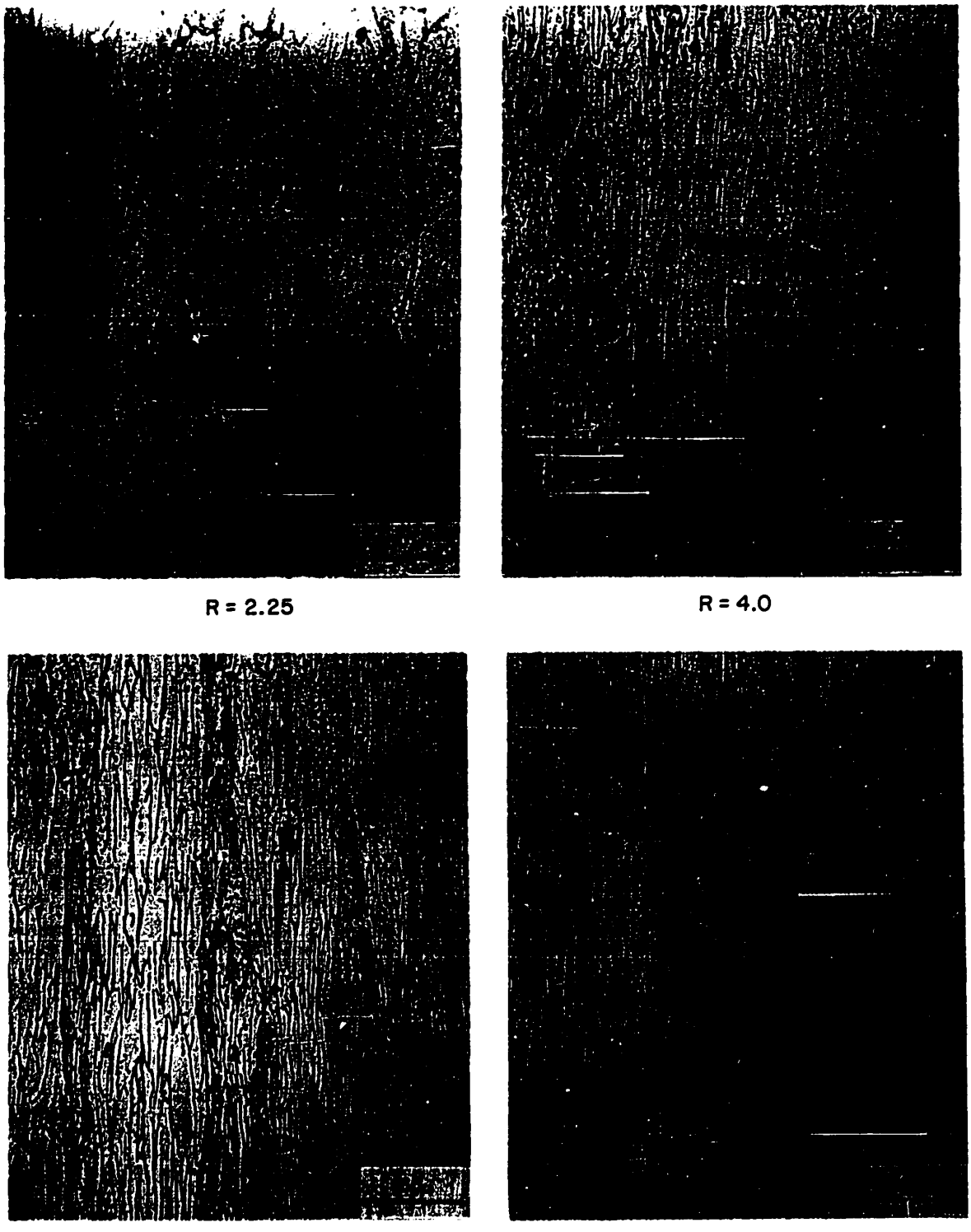

FIG. 45 LONGITUDINAL SECTIONS OF EXTRUDED ALCOA GRADE 1202 ALUMINUM POWDER COMPACTED AT 551 MN/m²

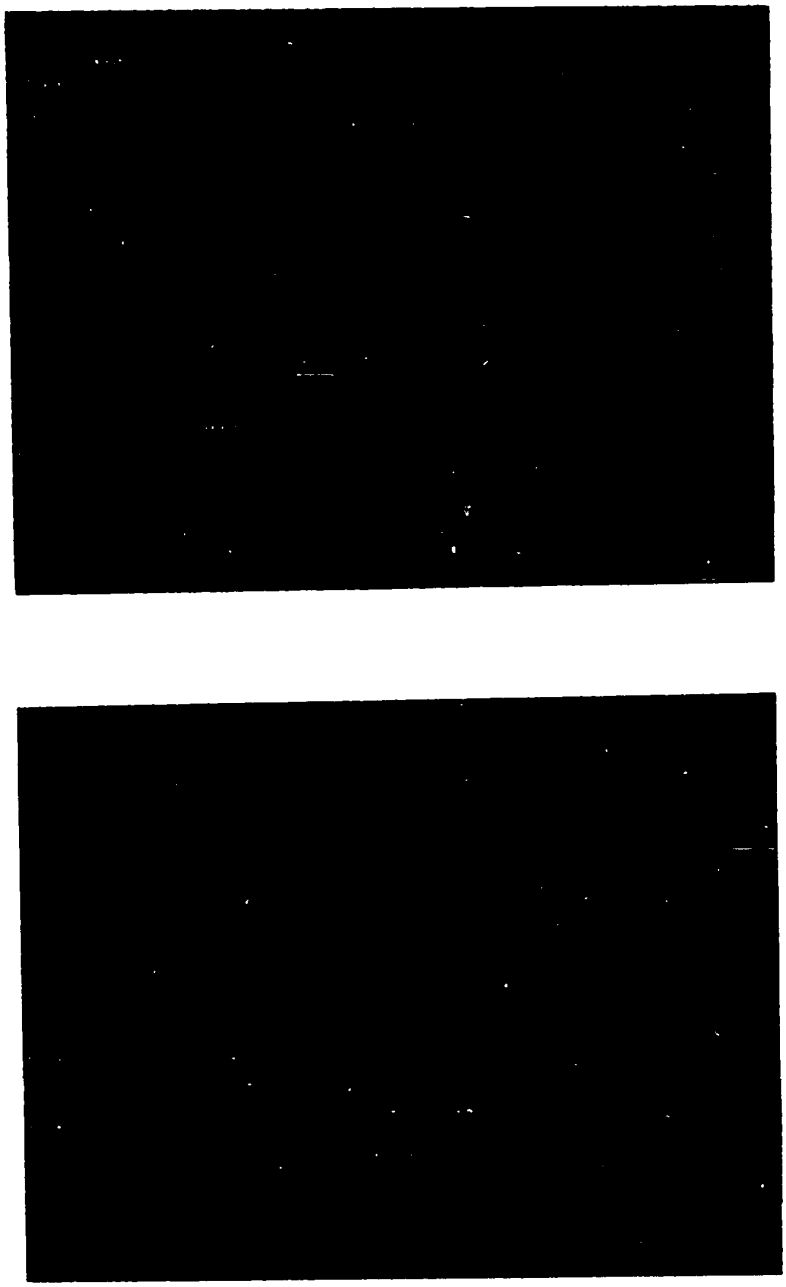

FIG. 46 CROSS SECTIONS OF ALCOA ALUMINUM 1202 POWDER COMPACT EXTRUDED THROUGH 2.25 REDUCTION RATIO SHOWING PATH OF LONGITUDINAL CRACKS IN RADIAL DIRECTION

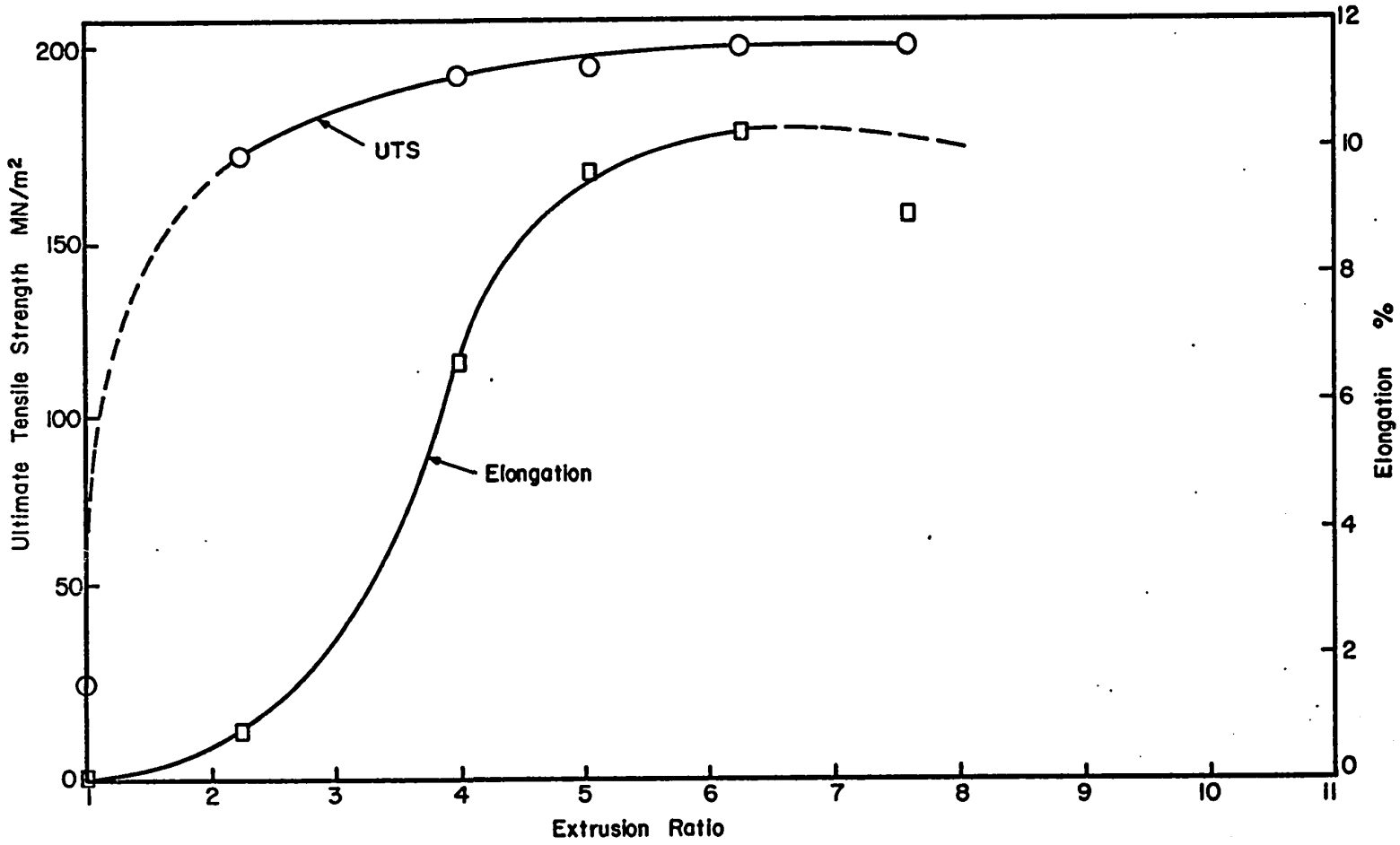

FIG. 47 ULTIMATE TENSILE STRENGTH AND ELONGATION OF EXTRUDED ALCOA 1202 ALUMINUM COMPACTS VERSUS EXTRUSION RATIO

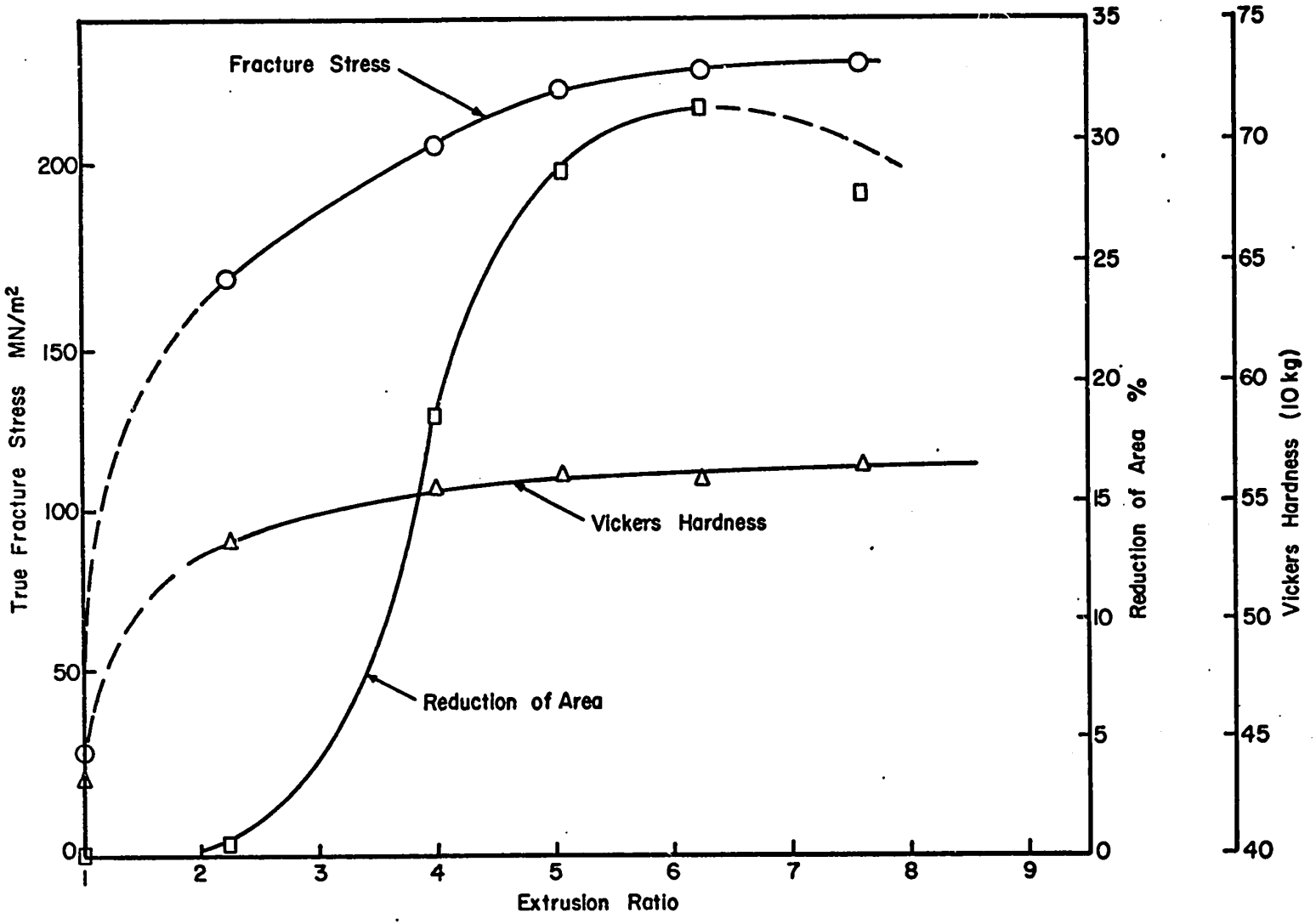

FIG. 48 TRUE FRACTURE STRESS, REDUCTION OF AREA AND HARDNESS OF EXTRUDED ALCOA 1202 ALUMINUM COMPACTS VERSUS EXTRUSION RATIO

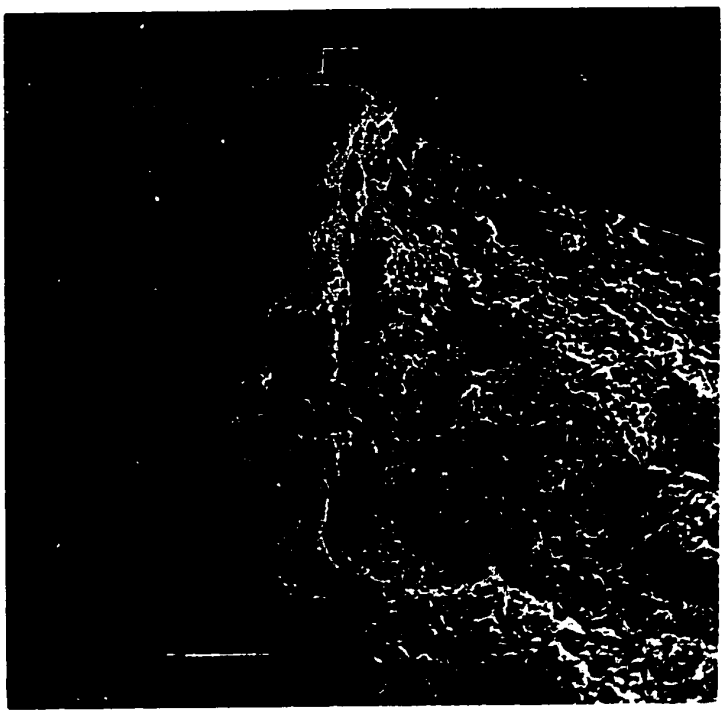

R = 4.0

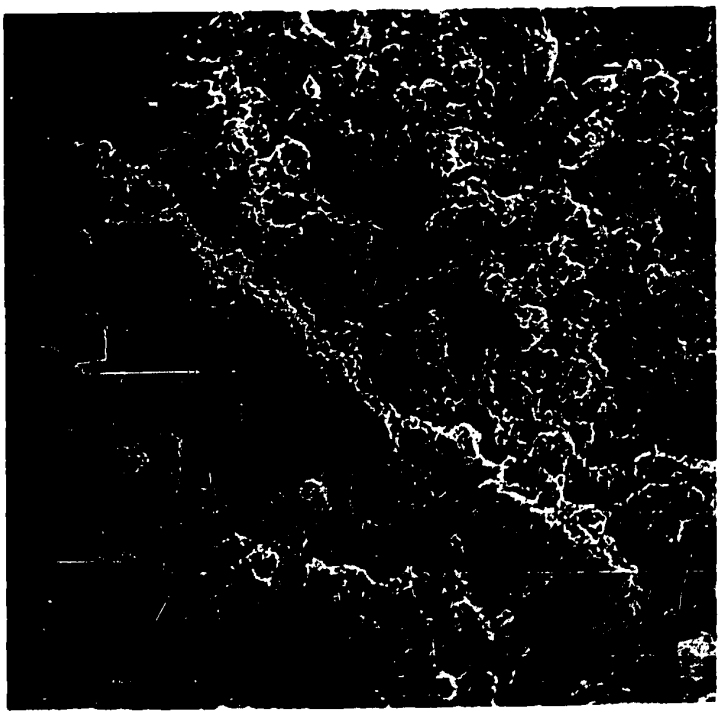

R = 2.25

FIG. 49 TENSILE FRACTURE SURFACES OF EXTRUDED ALCOA 1202 ALUMINUM COMPACTS SHOWING LONGITUDINAL CRACKING

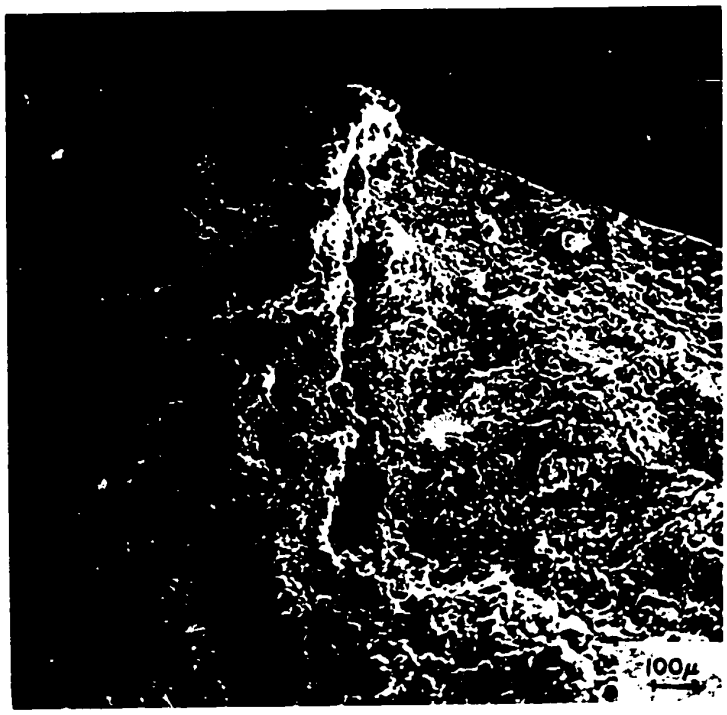

R = 4.0

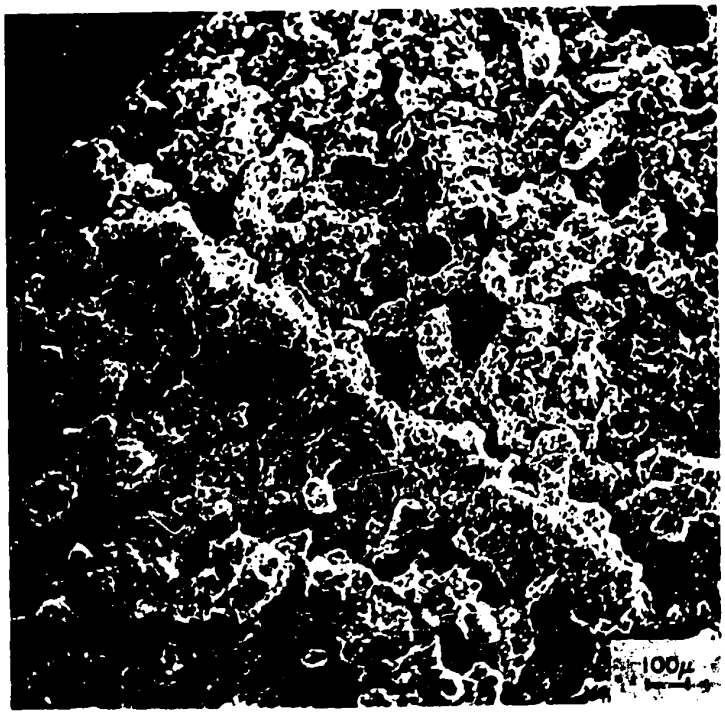

R = 2.25

FIG. 49 TENSILE FRACTURE SURFACES OF EXTRUDED ALCOA 1202 ALUMINUM COMPACTS SHOWING LONGITUDINAL CRACKING

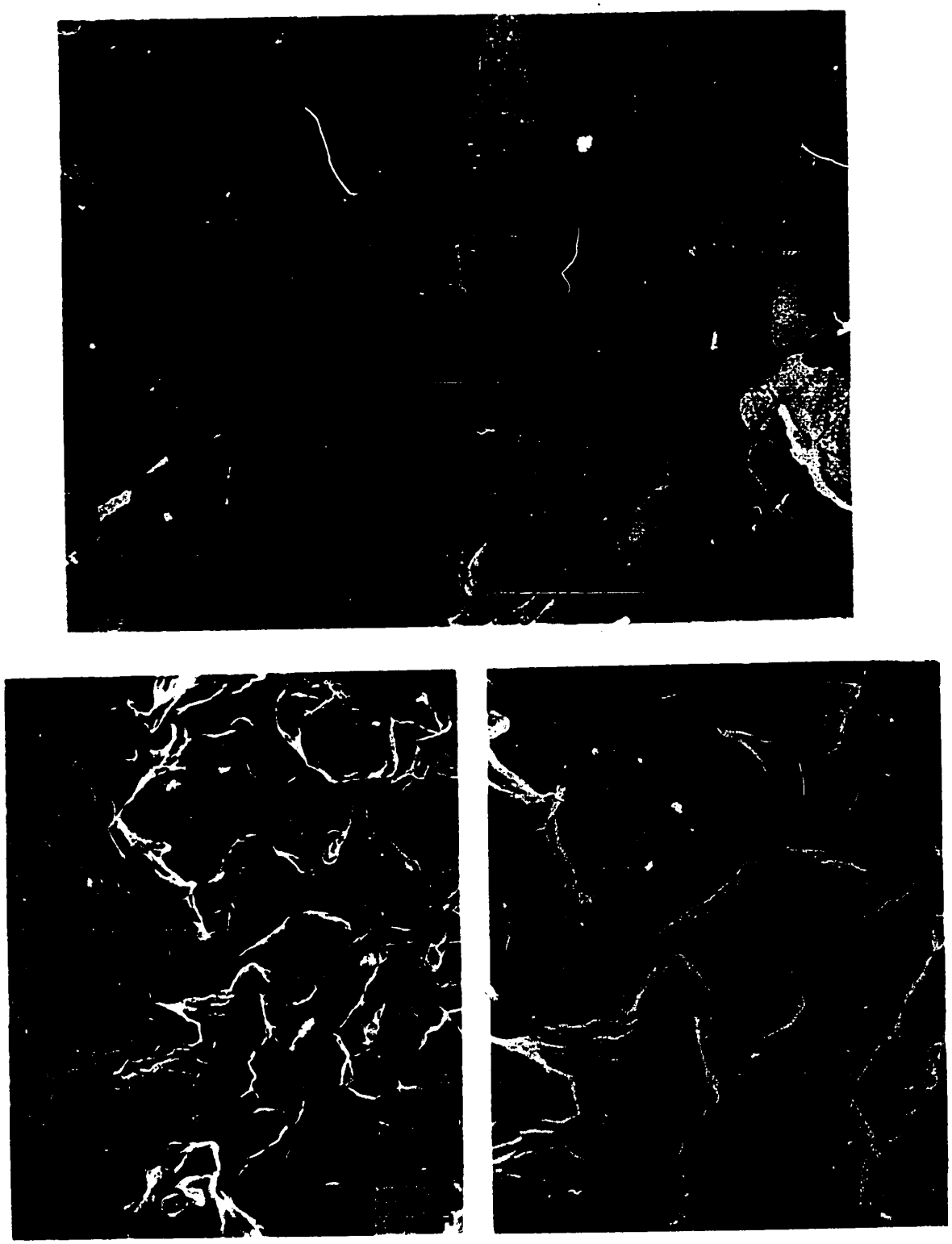

FIG. 50 TRANSMISSION AND SCANNING ELECTRON MICROGRAPHS OF TENSILE FRACTURE SURFACE OF AS-COMPACTED ALCOA 1202 ALUMINUM POWDER

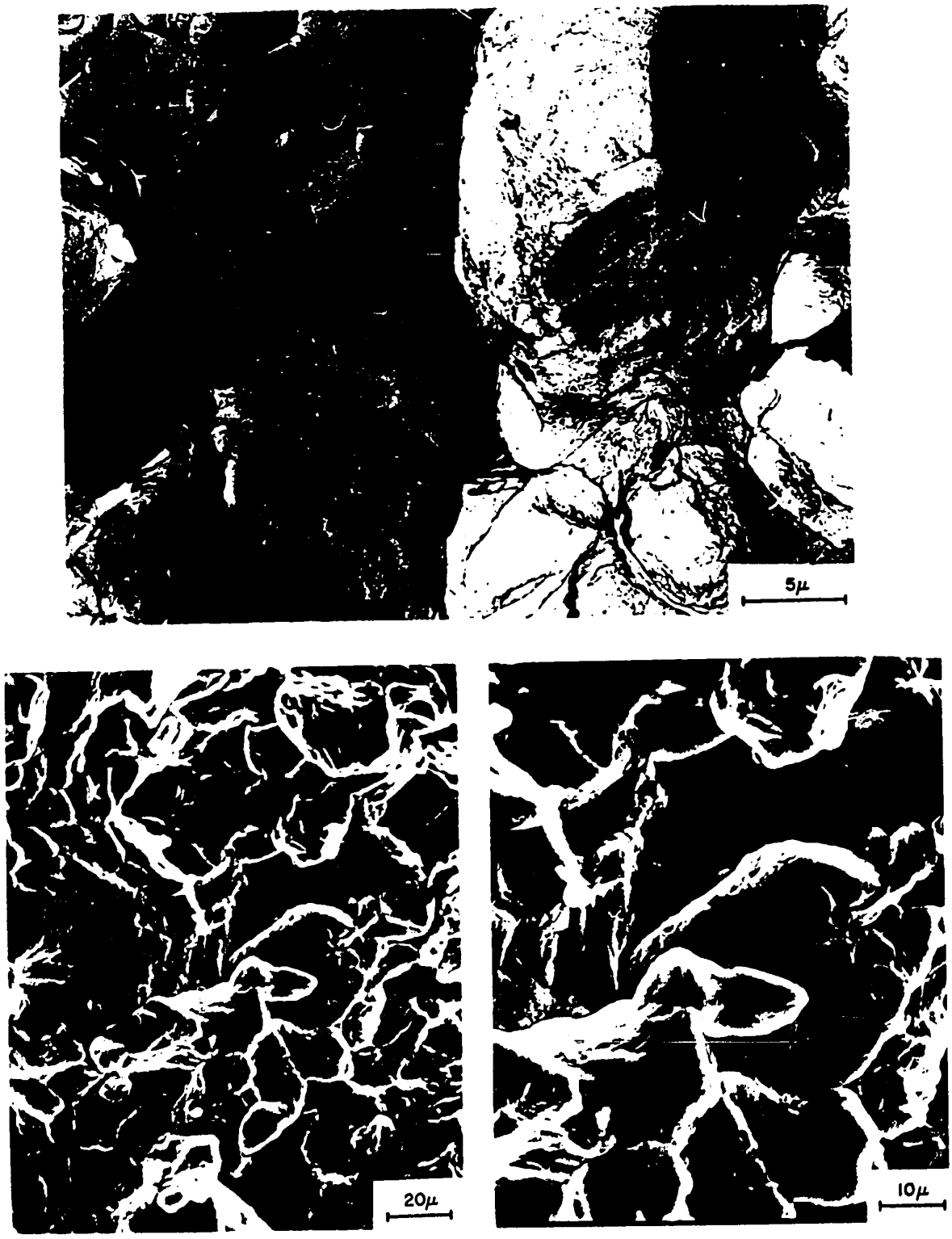

FIG. 50 TRANSMISSION AND SCANNING ELECTRON MICROGRAPHS OF TENSILE FRACTURE SURFACE OF AS-COMPACTED ALCOA 1202 ALUMINUM POWDER

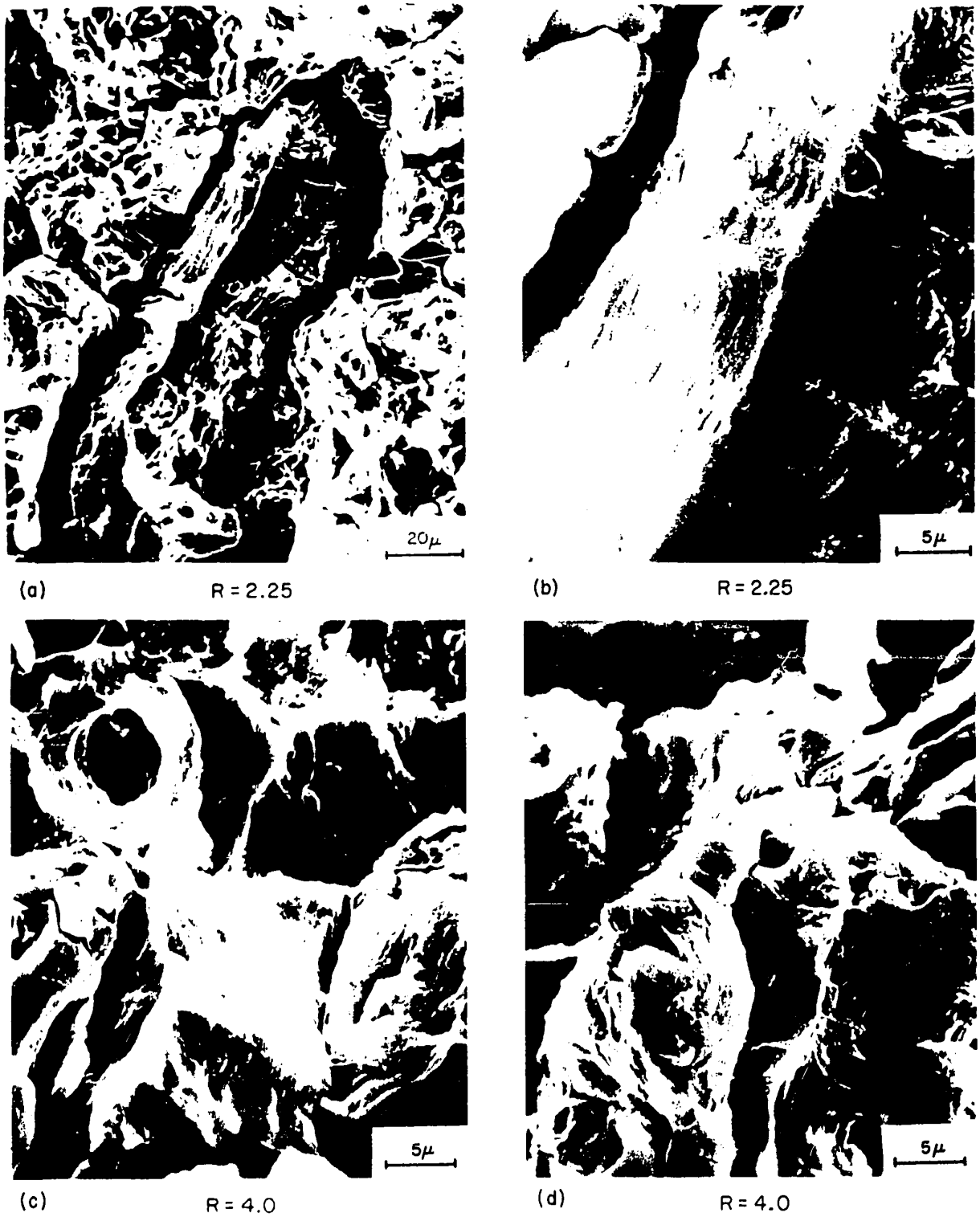

FIG. 51 SCANNING ELECTRON MICROGRAPHS OF TENSILE FRACTURE SURFACES OF ALCOA 1202 ALUMINUM POWDER COMPACTS EXTRUDED AT R=2.25 AND R=4.0

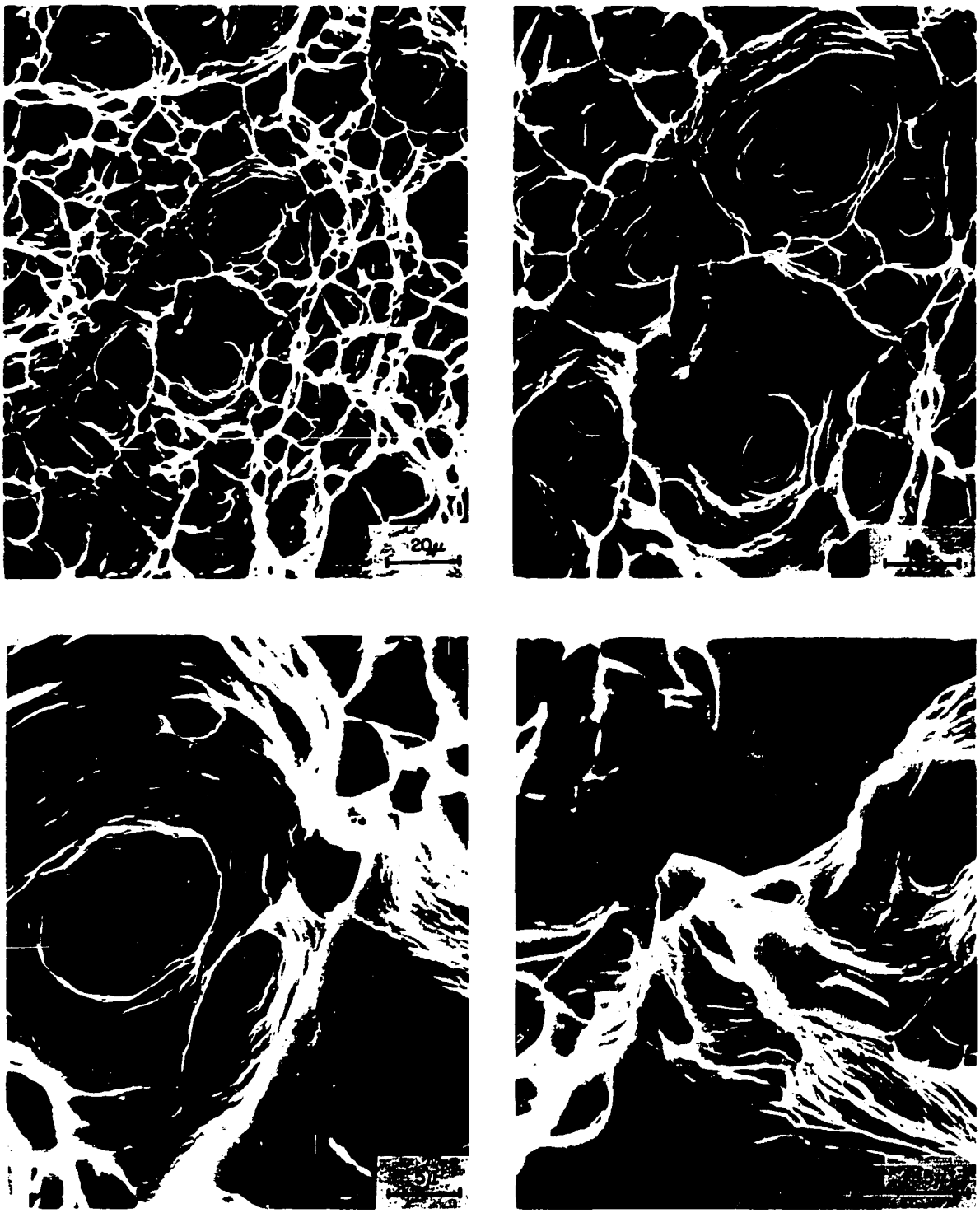

FIG. 52 SCANNING ELECTRON MICROGRAPHS OF TENSILE FRACTURE SURFACE OF WROUGHT IS ALUMINUM EXTRUDED AT R = 3.0

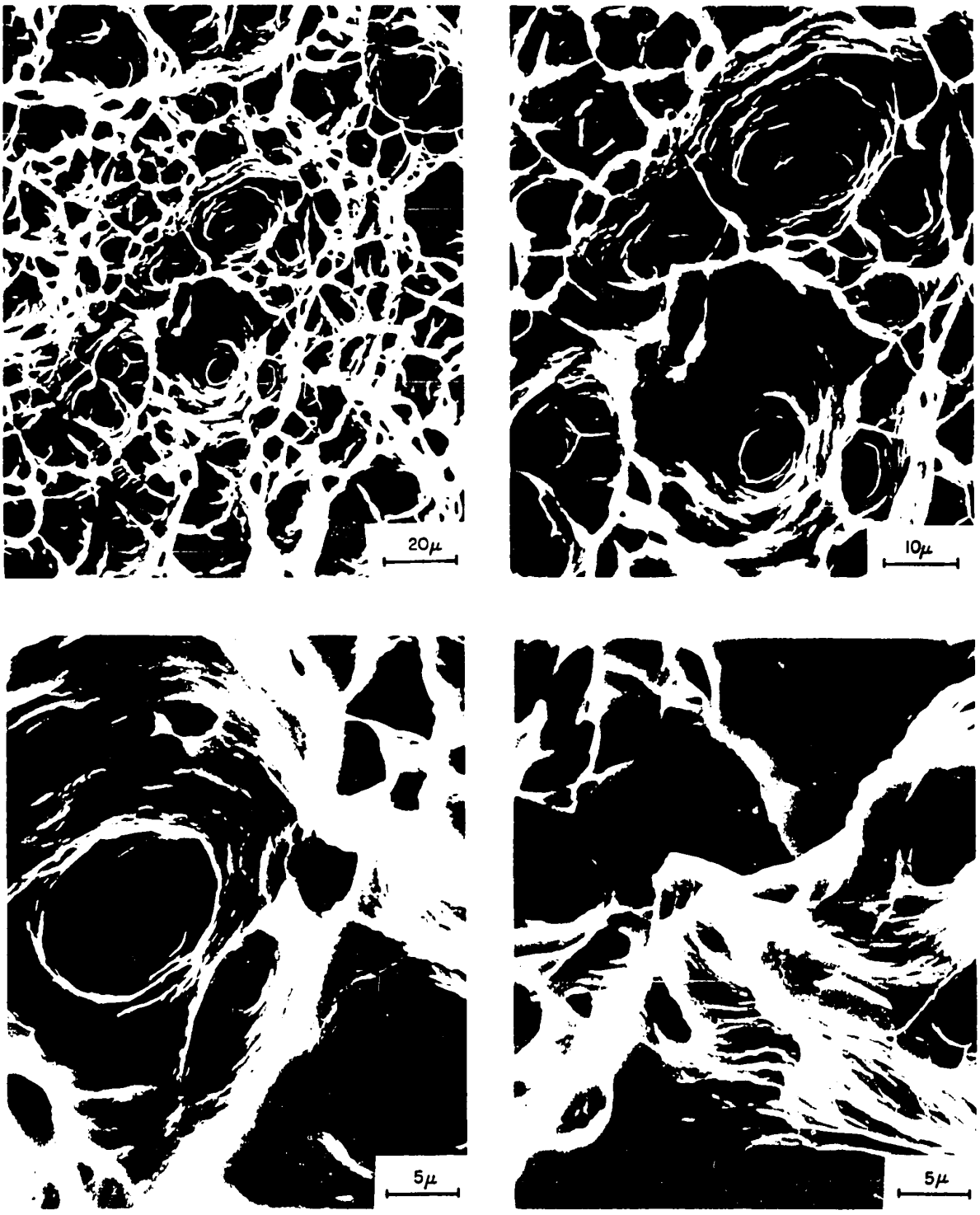

FIG. 52 SCANNING ELECTRON MICROGRAPHS OF TENSILE FRACTURE SURFACE OF WROUGHT IS ALUMINUM EXTRUDED AT R = 3.0

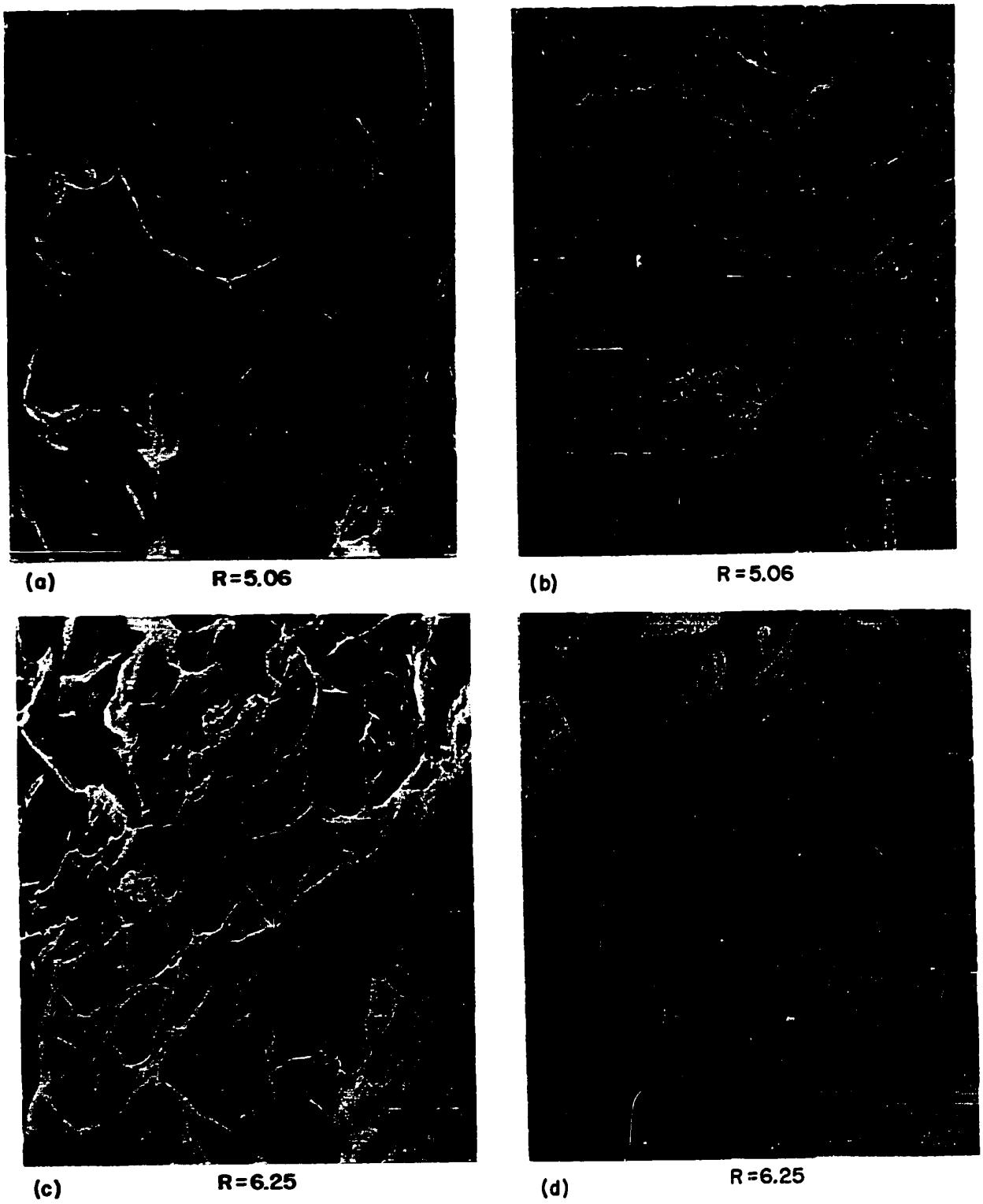

FIG.53 SCANNING ELECTRON MICROGRAPHS OF TENSILE FRACTURE SURFACES OF ALCOA 1202 ALUMINUM POWDER COMPACTS EXTRUDED AT R=5.06 AND R=6.25

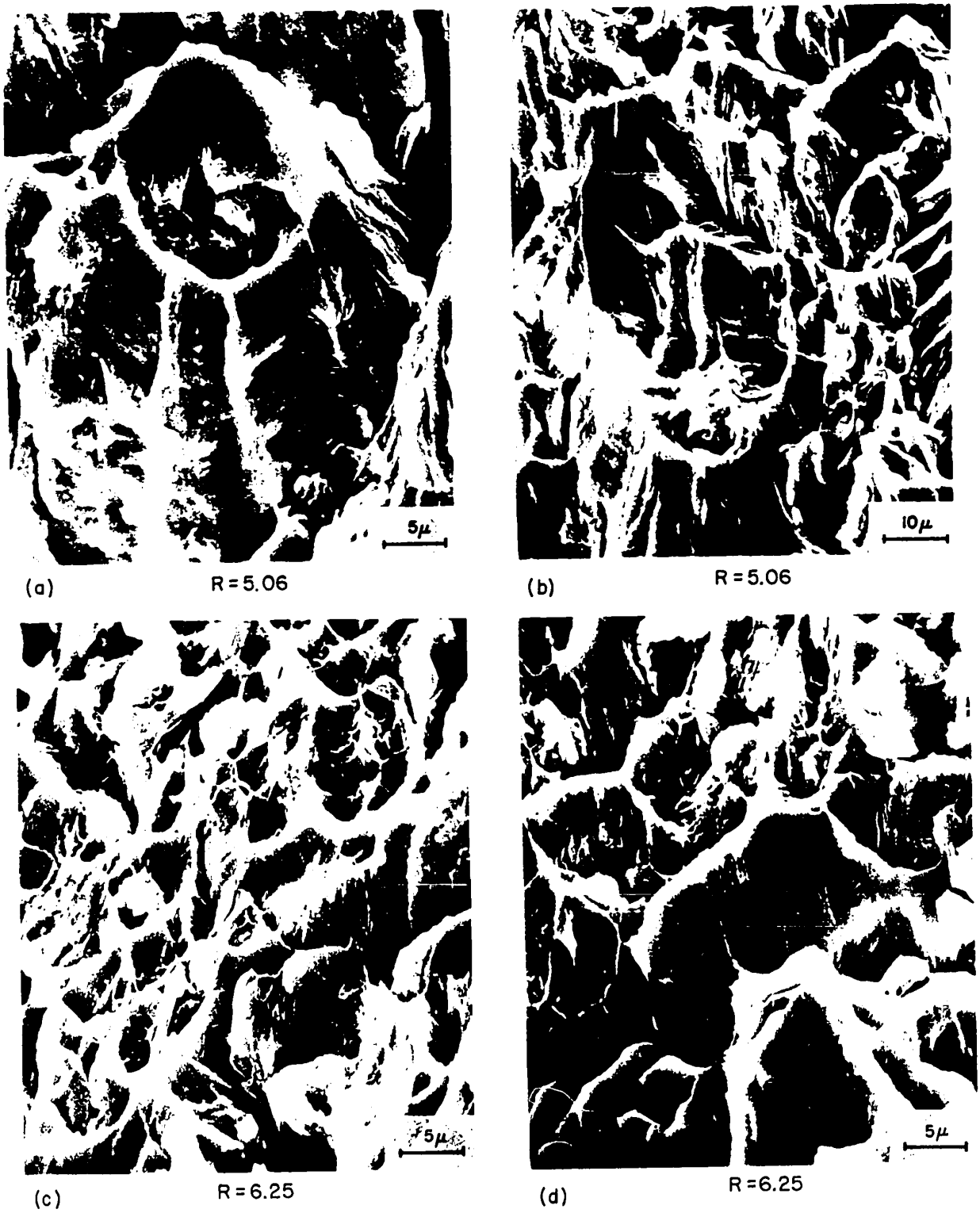

FIG. 53 SCANNING ELECTRON MICROGRAPHS OF TENSILE FRACTURE SURFACES OF ALCOA 1202 ALUMINUM POWDER COMPACTS EXTRUDED AT R = 5.06 AND R=6.25